

**DEVELOPMENT OF PROTECTIVE
NANO-COATINGS FOR ELECTRO-OPTICAL
SYSTEMS**

**A Thesis Submitted to
The Graduate School of Engineering and Sciences of
Izmir Institute of Technology
In Partial Fulfillment of the Requirements for the Degree of**

MASTER OF SCIENCE

in Chemical Engineering

**by
Merve ÖZPİRİN**

**July 2016
İZMİR**

We approve the thesis of **Merve ÖZPİRİN**

Examining Committee Members:

Assist. Prof. Dr. Özgeç EBİL

Department of Chemical Engineering, Izmir Institute of Technology

Prof. Dr. Mustafa M. DEMİR

Department of Material Science and Engineering, Izmir Institute of Technology

Assist. Prof. Dr. Güler NARİN

Department of Chemical Engineering, Usak University

13 July 2016

Assist. Prof. Dr. Özgeç EBİL

Supervisor, Department of Chemical Engineering, Izmir Institute of Technology

**Prof. Dr. S. Fehime ÇAKICIOĞLU
ÖZKAN**

Head of the Department of Chemical Engineering

Prof. Dr. Bilge KARAÇALI
Dean of the Graduate School of Engineering and Sciences

ACKNOWLEDGEMENTS

I am sincerely thankful to people who helped me in my M.Sc. thesis.

Initially, I would like to express my thankfulness to my supervisor, Assist. Prof. Dr. Özgenç EBİL that he provides me opportunities to work on the TUBITAK project, for his knowledge, encouragement, guidance, perceptiveness, precious advices during my study, many valuable and good ideas that offered me on my thesis subject, and his endless support to complete my M.Sc. thesis.

I would also like to thank my friends; especially Gizem PAYER, Sema KIRKÖSE and Selcan ATEŞ for their help in laboratory works and also their friendship.

I wish to thank Dr. Hüseyin ÖZGENER, Zeynep AY, Aysel TOMAK and staff at Center for Materials Research in Izmir Institute of Technology for their help in characterizations.

I am grateful and I express my special thanks to Emre DEMİRKAYA for his understanding, motivations which contribute to me in my work, limitless support ensured to my life, sincerity, friendship and helping me throughout my M.Sc. thesis.

Finally, I would especially like to thank and express my gratitude to my family because they always listen to me and show me the right ways for my future and also thank for their supports in every sense to overcome difficult times, understanding, motivations and valuable opinions.

ABSTRACT

DEVELOPMENT OF PROTECTIVE NANO-COATINGS FOR ELECTRO-OPTICAL SYSTEMS

Electro-optical (EO) systems have wide range of applications and in recent years, especially the use of EO imaging systems in military and civil aviation applications have substantially increased. In these applications, EO systems are exposed to quite harsh and unstable operating conditions like sudden changes in temperature and humidity, dust, fog, physical shock, vibration and radiation. If their optical surfaces such as prisms, lenses and mirrors are damaged due to these conditions, their repair usually is not possible. To overcome these problems, it is necessary to develop special protective coating layers for optical surfaces.

The main goal of this study is to produce protective, self-cleaning and super-hydrophobic polymeric thin films for optical surfaces of the electro-optical (EO) systems. Initiated chemical vapor deposition (iCVD) is a novel method for the fabrication of thin film coatings and it has many advantages such as low production cost, very low deposition temperature, 3D geometry coating performance and high deposition rate. Therefore, iCVD was employed to fabricate homopolymers of poly (glycidyl methacrylate) (PGMA) and poly (1H, 1H, 2H, 2H-Perfluorodecyl acrylate) (PPFDA) and P(GMA-PPFDA) copolymer thin-films as protective coatings for EO systems.

Optical modeling and simulations were performed to determine the effect of film thickness and refractive index on optical performance of substrates to be coated. Optical performance of fabricated coatings was also measured between 400 and 1000 nm range to confirm that protective coatings do not have any measureable impact on optical performance provided that the protective film thickness is kept between 50 nm to 1 μ m. The surface morphology of the protective coatings was evaluated using a variety of analytical tools such as Fourier Transform Infrared Spectroscopy (FTIR), Scanning Electron Microscopy (SEM), Atomic Force Microscopy (AFM) and Contact Angle measurements. Optical tests were performed by following MIL-F-48616 Military Standard (MIL-STD). The best protective coatings were obtained by using P(GMA-PPFDA) copolymer which yields good mechanical properties due to epoxy pendant group and super hydrophobicity due to incorporation of fluoro monomer.

ÖZET

ELEKTRO-OPTİK SİSTEMLER İÇİN KORUYUCU NANO KAPLAMALARIN GELİŞTİRİLMESİ

Elektro-optik (EO) sistemler çok geniş uygulama alanlarına sahiplerdir, son yıllarda, özellikle Elektro-optik görüntüleme sistemlerinin askeri ve sivil havacılık sektöründe kullanımı oldukça artmıştır. Bu alanlarda EO sistemler anlık sıcaklık değişimi, nem, toz, sis, fiziksel şok, titreşim ve radyasyon gibi oldukça zorlu ve değişken çalışma koşullarına maruz kalmaktadırlar. Bu sistemlerin sahip olduğu prizma, lens ve ayna gibi optik yüzeyler, bu şartlardan dolayı zarar görürlerse, tamirleri neredeyse mümkün olmamakta ve bu tip karşılaşılan problemlerin çözümlenebilmesi amacıyla, optik yüzeyler için özel koruyucu kaplamaların geliştirilmesine gerek duyulmaktadır.

Bu çalışmanın asıl amacı, EO sistemlerin optik yüzeyleri için koruyucu, kendi kendini temizleyebilen, süperhidrofobik polimerik ince filmlerin üretilmesidir. Başlatılmış Kimyasal Buhar Biriktirme (BKBB) yöntemi, ince film kaplamalarının üretiminde kullanılan oldukça yeni bir yöntemdir ve düşük üretim maliyeti, düşük sıcaklık koşulları, üç boyutlu yüzeyleri kaplama performansı ve yüksek biriktirme hızı gibi bir çok avantaja sahiptir. Bu nedenle, BKBB yöntemi kullanılarak EO sistemler için Poli(glisidil metakrilat) (PGMA) ve Poli(1H, 1H, 2H, 2H-Perflorodesil akrilat) (PPFDA) homopolimerleri ve P(GMA-PFDA) kopolimer ince filmlerinin üretimi yapılmıştır.

Film kalınlığı ve kırılma indisinin kaplanacak yüzeylerin optik performansına etkisini incelemek için optik modelleme ve simülasyonlar yapılmış bunun yanında film kalınlığı 50 nm ile 1 µm arasında tutularak üretilen koruyucu kaplamaların optik performansa herhangi bir etkisinin olmadığını doğrulamak amacıyla, kaplamaların 400-1000 nm aralığında ölçümleri alınmıştır. Koruyucu kaplamaların yüzey morfolojisinin belirlenmesi, Fourier Dönüşümlü Kızılötesi (FTIR) Spektroskopisi, Taramalı Elektron Mikroskopu (SEM), Atomik Güç Mikroskopu (AFM) ve Değme Açısı ölçümü gibi çeşitli analitik tekniklerin kullanılması ile gerçekleştirilmiştir. Ayrıca, MIL-F-48616 askeri standardı (MIL-STD) takip edilerek optik testler yapılmıştır. Sonuç olarak, en iyi koruyucu kaplama hem yapısındaki epoksi grubundan dolayı iyi mekanik özellik gösterip hem de fluoro monomerin sağladığı süperhidrofobik özelliğe sahip olduğu için P(GMA-PFDA) kopolimeriyle elde edilmiştir.

TABLE OF CONTENTS

LIST OF FIGURES	ix
LIST OF TABLES	xiii
CHAPTER 1. INTRODUCTION	1
1.1. Electro-Optical (EO) Systems	1
1.2. Optical Coating Technology and Applications	3
1.2.1. Optical Materials and Their Properties	4
1.2.1.1. Light Interactions with Materials	6
1.2.1.2. Crystalline Materials	11
1.2.1.3. Optical Glass Materials	14
1.2.1.4. Polymeric Materials	18
1.2.1.5. Metals	21
1.2.2. Optical Coating Techniques	23
1.2.2.1. Antireflection Coating	24
1.2.2.2. High Reflection Coating	25
1.2.2.3. Partial Reflectors	27
1.2.2.4. Optical Filters	27
1.2.3. Thin Film Production Methods	28
1.2.3.1. Initiated Chemical Vapor Deposition (iCVD)	32
CHAPTER 2. EXPERIMENTAL WORK	43
2.1. iCVD System	43
2.2. Materials	44
2.3. Cleaning Procedures of the Substrates	46
2.4. Polymeric Thin Film Coating Procedure in iCVD System	48
2.4.1. Startup of Thin Film Coating in iCVD System	48
2.4.2. Operating Mode in iCVD System	49
2.4.3. Shutdown Procedure in iCVD System	49
2.5. Characterization	50

CHAPTER 3. MODELING OF OPTICAL COATINGS.....	52
CHAPTER 4. RESULTS AND DISCUSSION.....	69
4.1. PGMA Deposition in iCVD System	69
4.1.1. Thickness Measurement with Reflectometer for PGMA Coatings	74
4.1.2. FTIR Analysis of GMA Monomer and PGMA Film.....	75
4.1.3. SEM Analysis of PGMA Film.....	77
4.1.4. AFM Results of PGMA Film.....	78
4.1.5. Contact Angle Measurement for PGMA Film.....	80
4.1.6. Surface Quality Test with Optical Microscopy for PGMA Film...	80
4.2. PPFDA Deposition in iCVD System	81
4.2.1. Thickness Measurement with Reflectometer for PPFDA Coatings	84
4.2.2. FTIR Analysis of PFDA Monomer and PPFDA Film.....	86
4.2.3. SEM Analysis of PPFDA Film	87
4.2.4. AFM Results of PPFDA Film.....	88
4.2.5. Contact Angle Measurement for PPFDA Film.....	89
4.2.6. Surface Quality Test with Optical Microscopy for PPFDA Film...	90
4.3. Copolymer P(GMA-PFDA) Deposition in iCVD System	91
4.3.1. Thickness Measurement with Reflectometer for Copolymer Films	92
4.3.2. FTIR Analysis of Copolymer Films	93
4.3.3. SEM Analysis of Copolymer Films.....	94
4.3.4. AFM Results of Copolymer P(GMA-PFDA) Films	95
4.3.5. Contact Angle Measurement for Copolymer Films.....	96
4.3.6. Surface Quality Test for Copolymer P(GMA-PFDA) Films.....	97
4.4. Performance Tests for Homopolymer and Copolymer Films	98
4.4.1. Humidity Test	98
4.4.2. Swelling-Solubility in Water Test	100
4.4.3. Salt Solubility Test.....	101
4.4.4. Solubility and Cleanability Test.....	103

4.4.5. Adhesion Test	103
CHAPTER 5. CONCLUSIONS	106
REFERENCES	108

LIST OF FIGURES

<u>Figure</u>	<u>Page</u>
Figure 1.1. An electromagnetic wave having electric field E, magnetic field B and the wavelength λ	4
Figure 1.2. Regions of electromagnetic spectrum	5
Figure 1.3. Refraction of light	6
Figure 1.4. Absorption mechanism of a photon.....	8
Figure 1.5. The electric field components; p-polarization and s-polarization	10
Figure 1.6. Constructive and destructive wave interference.....	24
Figure 1.7. Schematic representation of a single layer antireflection coating.....	24
Figure 1.8. Multilayer film that has quarter wavelength thicknesses	25
Figure 1.9. Reflectance curve of dielectric film stack	26
Figure 1.10. Atomic layer deposition (ALD) process steps	31
Figure 1.11. Schematic illustration of spin coating process	32
Figure 1.12. Initiated chemical vapor deposition (iCVD) system	34
Figure 1.13. General mechanism of iCVD technique	36
Figure 1.14. iCVD reaction mechanism, I: initiator, M: monomer, R: radical	36
Figure 2.1. Vacuum chamber of iCVD system.....	44
Figure 2.2. RCA cleaning procedure for c-Si substrates	47
Figure 2.3. Cleaning procedure for glass substrates	48
Figure 2.4. General substrate coating scheme in iCVD system.....	50
Figure 2.5. Mprobe-Vis system	50
Figure 3.1. Transmission curves of substrate materials.....	53
Figure 3.2. Film stack model of 1 pair PTFE/PMMA	54
Figure 3.3. Transmission graphs of 1 layer-100 nm PTFE/100 nm PMMA (black) and 10 layer-150 nm PTFE/150 nm PMMA (red) on sapphire substrates.....	55
Figure 3.4. Film stack model of 10 pair PTFE/PMMA	55
Figure 3.5. Transmission graphs of 10 layer-100 nm PTFE/100 nm PMMA (black)and 10 layer-150 nm PTFE/150 nm PMMA (red) on sapphire substrates	56
Figure 3.6. Film stack model of 100 pair PTFE/PMMA	56
Figure 3.7. Transmission graphs of 100 layer-100 nm PTFE/100 nm PMMA (black) and 100 layer-150 nm PTFE/150 nm PMMA (red) on sapphire substrates.....	57

Figure 3.8. BK7 transmission behavior (transmission scale between 95-96%)	59
Figure 3.9. Simulation graphs of modeling BK7 coated with different thickness of PGMA	60
Figure 3.10. Transmission graph of BK7 coated with PGMA from 50 nm to 1 μ m.....	61
Figure 3.11. Transmission graph of BK7 coated with FP from 50 nm to 1 μ m	62
Figure 3.12. Transmission graph of BK7 coated with copolymer (PGMA-FP) from 50 nm to 1 μ m.....	63
Figure 3.13. Microscope slide transmission curve	64
Figure 3.14. Transmission graph of MS coated with PGMA from 50 nm to 1 μ m.....	65
Figure 3.15. Transmission graph of MS coated with FP from 50 nm to 1 μ m.....	66
Figure 3.16. Transmission graph of Microscope slide coated with copolymer (PGMA- FP) from 50 nm to 1 μ m	66
Figure 3.17. Transmission graph of BK7 coated with Si ₃ N ₄ from 50 nm to 1 μ m.....	67
Figure 3.18. Transmission graph of MS coated with Si ₃ N ₄ from 50 nm to 1 μ m	68
Figure 4.1. Glycidyl methacrylate (GMA) structure	69
Figure 4.2. Calibration graphs of GMA in MFC2 and MMFC and TBPO in MFC1 and MFC3	71
Figure 4.3. Reflectometer results of (a) iCVD61, (b) iCVD40 and (c) iCVD53 depositions for PGMA coatings on c-Si	74
Figure 4.4. FTIR spectra of (a) GMA monomer and (b) PGMA film synthesized in iCVD system.....	76
Figure 4.5. SEM images of (a) uncoated c-Si substrate (b) c-Si coated with ~1 μ m PGMA Film	77
Figure 4.6. AFM results of bare c-Si substrate (a) color map (b) 3D view	78
Figure 4.7. AFM color map and 3D images of PGMA coating with (a) ~500 nm and (b) 1 μ m thickness	79
Figure 4.8. Contact angle results for bare c-Si substrate and c-Si coated with ~500 nm PGMA film	80
Figure 4.9. Surface images of 1 μ m PGMA film at (a) 40x and (b) 80x magnifications.	81
Figure 4.10. 1H, 1H, 2H, 2H, (Perfluorodecyl) acrylate (PFDA) structure	81
Figure 4.11. Calibration result of PFDA in MFC2	82
Figure 4.12. Reflectometer results of (a) iCVD73, (b) iCVD69 and (c) iCVD72 depositions for PPFDA coatings on c-Si	85

Figure 4.13. FTIR spectra of (a) PFDA monomer and (b) PPFDA film synthesized in iCVD system.....	86
Figure 4.14. SEM image of c-Si coated with 352 nm PPFDA film	87
Figure 4.15. SEM images of (a) uncoated napkin (b) coated napkin with PPFDA film..	88
Figure 4.16. AFM color map and 3D images of PPFDA coating with (a) medium thickness 352 nm and (b) 1.09 μ m thickness.....	89
Figure 4.17. Contact angle results for bare c-Si substrate and c-Si coated with 1.09 μ m PPFDA coating	90
Figure 4.18. Surface images of 1.09 μ m PPFDA film at (a) 40x and (b) 80x magnifications.....	91
Figure 4.19. Reflectometer result of (a) iCVD59 and (b) iCVD77 depositions for Copolymer coatings on c-Si.....	92
Figure 4.20. FTIR spectra of (a) homopolymer PGMA, (b) homopolymer PPFDA, (c) copolymer P(GMA-PFDA) deposited in iCVD59 and (d) copolymer P(GMA-PFDA) deposited in iCVD77.....	93
Figure 4.21. SEM image of c-Si coated with copolymer P(GMA-PFDA) film which contains higher amount of PGMA	94
Figure 4.22. SEM image of c-Si coated with copolymer P(GMA-PFDA) film which contains higher amount of PPFDA	95
Figure 4.23. AFM color map and 3D images of copolymer coatings synthesized in (a) iCVD59 run and (b) iCVD77 run	95
Figure 4.24. Contact angle results for c-Si substrate coated with copolymer films	97
Figure 4.25. Surface images of (a) iCVD59 and (b) iCVD77 deposition samples at 80x magnification	97
Figure 4.26. Thickness and reflection inspection of PGMA film produced in iCVD system before and after humidity test	99
Figure 4.27. Thickness and reflection inspection of PGMA film produced in iCVD system before and after swelling-solubility in water test	101
Figure 4.28. Thickness and reflection inspection of PGMA film produced in iCVD system before and after salt solubility test.....	102
Figure 4.29. Thickness measurement results before and after adhesion test for (a) Copolymer (iCVD59) and (b) Copolymer (iCVD77) films produced in iCVD system.....	104

Figure 4.30. Before and after adhesion test visual inspection results of (a) and (b)
Copolymer (iCVD59) and (c) and (d) Copolymer (iCVD77) film surface
images at 5x magnifications 104

LIST OF TABLES

<u>Table</u>	<u>Page</u>
Table 1.1. Type of EO systems and Applications.....	2
Table 1.2. The wavelength ranges for the primary color of the visible region.....	5
Table 1.3. Crystal Systems	12
Table 1.4. Physical and Optical Properties of Some Selected Crystalline Materials	12
Table 1.5. Mechanical and Thermal Properties of Some Selected Crystalline Materials.....	13
Table 1.6. Encoding Types and Densities of Some Selected Glasses	16
Table 1.7. Optical and Mechanical Properties of Some Selected Glasses.....	17
Table 1.8. Thermal Properties of Some Selected Glasses	18
Table 1.9. The Physical, Optical and Thermal Properties of Some Optical Polymers ...	19
Table 1.10. The Mechanical Properties of Some Optical Polymers.....	21
Table 1.11. The Physical and Mechanical Properties of Some Selected Metals	22
Table 1.12. The Thermal Properties of Some Selected Metals	22
Table 2.1. Properties of iCVD materials and substrate cleaning chemicals	45
Table 4.1. PGMA deposition experiment conditions and thickness results	72
Table 4.2. PPFDA deposition experiment conditions and thickness results	83
Table 4.3. Copolymer deposition experiment conditions and thickness results.....	92
Table 4.4. Thickness results of coated films on c-Si substrate.....	99
Table 4.5. Swelling-Solubility in Water Test results of coating films on c-Si substrate.....	100
Table 4.6. Salt Solubility Test results of coating films on c-Si substrate.....	102

CHAPTER 1

INTRODUCTION

The main aims of this study are to fabricate hydrophobic protective polymeric nano-coatings for optical surfaces of Electro-Optical (EO) systems. This thesis contains five chapters: in Chapter 1, general information about EO systems, optical coating technology and materials, and coating techniques, especially initiated chemical vapor deposition (iCVD) that used as a principal method in this study to form polymeric films, are mentioned. In Chapter 2, materials, characterization and fabrication methods including Initiated Chemical Vapor Deposition (iCVD) system are given. Modeling and simulation of the polymeric coatings on a variety of substrate materials are detailed in Chapter 3. Chapter 4 contains results and discussion of characterization and performance measurements of fabricated protective. Finally, conclusions are given in Chapter 5.

1.1. Electro-Optical (EO) Systems

The advancement of technology has enabled the emergence of innovations in many areas and one of them is the field of electro-optics. After the invention of lasers, this field has continued to develop rapidly and gained importance in different applications such as telecommunication, sensor systems and signal processing. In addition to these applications, imaging systems used in military and civil aviation showed great improvements due to advancements in EO systems. In EO imaging systems, in order to find a source and also provide visual display, electromagnetic radiation at optical wavelength is transformed to the electrical signals. The high data collection and human vision in different wavelength, distance and environmental conditions become easier thanks to EO imaging systems (Dudzik 1993, Driggers, Cox et al. 1999).

In terms of performance capabilities, EO systems can be divided into two main categories as passive and active EO systems. Types and application areas of EO systems are given in Table 1.1.

Table 1.1. Type of EO systems and Applications
(Source: Campana 1993, Fox 1996).

		Applications
Passive EO Systems	Starting-Sensor Systems	Commercial and military applications; <ul style="list-style-type: none"> • tracking • automatic identification • moving target demonstration • recognition
	Infrared Line Scanning (IRLS) Systems	<ul style="list-style-type: none"> • recognition of the check points • autonomous homing vehicles guidance
	Forward-Looking Infrared (FLIR) Systems	<ul style="list-style-type: none"> • night vision by using thermographic camera • search and rescue operations • target acquisition in military and civil aircraft
	Infrared Search and Track (IRST) Systems	Military applications; <ul style="list-style-type: none"> • determination and tracking of infrared emitting objects • tracking of multivarious targets • warning systems for air vehicles
Active EO Systems	Laser Radar	<ul style="list-style-type: none"> • target tracking • target identification and recognition • imaging • detection of the small objects • vibration sensing • wind shear identification
	Millimeter-Wave Radar	<ul style="list-style-type: none"> • missile guidance • fire control for ground targets • tracking for airborne targets • automotive braking systems • automotive warning systems
	Laser Rangefinders	Military and commercial applications; <ul style="list-style-type: none"> • long range tracking • tank fire control • cloud height measurement • missile command guidance
	Fiber Optic Systems	<ul style="list-style-type: none"> • telecommunication applications • transferring of data and information • endoscopic imaging applications • transportation systems • distribution of video and data services

Electro-Optical systems used in military and civil aviation applications such as night vision systems, remote sensing and sighting devices usually include prisms, lenses and mirrors as optical surfaces, and these surfaces are made of many different inorganic and organic materials. Such materials include sapphire, calcite (CaCO₃), silica, barium

fluoride (BaF_2), lithium fluoride (LiF), germanium (Ge), calcium fluoride (CaF_2), magnesium fluoride (MgF_2), quartz (SiO_2), F_2 , Urea, N-BK7, Teflon (PTFE), poly(methyl methacrylate) (PMMA), poly(styrene) (PS), zinc selenide (ZnSe), Ohara FPL glass (especially S-FPL51 and S-FPL53 equivalent), other dielectric (inorganic/organic) materials, and certain metals such as Al, Ag etc. (Nalwa and Miyata 1996, Wakaki 2012).

Electro-Optical systems are exposed to quite harsh and unstable operating conditions like sudden changes in temperature, humidity, dust, fog, physical shock, vibration, radiation, etc. If their optical surfaces are damaged because of these conditions, their repair usually is not possible. Scratches, cracks, stains, roughness and corrosion occurs due to the physical and chemical factors thus generally these usually very expensive optical surfaces are removed and replaced with new pieces. These are also financially negative factors. Therefore, it is necessary to develop a special coating for these surfaces. In addition, these optical surfaces should be protected against all corrosive vapors (jet fuel, diesel, gasoline etc.) and liquid spills.

The main goal of this study is to produce self-cleaning and super-hydrophobic polymeric or hybrid thin films for protection of optical surfaces of EO systems from physical and chemical elements without any measurable decrease in optical performance.

1.2. Optical Coating Technology and Applications

Nowadays, the complexity of the optical systems are increasing quickly therefore it has become even more important to protect these systems from elements and to make them more durable. As a result, surfaces of the optical components used in many areas are now coated with thin films and the optical properties of the components can be modified with use of inorganic coatings.

Optical technology is continuously evolving hence it is needed to develop available coating techniques or find novel and distinct ones to keep up with the new application requirements. In addition, the film material selection is also significant because the film materials that are coated to the surface of the optical components with the different techniques should have to provide sufficient environmental and mechanical protection. Materials used in the optical systems such as transparent materials which have

appropriate refractive indices and also high reflective opaque materials were limited in terms of diversity in the past.

However, with the advancements in materials science and optical coating technology a variety of materials have found use in distinct wavelength regions according to the operating conditions of the optical systems. In the next section, the types of the optical materials and their properties will be discussed.

1.2.1. Optical Materials and Their Properties

Various optical materials have evolved depending on the different application areas and operating conditions of the optical systems. Therefore, many sort of materials having a lot diverse optical properties came up and continues to emerge.

Optical property of a material can be defined as response of materials or their interactions taken place when they are exposed to the electromagnetic radiation, especially to visible light.

Electromagnetic radiation that travels as wave at speed of light consists of two reciprocally orthogonal electric and magnetic fields and they are also perpendicular to the propagation direction (Stuart 2004). The following figure shows the electromagnetic wave that have the electric and magnetic field and in this figure electric and magnetic field vectors are demonstrated with E and B respectively.

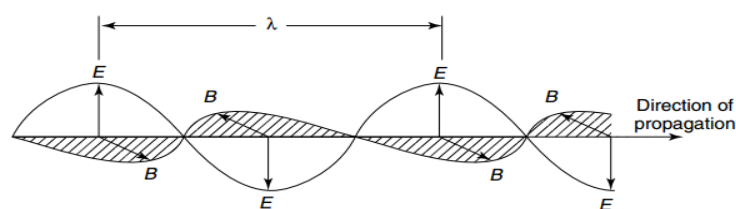


Figure 1.1. An electromagnetic wave having electric field E, magnetic field B and the wavelength λ (Source: Stuart 2004).

There are many forms of electromagnetic radiation and the range of all these forms is called as the electromagnetic spectrum. This spectrum contains different regions in order of increasing frequency, from lowest to highest energy, and decreasing wavelength, from longest to shortest wavelength, as radio waves, microwaves, infrared radiation, visible light, ultraviolet (UV) radiation, X-rays and γ -rays.

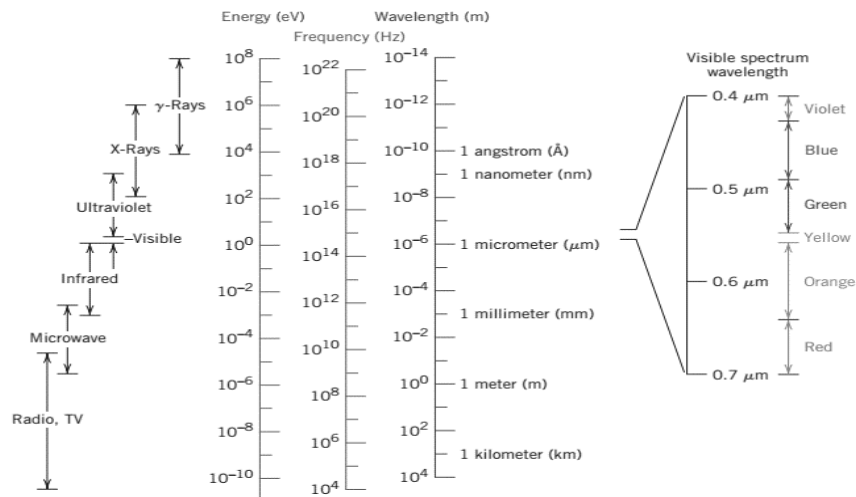


Figure 1.2. Regions of electromagnetic spectrum
(Source: Callister 2007).

The visible lights located in a small region of the electromagnetic spectrum which comes about the wavelengths range between $0.4 \mu\text{m}$ and $0.7 \mu\text{m}$. Moreover, certain colors appear at certain wavelength ranges in the visible region and these were shown in the table below.

Table 1.2. The wavelength ranges for the primary color of the visible region
(Source: Andrews 2009).

Color	Wavelength (nm)
Red	780-625
Orange	625-590
Yellow	590-565
Green	565-500
Blue	500-435
Violet	435-380

Furthermore, infrared region lies between the visible and microwave regions in the electromagnetic spectrum and it can be separated into three regions as near, middle and far infrared (IR). The near infrared region falls into the wavelength between approximately $0.78\text{-}3 \mu\text{m}$, also the mid and far IR regions are located in the range of wavelength as $3\text{-}30 \mu\text{m}$ and $30\text{-}300 \mu\text{m}$, respectively (Stuart 2004).

1.2.1.1. Light Interactions with Materials

Light is formed from the particles that are defined as photons and when the light interacts with the material, few phenomena may take place such as refraction, reflection, absorption and transmission. After the interaction of the light with the materials such as progressing from one medium to another, it may move to distinct directions. This can be explained as the light may be transmitted through the sample, it will be reflected from the surface of the sample or absorbed at the surface (Stenzel 2006).

Refraction:

When the light is transmitted into the material and enters the medium where the velocity of light is different, bending of the light ray occurs and this case is called as the refraction. In this phenomenon, light ray is bent close to the normal to boundary between two media if light passes from the fast to the slow medium. Besides, bend percentage alters with the index of refraction of the medium (Callister 2007). The index of refraction, n , can be defined as the velocity of light in vacuum, c , divided by its velocity in the medium, v like the following equation.

$$n = \frac{c}{v} \quad (1.1)$$

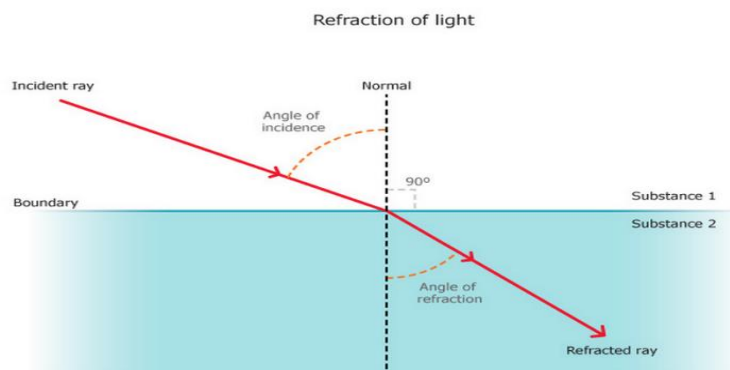


Figure 1.3. Refraction of light
(Source: Web-1 2012).

In addition to the equation 1.1, if the incidence angle is taken as θ_i and the angle of refraction is θ_r , index of refraction, n , of the medium can be found from the equation 1.2 as;

$$n = \frac{\sin\theta_i}{\sin\theta_r} \quad (1.2)$$

In this equation, the incident light come from the vacuum or air which has the small index of refraction. Moreover, there is a relationship between the incidence and refraction angles and the refractive indices of two media, this is called as the Snell's law which is the law of refraction (Driggers, Cox et al. 1999). Snell's law is expressed as the following equation;

$$n_1 \sin\theta_i = n_2 \sin\theta_r \quad (1.3)$$

In the equation above, n_1 is the refractive index of medium 1, n_2 is the refractive index of medium 2, θ_i is the incidence angle and also θ_r is the refractive angle.

Reflection:

When the light ray passes from one medium to another that both have different refractive indices and the transparent surfaces, it strikes the interface between these media and splits into two components. One of them is the reflected ray which leaves from the interface of two media and the other one is the transmitted ray continued to pass into the second medium (Driggers, Cox et al. 1999, Callister 2007). The reflectivity, R , is directly proportional to the intensity of reflected light, I_r , while inversely proportional to the incident light, I_i ;

$$R = \frac{I_r}{I_i} \quad (1.4)$$

When the light ray hits to the interface of these media, normal line which is the perpendicular to the interface plane divides the angle that is between the incident and the reflected rays to two equal angles. One of these formed angles is referred to as incidence

angle because it is placed between the incident light and the normal line, and the other angle is called as the reflection angle and it is located between the normal line and the reflected ray. This case is called as the law of reflection because this law states that the angle of incidence and reflection equals to each other when a light ray reflects from interface of two media (Driggers, Cox et al. 1999).

Absorption:

Absorption is especially a quantum process and in this process transferring of the energy of incident photon to an electron of absorbing molecule or atom takes place. Therefore, electron is excited and is removed from its lowest energy state (ground level) to the highest energy state (excited state) and energy rising leads to temperature change. For this situation, the energy of the incident photon, E_{photon} must be greater than the energy gap E_g and if this condition is satisfied, absorption occurs (Driggers, Cox et al. 1999). Additionally, in order to absorb the energy of photon by the molecule, it should be at the desired wavelength, otherwise absorption does not happen appropriately. For instance, the absorption cannot actualize at visible wavelengths for some molecules whereas it can eventuate at the infrared (IR) wavelengths (Driggers, Cox et al. 1999, Callister 2007). The following figure shows the schematic representation of the absorption mechanism.

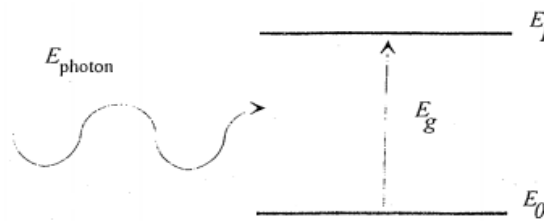


Figure 1.4. Absorption mechanism of a photon
(Source: Driggers, Cox et al. 1999).

Besides, absorption increases with increasing of the intensity of the absorbed ray and decreases with the incident ray as;

$$A = \frac{I_a}{I_i} \tag{1.5}$$

Transmission:

Transmission is realized when the incident light, which is not reflected or absorbed, passes through the material. There are three types of this process as direct, diffuse and selective. In the direct transmission, incident light goes through the material without any direction change. Besides, diffuse transmission occurs when the incident light pass through the material and light is not only move in one direction, is also dispersed in distinct directions. In addition to these processes, selective transmission takes place when the light progresses through a colored transparent material. In this process, some of the incident light are absorbed by the material and some parts transmitted according to the colors at certain wavelengths (Web-2 , Callister 2007).

Furthermore, transmittance is directly related with the intensity of transmitted light, I_t , whereas there is an inverse ratio between transmittance and the incident light, I_i as;

$$T = \frac{I_t}{I_i} \quad (1.6)$$

The intensity of the incident light, I_i , ray equals to the sum of the intensities of the reflected, absorbed and transmitted lights as;

$$I_i = I_r + I_a + I_t \quad (1.7)$$

Besides of this equation, the sum of the reflectivity, R , absorptivity, A , and transmittance, T , should be equal to the unity because all the incident light that impinges to the surface of the material reflected, transmitted or absorbed (Callister 2007).

Fresnel's Equations:

The transmission and reflection coefficients of the electromagnetic wave at surfaces and interfaces can be identified by using the Fresnel's equations. When the incident light comes through the surface of the material and enters the interface of distinct media, two different polarization components occur from field incident at the interface as "p" and "s" polarizations. P-polarization can be defined as the electric field component

parallel to the plane of incidence while s-polarization is the component that is perpendicular to this plane (Stenzel 2006, Lvovsky 2013). These polarizations were shown clearly in the following figure.

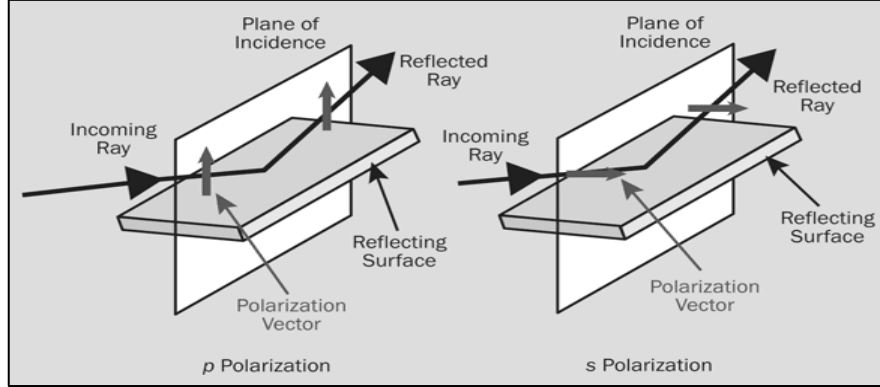


Figure 1.5. The electric field components; p-polarization and s-polarization (Source: Turner and Kirschner).

The transmission and reflection coefficients of electromagnetic waves according to the p and s polarizations are expressed by using equations from (1.8) to (1.11) as;

$$r_p = \frac{n_2 \cos \theta_1 - n_1 \cos \theta_2}{n_2 \cos \theta_1 + n_1 \cos \theta_2} \quad (1.8)$$

$$t_p = \frac{2 n_1 \cos \theta_1}{n_2 \cos \theta_1 + n_1 \cos \theta_2} \quad (1.9)$$

$$r_s = \frac{n_1 \cos \theta_1 - n_2 \cos \theta_2}{n_1 \cos \theta_1 + n_2 \cos \theta_2} \quad (1.10)$$

$$t_s = \frac{2 n_1 \cos \theta_1}{n_1 \cos \theta_1 + n_2 \cos \theta_2} \quad (1.11)$$

In these formulas, r is reflection and t is the transmission coefficients, n_1 is the refractive index of medium 1 and n_2 is the refractive index of medium 2 and also θ_1 and θ_2 are the angles of reflected and transmitted waves, respectively. These coefficients are not intensity fractions, they are amplitude fractions. In order to find the intensity relation, these coefficients must be squared as such:

$$\begin{aligned}
R_p &= |r_p|^2 & , & & T_p &= |t_p|^2 \\
R_s &= |r_s|^2 & , & & T_s &= |t_s|^2
\end{aligned}
\tag{1.12}$$

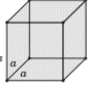
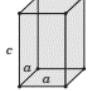
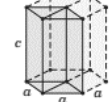
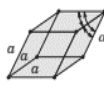
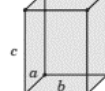
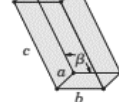
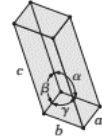
Interaction of light with optical materials and how optical properties of materials change in terms of these interactions have been explained above. The materials that have different optical features as a result of light interactions also have diverse electrical, thermal and mechanical properties. Therefore, these materials can be used suitably in distinct application areas of the electro-optical systems. The optical materials can be grouped under four main headings as crystalline materials, glasses, polymeric materials and metals. In the next sections, these materials and their physical, optical, mechanical and thermal properties will be explained.

1.2.1.2. Crystalline Materials

The optical crystalline materials are usually employed at the wavelengths from 100nm to 100 μ m in the electromagnetic spectrum and they are mostly transparent from the ultraviolet (UV) to infrared region despite of seeming as opaque in only small parts of this range. The optical crystals can be divided into two main groups as isotropic and anisotropic crystals (Weber 2002).

In isotropic crystals, light exhibits the same behavior regardless of its movement direction in the medium thus their properties do not alter in any directions. However, in anisotropic crystals, light ray acts distinctly different in different directions through the medium since material properties depend on geometries of crystals (Weber 2002). Besides, the anisotropic crystals can be classified as uniaxial and biaxial crystals. The uniaxial crystals, which possess only one optic axis, contain three different crystal geometries as tetragonal, hexagonal and trigonal. In addition to this, there are two specific refractive indices as ω and ϵ . Moreover, the biaxial crystals are called with this name due to having two optic axes and orthorhombic, monoclinic and triclinic crystal systems fall into biaxial category. Unlike the uniaxial crystals, this crystal type has three unique refractive indices according to the increasing value as α , β and γ , respectively (Web-3 , Weber 2002).

Table 1.3. Crystal Systems
(Source: Callister 2007).

	Isotropic Crystals	Anisotropic Crystals					
		Uniaxial			Biaxial		
Crystal System	Cubic	Tetragonal	Hexagonal	Trigonal	Orthorhombic	Monoclinic	Triclinic
Unit Cell Geometry							

If the optical implementation areas are examined according to the crystal systems, it can be found that anisotropic crystals mostly utilized in optical wave plates and polarizers while the usage areas of the isotropic crystals are lenses and windows.

The general properties of most commonly used crystalline materials in the optical systems were tabulated and physical and optical properties were given in the Table 1.4 whereas mechanical and thermal properties were shown in the Table 1.5.

In the following table, density values were listed as physical property and the transmission range and refractive index values were denoted as optical properties of the crystalline materials.

Table 1.4. Physical and Optical Properties of Some Selected Crystalline Materials
(Source: Weber 2002).

Name	Formula	Crystal System	Density (g/cm ³)	Transmission Range (μm)	Refractive Index, n _d
Aluminum oxide (sapphire, alumina)	Al ₂ O ₃	Trigonal	3.98	0.19-5.2	1.7579 (ε) 1.7659 (ω)
Barium fluoride	BaF ₂	Cubic	4.83	0.14-13	1.4733
Calcium Carbonate (calcite)	CaCO ₃	Trigonal	2.715	0.2-5.5	1.486 (ε) 1.658 (ω)
Calcium Fluoride	CaF ₂	Cubic	3.180	0.12-10	1.433
Germanium	Ge	Cubic	5.35	1.8-15	4.052 (2.8 μm)
Lithium Fluoride	LiF	Cubic	2.635	0.12-6.6	1.3912

(Cont. on next page)

Table 1.4. (Cont.)

Name	Formula	Crystal System	Density (g/cm ³)	Transmission Range (μm)	Refractive Index, n _d
Lithium Niobate	LiNbO ₃	Trigonal	4.644	0.35-5.0	2.156 (ε) 2.232 (ω)
Magnesium Fluoride	MgF ₂	Tetragonal	3.18	0.13-7.7	1.3886 (ε) 1.3768 (ω)
Silicon	Si	Cubic	2.33	1.1-6.5	3.4777 (1.55 μm)
Silicon Dioxide (α-quartz)	SiO ₂	Trigonal	2.65	0.16-4.0	1.56 (ε) 1.55 (ω)
Zinc Selenide	ZnSe	Cubic	5.42	0.5-20	2.5907

In the Table 1.5 below, young's modulus, poisson's ratio and knoop hardness values were given as mechanical properties and also thermal properties contain melting point, heat capacity, thermal expansion and thermal conductivity.

Young's modulus is one of the elastic moduli types and it can be expressed clearly as the rigidity of a material. Poisson's ratio can be identified as the minus sign of division of the lateral to lengthwise strain when a longitudinal stress applied to the material. Additionally, knoop hardness is a stiffness measurement of a material and in this measurement a diamond indenter is used to create notch on the surface of the material, then produced indentation is measured. The materials can be classified as the smooth materials if the knoop hardness value is smaller than 100 kg/mm², and can be termed as tough materials when the value is larger than the 750 kg/mm² (Bass, DeCusatis et al. 2009).

Table 1.5. Mechanical and Thermal Properties of Some Selected Crystalline Materials (Source: Weber 2002, Bass, DeCusatis et al. 2009).

Name	Formula	Young's Modulus (GPa)	Poisson's Ratio	Knoop Hardness (kg/mm ²)	Melting Point (K)
Aluminum oxide (sapphire, alumina)	Al ₂ O ₃	400	0.23	2250	2319
Barium fluoride	BaF ₂	65.8	0.31	78	1150
Calcium Carbonate (calcite)	CaCO ₃	83	0.31	100	323p 1610
Calcium Fluoride	CaF ₂	110	0.29	170	1424p 1630
Germanium	Ge	132	0.20	850	1211

(Cont. on next page)

Table 1.5. (Cont.)

Name	Formula	Young's Modulus (GPa)	Poisson's Ratio	Knoop Hardness (kg/mm ²)	Melting Point (K)
Lithium Fluoride	LiF	110	0.22	115	1115
Lithium Niobate	LiNbO ₃	170	0.25	630	1523
Magnesium Fluoride	MgF ₂	137	0.26	500	1536
Silicon	Si	162	0.22	1150	1680
Silicon Dioxide (α -quartz)	SiO ₂	95	0.08	740	845p
Zinc Selenide	ZnSe	75.4	0.30	115	1790

p-phase change

Table 1.5. (Cont.) Mechanical and Thermal Properties of Some Selected Crystalline Materials (Source: Weber 2002, Bass, DeCusatis et al. 2009).

Name	Formula	Heat Capacity (J/gK)	Thermal Expansion (10 ⁻⁶ K ⁻¹)	Thermal Conductivity (W/mK) @ 300K
Aluminum oxide (sapphire, alumina)	Al ₂ O ₃	0.777	6.65 to a axis 7.15 to c axis	46
Barium fluoride	BaF ₂	0.4474	18.4	12
Calcium Carbonate (calcite)	CaCO ₃	0.8820	-3.7 to a axis 25.1 to c axis	4.5 to a axis 5.4 to c axis
Calcium Fluoride	CaF ₂	0.9113	18.9	9.7
Germanium	Ge	0.3230	5.7	59.9
Lithium Fluoride	LiF	1.62	34.4	14
Lithium Niobate	LiNbO ₃	0.63	14.8 to a axis 4.1 to c axis	5.6
Magnesium Fluoride	MgF ₂	1.0236	9.4 to a axis 13.6 to c axis	30 to a axis 21 to c axis
Silicon	Si	0.7139	2.62	140
Silicon Dioxide (α -quartz)	SiO ₂	0.7400	12.38 to a axis 6.88 to c axis	6.2 to a axis 10.4 to c axis
Zinc Selenide	ZnSe	0.339	7.1	13

1.2.1.3. Optical Glass Materials

The refractive index and dispersion properties are very significant for identifying the optical glasses and also in making a group or classification of these materials, their

components, which constitute them, play substantial roles. The refractive index that was explained in detail in the refraction part of the light interactions with materials section of this study can be described briefly as a bending measure of a light. It occurs when a light ray goes from one medium to another where is the velocity of light different. Moreover, dispersion property can be expressed with the abbe number, v_d , and it is identified as dispersion measure of a light (Weber 2002). Abbe number can be found by using the following equation;

$$v_d = \frac{n_d - 1}{n_F - n_C} \quad (1.13)$$

In this equation, n_d , n_F and n_C are the refractive indices at the specific wavelengths of the Fraunhofer's lines which are the absorption lines seen in the spectrum owing to the absorption of the light ray. Besides, the letter d, F and C represent the d-, F- and C-spectral lines at wavelengths of 589.3, 486.1 and 656.3 nm, respectively (Weber 2002).

There are many types of the optical glasses and they are usually encoded for universal identification. The glass materials receive the crown (K) name if their refractive index and abbe numbers are larger than 1.60 and 50, respectively, or refractive index value is smaller than 1.60 but abbe number value is greater than 55. On the other hand, flint (F) name is given to the glass materials if they have high refractive index (range from 1.45 to 2.00) and low abbe number values ($v_d < 55$). Additionally, different abbreviations are applied to the names of the components formed the glass materials by the manufacturers of them such as Hoya Glass Works Ltd, Schott Optical Glass Inc., Ohara Optical Glass Inc. etc. For instance, borosilicate Crown glass is encoded as "BSC" by Hoya, "BK" by Schott and "BSL" by Ohara Inc (Weber 2002, Bass, DeCusatis et al. 2009). Another encoding type is "mil spec" and in this type, the glass materials are identified with the six digit number. The first three digit of the number demonstrates the refractive index value of related material and the other three digit displays the abbe number of the material. For example, refractive index and the abbe number of borosilicate crown glass are 1.517 and 64.17, respectively. When this glass type is encoded according to the mil spec, in the refractive index value the next three digits after the number "1" is taken and in the abbe number value, decimal point is ignored. Therefore, the coding for borosilicate crown glass is made as 517-642 (Weber 2002).

The following tables shows the optical, thermal and mechanical properties of the common glass materials used in the optical systems. In Table 1.6, encoding types and densities of the glass materials are given, optical and mechanical properties are shown in Table 1.7 and also thermal properties of the materials are displayed in Table 1.8.

Table 1.6. Encoding Types and Densities of Some Selected Glasses
(Source: Weber 2002, Bass, DeCusatis et al. 2009).

Glass Type	Encoding Types			
	Schott Type	Ohara Type	Hoya Type	Corning Type
Borosilicate Crown	N-BK 7 (517-642) $\rho=2.51$	S-BSL7 (516-614) $\rho=2.52$	BSC7 (517-642) $\rho=2.52$	B16-64
Fluoro Crown	N-FK 5 (487-704) $\rho=2.45$	S-FSL5 (487-702) $\rho=2.46$	FC5 (487-704) $\rho=2.45$	A87-70
Phosphate Crown	N-PK52A (497-816) $\rho=3.70$	S-FPL51 (497-816) $\rho=3.62$	FCD1 (497-816) $\rho=3.70$	-
Barium Crown	N-BaK4 (569-560) $\rho=3.05$	S-BAL14 (569-563) $\rho=2.89$	BAC4 (569-560) $\rho=2.85$	B69-56
Crown	N-K5 (522-595) $\rho=2.59$	S-NSL5 (522-598) $\rho=2.49$	-	B23-59
Fluoro Flint	TiF1 (511-510) $\rho=2.48$	S-FTM16 (593-353) $\rho=2.64$	FF5 (593-354) $\rho=2.64$	-
Barium Flint	N-BaF10 (670-471) $\rho=3.75$	S-BAH10 (670-473) $\rho=3.48$	BAF10 (670-472) $\rho=3.61$	-
Flint	N-F2 (620-364) $\rho=2.65$	S-TIM1 (626-357) $\rho=2.71$	E-F2 (620-363) $\rho=2.67$	C20-36
Antimony Flint	KzFN1 (551-496) $\rho=2.71$	-	SbF1 (551-495) $\rho=2.72$	-

Density, ρ (g/cm³) @ 25°C

(Cont. on next page)

Table 1.6. (Cont.)

Unique Glasses				
Fused Silica (UV)	Lithosil-Q (458-678) $\rho=2.20$	-	-	-
Pyrex	-	-	-	(474-660) $\rho=2.23$
CORTRAN 9754	-	-	-	(660-465) $\rho=3.581$

Density, ρ (g/cm³) @ 25°C

Table 1.7. Optical and Mechanical Properties of Some Selected Glasses
(Source: Weber 2002, Bass, DeCusatis et al. 2009).

Glass Type	Refractive Index, n_d	Abbe Number, v_d	Young's Modulus (GPa)	Poisson's Ratio	Knoop Hardness (kg/mm ²)
BK 7	1.517	64.17	81	0.206	610
FK 5	1.487	70.41	62	0.232	520
PK52A	1.497	81.60	71	0.298	355
BaK 4	1.569	56.0	77	0.24	550
K 5	1.522	59.48	71	0.224	530
TiF1	1.511	51.01	58	0.263	440
BaF10	1.670	47.11	89	0.271	620
F 2	1.620	36.37	82	0.228	600
KzFN1	1.551	49.64	60	0.276	500
Fused Silica (UV)	1.458	67.70	72.6	0.164	635
Pyrex	1.474	66.0	62.8	0.200	418
CORTRAN 9754	1.660	46.5	84.1	0.290	560

Table 1.8. Thermal Properties of Some Selected Glasses
(Source: Weber 2002, Bass, DeCusatis et al. 2009).

Glass Type	Heat Capacity (J/gK)	Thermal Expansion (10^{-6} K^{-1})	Thermal Conductivity (W/mK) @ 300K
BK 7	0.858	7.1	1.114
FK 5	0.808	9.2	0.925
PK52A	0.67	13.01	0.73
BaK 4	0.680	6.99	0.88
K 5	0.783	8.2	0.95
TiF1	0.842	10.3	0.773
BaF10	0.56	6.18	0.78
F 2	0.81	7.84	1.05
KzFN1	-	7.5	-
Fused Silica (UV)	0.746	0.51	1.38
Pyrex	1.05	3.25	1.13
CORTRAN 9754	0.54	6.2	0.81

1.2.1.4. Polymeric Materials

The glass materials possess very significant optical properties and are used efficiently in the optical systems. In addition to glasses some plastic materials are also utilized suitably in these systems. Although they show some shortcomings in terms of the main features compared with glass like having low refractive indices, they may have better features than many other glass properties (Bass, DeCusatis et al. 2009). For instances, plastic materials are much lighter than the optical glass materials and this property makes them more valuable in the applications which the weight is a significant parameter. Besides, the impact resistance is much better for plastic materials than the glasses that have more fragile structures and this property is required particularly in the military applications and is also desired in many other EO systems. Moreover, physical properties of the plastic materials make them much versatile for the optical and mechanical design requirements because they have advantages in terms of improvement or reconstruction of the optical components or the systems that are not easy and unlikely with glass materials (Bass, DeCusatis et al. 2009).

The plastic materials can be categorized into two main groups as thermosets and thermoplastics. In thermoset plastics, phase change takes place from liquid to solid form permanently as a result of a chemical reaction. After this reaction, they don't melt or are recycled again because they remain in solid state form. Also, they are more durable than the thermoplastics and resistant to high temperatures and solvents thus they are used in the electronic chips, eyewear lenses and also polymeric coatings. On the other hand, the thermoplastics can be recycled and remolded easily although they have final solid shape after the curing process. They possess chemical and high impact resistant and are generally used in the military optics, electrical and thermal insulation applications. While the thermosets include the epoxy resins, unsaturated polyesters, phenolic and amino resins, thermoplastics contain the nylons, polypropylene (PP), polyethylene (PE), polystyrene (PS), polysulfone (PSU), polyvinyl chloride (PVC), polytetrafluoroethylene (PTFE, Teflon) etc. (Bass, DeCusatis et al. 2009, Schaub 2009).

The following tables show the physical, optical, thermal and mechanical properties of the common optical plastics.

Table 1.9. The Physical, Optical and Thermal Properties of Some Optical Polymers
(Source: Weber 2002, Bass, DeCusatis et al. 2009, Wypych 2011).

Name	Density (g/cm ³)	Refractive Index, n _d	Abbe Number v _d	Thermal Expansion (10 ⁻⁵ K ⁻¹)	Thermal Conductivity (W/mK) @ 300K	Typical Solvents
Polymethyl methacrylate (PMMA)	1.18	1.491	57.4	3.6–6.5	0.16–0.24	<ul style="list-style-type: none"> • Ethanol • Isopropanol • Formic acid • Methyl ethyl ketone
Polystyrene (PS)	1.05	1.589	31	6.0–8.0	0.10–0.13	<ul style="list-style-type: none"> • Chloroform • Ethyl acetate • Tetrahydrofuran (THF)
Polyetherimide (PEI)	1.27	1.658	-	1-5.6	0.17-0.26	<ul style="list-style-type: none"> • Dichloro methane • N-methyl pyrrolidone
Polysulfone (PSU)	1.24	1.651	-	2.5	0.11	<ul style="list-style-type: none"> • N-methyl pyrrolidone • Trichloro ethylene • Dimethyl formamide (DMF)
Polytetrafluoroethylene (PTFE)	1.80	1.32	92	11-22	0.234-0.25	<ul style="list-style-type: none"> • Perfluoro kerosene @ 350°C

(Cont. on next page)

Table 1.9. (Cont.)

Name	Density (g/cm ³)	Refractive Index, n _d	Abbe Number v _d	Thermal Expansion (10 ⁻⁵ K ⁻¹)	Thermal Conductivity (W/mK) @ 300K	Typical Solvents
Polycarbonate (PC)	1.25	1.586	30	6.6–7.0	0.19	<ul style="list-style-type: none"> • Chloroform • Cresol • Methylene chloride • Benzene (hot) • Aniline (hot)
Polyamide (Nylon)	1.185	1.588	-	8.2	0.2–0.23	<ul style="list-style-type: none"> • Acetic acid • Chlorophenol • M-cresol • Formic acid • Sulfuric acid • Phosphoric acid • Formic acid
Poly(4-methylpentene-1) (TPX)	0.833	1.463	56.3	11.7	0.16	<ul style="list-style-type: none"> • Cyclohexane • Decalin • Tetralin • Xylene (above 100°C)
Polyurethane (PU)	1.20	1.64-1.65	-	18	0.13	DMF
Polystyrene-coacrylonitrile (SAN)	1.07	1.57	35.3	6.4–6.7	0.11	<ul style="list-style-type: none"> • Acetone • Acetophenone • Butyl acetate • Diethyl ether • THF

The tensile strength, young's modulus and impact strength were given in the table 1.10 as mechanical properties of the optical polymers.

The tensile strength is the material capability shown against the tensile force applied to the material. Also, impact strength can be defined as the resistance exhibited by the material against deformation or fracture which will occur as a result of an impact. Izod impact strength test is a plastic durability test. In this method, a notch is formed at the midpoint of a sample then this sample is placed facing the pendulum tip as vertically into the test equipment. After that, in order to hit to the sample, pendulum is released and the resistance of this sample against the impact is measured.

Table 1.10. The Mechanical Properties of Some Optical Polymers
(Source: Weber 2002, Wypych 2011).

Name	Tensile Strength, MPa	Young's Modulus GPa	Izod Impact Strength, notched, J/m @ 23°C
Polymethyl methacrylate (PMMA)	64.8-74.5	1.3	19
Polystyrene (PS)	34-82	3-3.5	12-20
Polyetherimide (PEI)	53-124	3	27-69
Polysulfone (PSU)	84	-	69
Polytetrafluoroethylene (PTFE)	20-35	-	188
Polycarbonate (PC)	55-88	2.39-2.6	12-736
Polyamide (Nylon)	74-106	0.235-0.337	-
Poly(4-methylpentene-1) (TPX)	16-33	1.9	267
Polyurethane (PU)	7.6-66	-	-
Polystyrene-coacrylonitrile (SAN)	61-79	0.022-0.171	-

1.2.1.5. Metals

Some selected metals, not all metals, can be used appropriately in different optical applications as optical thin films, substrate materials (mirrors) and structural elements. Metals are usually used in application where high reflectivity such as telescope mirrors, filters etc. However, due to oxidation problem, a thin protective inorganic coating is mostly necessary. The following tables display the physical, thermal and mechanical properties of these metals.

Table 1.11. The Physical and Mechanical Properties of Some Selected Metals
(Source: Weber 2002, Bass, DeCusatis et al. 2009).

Name	Symbol	Crystal Structure	Density (g/cm ³)	Young's Modulus GPa	Poisson's Ratio
Aluminum 5086-O 6061-T6	Al	Cubic	2.70	71.0 68.9	0.33
Copper	Cu	Cubic	8.96	129.8	0.343
Gold	Au	Cubic	19.3	78.5	0.42
Nickel	Ni	Cubic	8.9	199.5	0.312
Platinum	Pt	Cubic	21.5	170.0	0.39
Silver	Ag	Cubic	10.50	82.7	0.367
Tantalum	Ta	Cubic	16.4	185.7	0.342

Table 1.12. The Thermal Properties of Some Selected Metals
(Source: Weber 2002).

Name	Symbol	Melting Point (°C)	Heat Capacity (J/gK)	Thermal Expansion (10 ⁻⁶ K ⁻¹)	Thermal Conductivity (W/mK) @ 300K
Aluminum	Al	660.3	0.897	23.1	237
Copper	Cu	1084.6	0.385	16.5	401
Gold	Au	1064.3	0.129	14.2	317
Nickel	Ni	1455	0.444	13.4	90.7
Platinum	Pt	1768.4	0.133	8.8	71.6
Silver	Ag	961.8	0.235	18.9	429
Tantalum	Ta	3017	0.140	6.3	57.5

1.2.2. Optical Coating Techniques

The optical components used in the optical systems are composed of different materials and also they can be coated with thin films of the unique materials in order to

possess some specific features that might be required by the application and operating environment of the optical systems. Actually, these specific features are the reflection and transmission properties and they can be easily altered and improved to achieve desired conditions with the thin film coatings.

When the light ray goes from one medium to another which have distinct optical properties, especially different refractive indices, some of the light is transmitted whereas some of them is reflected. In the optical component designs, the percentages of the transmission and the reflection of light occupy the important positions one can run into undesirable cases due to lack of the transmitted or reflected lights.

For instance, lenses can cause some visual disorders such as ghost images that can be defined as forming two images instead of one and they occur with the reflection of light as a result of the failure to transmit the certain amount of light. In order to prevent such undesired events thin film coating designs must be performed carefully before fabrication. According to the implementation of the optical components such as optical transmitters, reflective optics etc., coating designs are changed. In the optical transmitters like lenses, it is required that the transmitting section of the light becomes 100 percent while the reflection part goes to zero. However, for reflective optics like the mirrors, 100% reflection it is desired.

There are different coating techniques to meet the desired conditions explained above as antireflection coating, high reflection coating and also coatings for partial reflectors and optical filters. In the next sections, these coating techniques will be described briefly.

1.2.2.1. Antireflection Coating

Antireflection (AR) coating is a commonly used coating type that is used to reduce the reflection of light and also improve the transmission. A phase change of 180° is used to eliminate light transmission losses in antireflection coatings of the thin films.

Light also behaves like wave, therefore it creates interference effects that can be described as the waves' interactions formed between them. This effect is very useful in design of optical devices. This interference can be divided into two distinct types as constructive and destructive interference. In constructive interference, when waves are progressed in phase and a peak of one wave coincides with the peak of the other wave at

the same point, the resultant wave which has a magnitude equal to the sum of the magnitude of individual waves. In destructive interference, wave interactions take place and the resultant wave magnitude is equal to the difference of the magnitudes of individual ones when a peak of a wave encounters with a pit of the other wave. The following figure shows the constructive and destructive interferences.

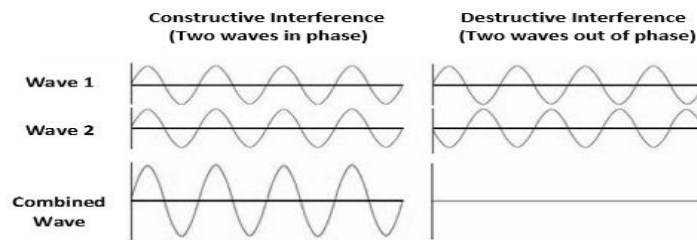


Figure 1.6. Constructive and destructive wave interference
(Source: Web-4).

In a single layer antireflection coating, to reduce the reflection of light completely, two interfaces should be formed by a thin film coating on the substrate (that can be glass, quartz etc.) because two reflected waves are created from these interfaces. When the light is reflected from the medium with higher refractive index, 180 degrees (π radians) phase change occurs but phase change does not occur when it reflects from the medium with smaller index. The film thickness that is formed by coating of the thin layer of a unique material is commonly designed to be quarter wavelength ($\lambda/4$). If the refractive index of the film is between 1 and 1.52 which are refractive indices of air and glass (minimum value), respectively, one reflection occurs from the interface between the air and film and the other reflection occurs from the interface between film and substrate (MacLeod 2001). In these conditions, these two reflections are 180 degrees out of phase and they eliminate each other by destructive interference. As a result, the intensity of the incident light completely equals to the transmitted light.

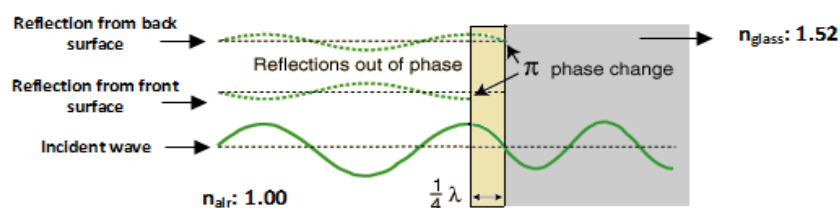


Figure 1.7. Schematic representation of a single layer antireflection coating
(Source: Web-5).

There is no unique material that has the refractive index needed to reduce reflectance to zero, in a single layer coating. This is a serious disadvantage of the single layer antireflection coatings and multilayer antireflection coating is needed. The multilayer coating efficiently eliminates the reflections over a wider range of the wavelengths while a single layer coating can reduce the reflection of light at only one wavelength. Besides, a wide variety of materials can be used appropriately in a multilayer antireflection coating to completely diminish light transmission losses. In multilayer antireflection coatings, quarter-quarter, quarter-half-quarter and broadband coating designs can be applied (Web-5).

1.2.2.2. High Reflection Coating

High reflection (HR) coating is needed for the applications that require high reflectance and also extremely low scattering and absorption properties like laser applications. Besides, in many optical systems, mirrors are used and they should have high reflectivity characteristics in order to increase the performance of these systems. High reflection coatings play an important role in maintaining the optical durability and reflectance property (MacLeod 2001). There are two types of high reflection coatings: dielectric and metallic coatings.

In a dielectric coating, multilayer film is formed with two different optical materials that have high and low refractive indices on the substrate material to produce extremely high reflection, nearly 100 percent. Dielectric mirrors are produced by using this coating technique and “*Bragg mirror*” is the most general design of the dielectric mirrors and in this mirror type each layer has a quarter wavelength thickness.

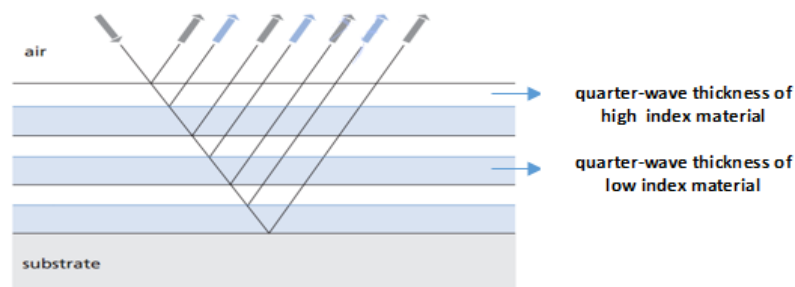


Figure 1.8. Multilayer film that has quarter wavelength thicknesses (Source: Web-6).

The following figure shows a typical reflection versus wavelength curve of the dielectric film stack.

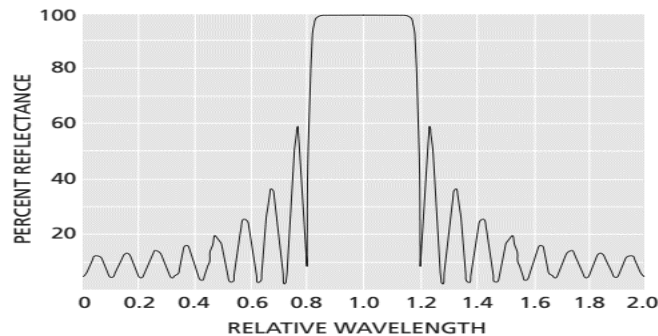


Figure 1.9. Reflectance curve of dielectric film stack
(Source: Web-6).

In this figure, the reflection has the maximum value at certain wavelength range and in this range the materials that have the high and low refractive indices possess the quarter wavelength ($\lambda/4$) thickness. Also, in the regions outside of high reflectance field, it is seen that reflection declines with oscillation towards to zero percent. The region in which high reflection is observed can be affected from the number of layer and the refractive index values of the optical materials. When the layer number of film stack and the differences between refractive indices of the layers increase, the height of the high reflection region increases also. Furthermore, width of the region increases with increasing of the ratio between high and low refractive indices of two materials.

Another type of high reflection coating is the metallic coating and it is applied by using the common metals such as aluminum, copper, gold, silver etc. also the reflection performance is not high as dielectric coating. However, its high reflection spectrum contains the region of near-ultraviolet, visible and near-infrared. This demonstrates that metallic coating is performed when the high reflection is required in wide spectral range (MacLeod 2001). Moreover, the high reflection requirements can be much more than that provided by metallic coatings in some applications therefore dielectric layers can be added to the film to increase the high reflection performance of the optical component.

1.2.2.3. Partial Reflectors

Beam splitters are known as partial reflectors which reflect the incident light ray not completely but partially and some parts of the light ray are transmitted. This type of optical component is generated with the metal coating on generally glass substrate and the metal selection is performed according to the reflection and transmission characteristics. Beam splitters have a plane surface and commonly their surface are inclined to realize the separating of the light ray into transmitted and reflected parts and percentages of them alter according to the application but generally beam splitters have equal percentage of transmission and reflection as 50/50 (T/R) (MacLeod 2001). Moreover, silver is common metal type used in the metal deposition process on the substrate.

1.2.2.4. Optical Filters

Optical filters are optical components that are designed to have selective transmissivity and rejection property against certain wavelengths or ranges of wavelengths. They are utilized in a variety of applications such as lasers systems, imaging, defense and sensing applications. There are distinct types of filters as bandpass filters, notch filters and edge filters. For all these filter types, single or multilayer film stacks that have quarter wavelength thickness and also antireflection coatings explained the previous sections can be applied according to the requirements by using suitable optical materials in terms of transmission and reflection properties (MacLeod 2001).

The bandpass filters transmit a certain range of wavelengths and reject all the others whereas the notch filters are design to reject a certain range of wavelengths and transmit all the others. In addition to these types, edge filters are defined as the filters that transmit the wavelengths which are over or beneath given values therefore they can be categorized as longwave pass and shortwave pass filters (MacLeod 2001). Also, hot and cold mirrors that are known as heat control filters are other types of edge filters. The hot mirror is formed by coating on the glass substrate, generally borosilicate glass, with multilayer dielectric coating technique and it has the unique property as reducing temperature of the light beam through the reflection of heat. The hot mirrors transmit approximately 85% of visible light, which is in the region between 420 and 700nm and

reflect nearly 95% of infrared (IR) radiation, range between 750-1100nm (Web-7 , Web-8). Moreover, the same coating technique is used for the cold mirrors like hot mirrors however the cold mirrors are designed to reflect the visible light as nearly 95% and transmit the 85% of infrared radiation. The hot and cold mirrors are commonly used in projection, illumination systems and scientific instruments (Web-7 , Web-8).

There are several types of coating production methods. In addition to application requirements, optical, mechanical and chemical properties, evaporation or condensation properties and also the cost of the materials are very significant points for selecting suitable coating method. In the next section, the coating production methods will be discussed clearly.

1.2.3. Thin Film Production Methods

Thin film optical coatings are fabricated using optical materials on desired substrates by using compatible methods. The material selection need to be done carefully for the thin film deposition methods because all optical materials have different properties thus they must comply with distinct operating conditions. For instance, the materials in the oxide class are used in the applications in the visible and near-infrared region while in the ultraviolet region, fluorides are used instead of oxides.

Although there are many types of the deposition processes for thin film coatings, generally they are operated under vacuum conditions thus they can be grouped into two main headings as physical vapor deposition (PVD) and chemical vapor deposition (CVD) (Träger 2012).

Physical Vapor Deposition (PVD):

In PVD processes, the main goal is the deposition of thin film coating by condensation of the desired material from the vapor phase. PVD also can be categorized into two diverse process types as thermal evaporation and energetic.

Thermal evaporation is a simple method to produce thin films. In this method, the desired thin film material is heated under vacuum and then evaporated material condenses on the substrate to form thin film coating. In energetic processes, extra energy is supplemented to the process to facilitate the movement of condensing particles that are

effective in thin film coating. Energetic processes include the most common methods as cathodic arc deposition, ion assisted deposition and sputter deposition.

In the cathodic arc deposition, vacuum conditions are supplied and low voltage and high current are applied to the system, then arc is created on the cathode surface. The temperature reaches quite high values at the points on the cathode surface where the arc forms, as a result of this, the desired materials are evaporated from the cathode and then highly ionized plasma composed of evaporated materials takes place and materials are deposited on the substrate under vacuum (Piegari and Flory 2013). The abrasion resistant and rigid coatings are produced with this method. Ion assisted deposition (IAD) is another PVD process and is also called as ion beam assisted deposition (IBAD). In this method, high vacuum conditions are provided like the cathodic arc deposition and desired coating material is evaporated by using an electron beam evaporator. After that, the coating molecules condense and cling to the substrate surface and at the same time ion beam bombardment which helps achieving desired density of the film (Träger 2012). The last method is the sputter deposition and in this method, the vacuum is supplied again in the system like the other energetic processes. The target material that is desired to be coated on the substrate forms the cathode while the substrate is located in the anode. The plasma is generated with gas ionization. Argon is common choice for gas. Ions strike to the surface of the target material and they remove atoms and molecules from there. This event is called as sputtering. Thereafter, ejected atoms and molecules from the target material condense and deposit on the substrate hence thin film coating is produced (Träger 2012, Piegari and Flory 2013).

Chemical Vapor Deposition (CVD):

CVD processes are similar to the PVD processes but the important difference is that chemical reaction takes place in CVD processes. The gaseous reactants called as precursors are carried into the reaction chamber under vacuum conditions, sometimes by using carrier gases, then deposition occurs on substrate and thin film coating is achieved (Piegari and Flory 2013). There are many types of CVD processes and diversity between them has evolved due to a variety of reaction activation techniques such as plasma enhanced, photo initiated and hot wire although there are other reasons such as reactor type and cost (Träger 2012). CVD is commonly utilized in thin and hard film coatings to ensure preservation of the coated product against external influences.

In the plasma enhanced chemical vapor deposition (PECVD), electrical energy is utilized instead of thermal energy used in general CVD process to provide the activation of the reaction (Pierson 1999). In this technique, plasma is created from the reactant gases via electrical energy and from that plasma a solid layer is formed on the desired substrate (Jones and Hitchman 2009). When it is compared with CVD, the significant point in this technique is that approximately 250-350°C is enough substrate temperature value to execute the deposition process whereas temperature is needed in common CVD process is nearly 800°C (Pierson 1999). Photo initiated chemical vapor deposition (PICVD) is another CVD technique and UV light is used to generate photo-initiators that trigger free radical polymerization reaction and heat is not needed to perform the deposition as in plasma enhanced CVD (Pierson 1999). More regular structured polymers are created by this technique compared to PECVD (Dorval Dion and Tavares 2013). Hot wire chemical vapor deposition (HWCVD) is a thermal CVD process in which reaction takes place by heat. In this technique, heat is supplied to the gas mixture for the decomposition of chemical by the hot wire then reaction is started and after a certain time, layer is formed on the substrate. The main disadvantage of this technique is that there is a restriction in polymeric materials deposition. Monomers that will be used in the HWCVD process might not be resistant to the heat and when they undergo to thermal conditions, some of them decompose (Dorval Dion and Tavares 2013).

In addition to these methods, there is also a coating technique that is very similar to CVD processes called as atomic layer deposition (ALD). The main difference between these two methods is that in CVD process, various precursors can be delivered to the reaction chamber at the same time to generate the coating film, on the other hand, in the ALD technique, the desired precursors are transported consecutively into the reactor under vacuum (Johnson, Hultqvist et al. 2014). Owing to carrying of the various precursors successively into the reactor, individual reactions occur by each precursor. The reaction takes place completely on the surface of the substrate by striking of the first precursor to the surface and only one atomic layer is produced. After that, the new monolayer is deposited on the layer which was formed previously and this process continues and can be cycled until the desired film is obtained. Besides, the important thing during the ALD process is that after forming monolayer by the precursor, purging operation is done by using the inert gas like nitrogen or argon in order to eliminate unwanted byproducts occurred in the reaction and this is maintained after every layer is created. Therefore, ALD is slow process but there are many significant advantages as

forming quietly uniform thin films, coating suitably three dimensional, very small like pinhole and also very large surfaces (Piegari and Flory 2013, Johnson, Hultqvist et al. 2014). The following figure demonstrates the ALD process schema.

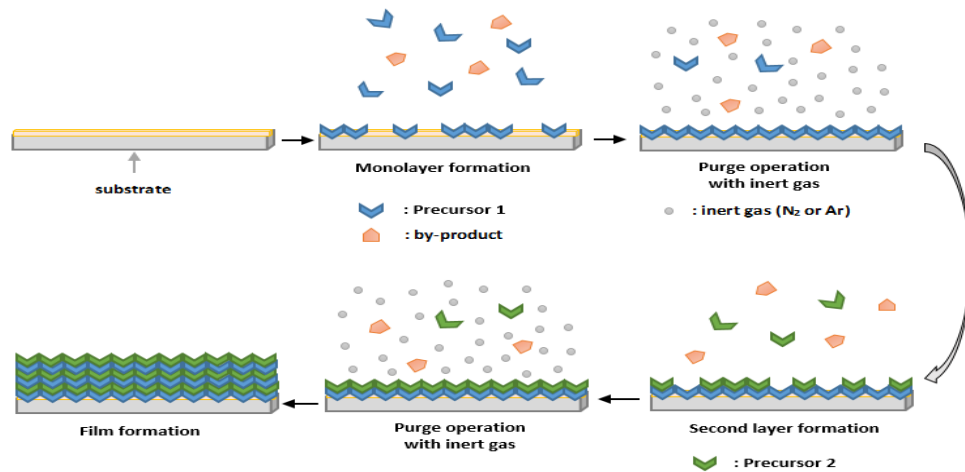


Figure 1.10. Atomic layer deposition (ALD) process steps.

Other Thin Film Coating Methods:

There are distinct optical thin film coating methods than PVD and CVD processes as sol-gel, dip-coating and spin coating processes. In sol-gel process, there is a colloidal solution which is known as “sol” and aggregation of the colloidal particles convert “sol” to the gel, then this gel is deposited on the desired surface (Träger 2012, Piegari and Flory 2013). Besides, in the dip-coating process, in order to form a layer, a substrate is immersed into a solution and after a certain time it is removed from there and formation of layer on the substrate surface is accomplished (Träger 2012). Moreover, spin-coating is another important process for the thin film coating. In this process, sufficient amount of solution is dropped onto the flat substrate surface and then it is rotated at high speed to spread of the solution so as to cover entire surface of the substrate (Träger 2012). In this spreading process, centrifugal force has very significant effect and the excess quantity of solution collected at the edge of the substrate as the result of the spreading is ejected with the influence of centrifugal force. Film thickness is affected from properties of the solution as viscosity and surface tension and parameters of spin process such as acceleration, rotation speed, drying time etc.

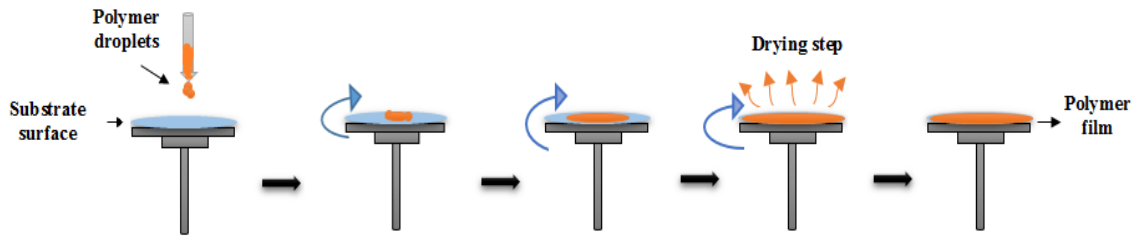


Figure 1.11. Schematic illustration of spin coating process.

In the methods explained briefly above, many inorganic or organic materials are used but particularly inorganic materials are widely utilized in the PVD processes for optical film coatings. The optical inorganic materials are quite expensive in terms of raw materials and they are processed with high precision. These cases lead to the higher production cost for the EO systems that include the optical components. Also, EO systems are especially used in defense and aerospace sectors thus they are exposed to severe operating conditions. Furthermore, in the optical surfaces made of inorganic materials, scratches, cracks and corrosion caused by physical and chemical factors occur easily. Because of all these reasons, protective coatings that will not adversely affect the optical performance are needed to preserve optical surfaces against the physical and chemical factors. Therefore, it was started to produce the polymeric thin films as these protective coatings for the purposes explained above.

Also, optical surfaces made from the optical materials rarely have a flat surface and they are usually produced different geometries as parabolic or hyperbolic to break, focus and sputter the electromagnetic waves which lie between certain waves. Therefore, the special thin film coating method is required to coat the polymeric films.

In this study, the initiated chemical vapor deposition (iCVD) method which is one of the CVD processes was used as the unique coating process of the polymeric thin films because it fully provides the required conditions through its important properties as low production cost, low temperature conditions, and especially three-dimensional geometry coating performance. In the next section, iCVD method will be explained clearly.

1.2.3.1. Initiated Chemical Vapor Deposition (iCVD)

In the previous section, it was mentioned about the requirements of the polymeric thin film coatings to protect the optical components used in the electro optical systems

against physical and chemical influences. The polymeric thin films are generally produced with polymerization reactions by using solvents in liquid phase, however, solvents can produce very unfavorable effects for the applications. For instance, they can disrupt the substrate materials and also they cannot be removed completely from the coatings at the end of the operations hence this may cause harmful effects (Bose, Lau et al. 2011).

Solventless CVD processes are suitable for coating of the optical components because optical surfaces generally have three dimensional shapes. Coatings of these surfaces are easily performed with the processes taken place in vapor phase like the CVD. Also the thicknesses of the polymeric films can be produced in nm and μm sizes by using this method (Parker, Baechle et al. 2011). However, in CVD processes, high temperature values are used to realize the deposition successfully. Actually, it is an undesirable case because at high temperatures the substrates and polymers can experience unwanted alterations and degradation. Therefore, a novel CVD technique has been evolved which is called as initiated chemical vapor deposition (iCVD) (Parker, Baechle et al. 2011) for deposition of polymeric thin films. The iCVD utilizes thermal energy instead of high electrical energy used in plasma enhanced CVD technique for initiation of the polymerization reaction thus it is similar to hot wire CVD (Chan, Kostun et al. 2006). On the other hand the main differences between the iCVD and hot wire CVD are that initiators are used in iCVD technique to create the radicals that play significant role in starting of the polymerization whereas monomer fragmentation occur in HWCVD for generation of the radicals and in these radical formations, filament temperature is lower in iCVD because the temperature range between 200-400°C (Lau and Gleason 2007) is adequate for the decomposition of the initiators while the higher temperature values (greater than 400°C) are needed to decompose the monomers (Coclite 2013). Therefore, iCVD process can be considered as the most suitable process that will be used in the thin film polymer coatings among the other CVD techniques in terms of using low energy and higher deposition rate.

The mechanism of the iCVD technique:

In iCVD technique, vacuum condition is ensured between 0.1 and 1 Torr in the reaction chamber then the initiator and monomer are introduced to the system. Monomer and initiator can be heated to provide enough vapor pressure, if necessary. Also a filament array is placed 2 or 3 cm above the substrate surface. (Coclite 2013). The monomer and

initiator are carried in the vapor phase into the reaction chamber and in order to bring about the thermal decomposition of the initiator, the filament is heated in the range between 200 and 400°C described above (Lau and Gleason 2006). While the initiator decompose in these temperature ranges, monomer fragmentation does not occur and it directly comes on the substrate surface without any changes in its functionalities (Coclite 2013). By thermal decomposition of the initiator on heated filament surface, free radicals are created in the gas phase. Then these radicals also come to the substrate surface and attack to the monomer units to create active monomers that are known as monomer radicals hence polymerization reaction is initiated. The backside cooling is performed generally less than 50°C to decrease the substrate temperature because this enhances the adsorption of the monomer units to the substrate surface (Lau and Gleason 2006, Lau and Gleason 2008).

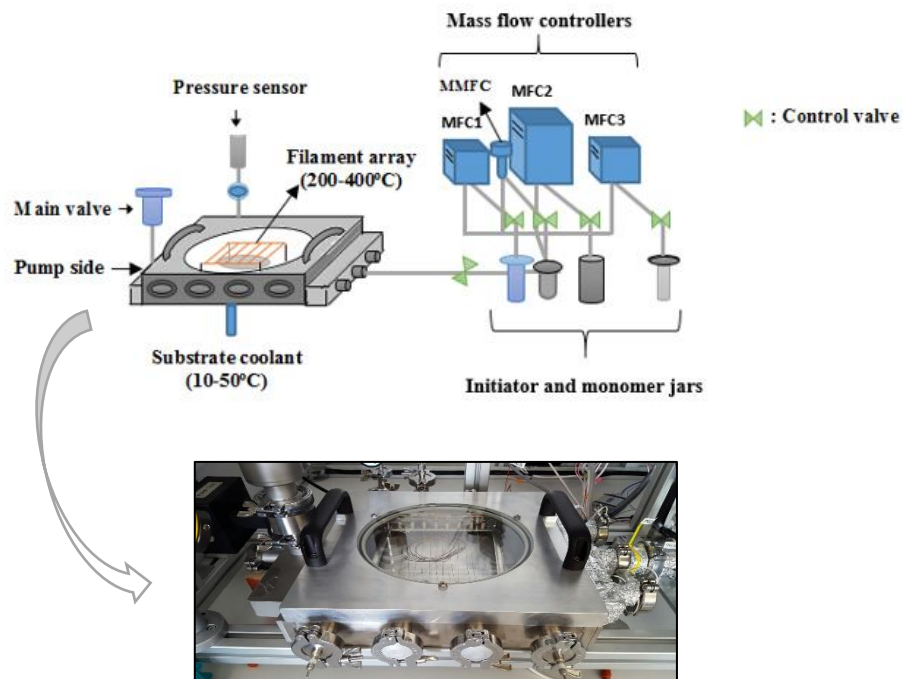


Figure 1.12. Initiated chemical vapor deposition (iCVD) system.

Free radical polymerization take place as polymerization reaction in the iCVD technique and in this reaction free radicals attack the monomer molecules to active them and active monomers carry unpaired electrons. After that, a monomer radical also attack the other monomer that does not possess an active site and unpaired electron is delivered to growing chain end thus the free radical polymerization is realized whereby addition of the radicals to the growing chain in each step (Allcock, Lampe et al. 2003). There are

three main steps as initiation, propagation and termination in the free radical polymerization.

Initiation: In this step, the reactive molecules that have the active sites are created (Allcock, Lampe et al. 2003). The initiation step of the iCVD polymerization includes the free radical formation from the initiator and also monomer activation. Free radicals are formed with the initiator decomposition in gas phase. After the adsorption of the free radicals and monomer molecules on the substrate surface, monomer radical formation occurs by free radicals but this process eventuates on the surface of the substrate not in the gas phase (Lau and Gleason 2006).

Propagation: Active monomer molecule attacks the other monomer unit that has not an active site and chain growth occurs. Active monomer transposes its unpaired electron to the end of the growing chain and transfer of this electron continues through chain growth process (Allcock, Lampe et al. 2003). This step is realized on the surface of the substrate in iCVD technique (Lau and Gleason 2006).

Termination: In termination step, polymerization immediately stops when the active site of the growing chain is eliminated and final product, that is polymer, is formed. If this reaction takes place between a free radical and growing chain radical, reaction called as primary radical termination. In addition to this, if there are two growing active chains exist in the reaction medium, termination can consist in two different ways as combination and disproportionation (Lau and Gleason 2006). In combination, growing chain radical is terminated with another one and only single molecule is formed at the end of the reaction. However, in the disproportionation, one of two growing chain radicals removes a hydrogen atom from its active site and transfers this atom to the other growing chain radical. Therefore, between the carbon atoms, double bond occurs due to losing of the hydrogen in the transfer molecule and at the end of the disproportionation reaction two distinct polymer molecules are created (Allcock, Lampe et al. 2003). Also, recombination of the radicals occurs if two free radicals collide with each other. All free radical polymerization steps take place on the surface of the substrate in iCVD except the initiator decomposition for producing the free radicals (Lau and Gleason 2006).

According to the explanations above the mechanism of the iCVD technique can be specified in four general steps (Lau and Gleason 2007):

- 1) Transport of the monomer and initiator into the reaction chamber (in vapor phase).
- 2) The decomposition of the initiator by heating filament (200-400°C) to form the free radicals (in vapor phase).

- 3) Adsorption of the monomer molecules and free radicals created in step 2 on the cooled substrate surface (vapor to surface process).
- 4) Free radical polymerization reaction that contains initiation, propagation and termination steps for producing the polymer thin film on the substrate (surface process).

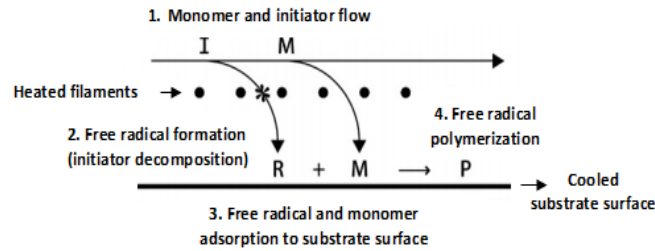


Figure 1.13. General mechanism of iCVD technique (Source: Lau and Gleason 2007).

The reaction mechanisms of the free radical polymerization for iCVD are given below respectively.

Vapor phase



Vapor to surface



Surface reactions

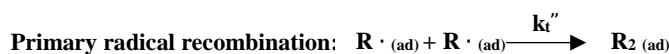
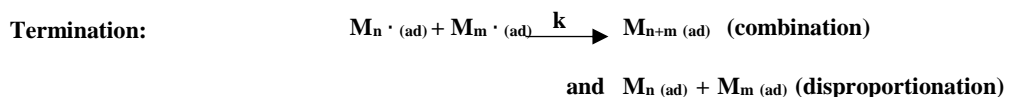


Figure 1.14. iCVD reaction mechanism, I: initiator, M: monomer, R: radical (Source: Lau and Gleason 2006).

In these reactions, k_d is rate constant for initiator decomposition, $k_{ad,R}$ and $k_{ad,M}$ are the adsorption rate constants for radical and monomer, respectively. Also, k_i , k_p , k_t , k_t' and k_t'' are the rate constants for initiation, propagation, termination, primary radical termination and radical recombination, respectively.

Some suitable assumptions should be made to derive the kinetic equations for the reactions that occur in different steps of the free radical polymerization.

i) The first assumption is the initiation rate, r_i , equals to the rate of initiator decomposition, r_d .

$$r_i = r_d = k_i [M][R \cdot] = 2fk_d[I] \quad (1.14)$$

In this reaction rate equation, initiating radicals' fraction is indicated as "f" (Allcock, Lampe et al. 2003) and from each initiator decomposition, two radicals are generated thus fraction is multiplied by 2 in the rate equation of the initiator decomposition. Besides, the termination rate can be expressed as the following relation;

$$r_t = 2k_t [M \cdot]^2 \quad (1.15)$$

The growing chain is terminated with the collision of two radicals hence the factor of 2 presents in the termination rate equation.

ii) The second assumption is the steady state approximation for the total radical concentration.

$$\frac{d[M \cdot]}{dt} = r_i - r_t = 0 \quad (1.16)$$

Equation (1.16) explained that there is no any effect of the reactions in propagating step on the total radical concentration because in this step radicals are created and destroyed consecutively (Allcock, Lampe et al. 2003). Therefore the rate of propagating radicals' initiation becomes equal to termination rate due to the steady state approximation. The total radical concentration is found from the following derivation;

$$\begin{aligned}
r_i &= r_t \\
2fk_d[I] &= 2k_t [M \cdot]^2 \\
[M \cdot] &= \left(\frac{fk_d[I]}{k_t} \right)^{1/2}
\end{aligned} \tag{1.17}$$

Additionally, the rate of polymerization, r_p , can be defined as the rate of depletion of the monomer concentration in accordance with time and this occurs in both initiation and propagation steps (Allcock, Lampe et al. 2003).

$$r_p = -\frac{d[M]}{dt} = k_i [M][R \cdot] + k_p [M][M \cdot] \tag{1.18}$$

iii) The last assumption is the lengths of the kinetic chain which can be expressed as the number of monomer units consumed per active center are too much. According to this assumption, it is observed that the number of monomer units depleted in the chain propagation step are very high when compared with the chain initiation step. Therefore, rate of polymerization becomes equal to the only rate of propagation (Allcock, Lampe et al. 2003).

$$r_p = -\frac{d[M]}{dt} = k_p [M][M \cdot] \tag{1.19}$$

The kinetic chain length, v , was defined above and it is calculated by dividing of rate of polymerization to initiation rate (Allcock, Lampe et al. 2003).

$$v = \frac{r_p}{r_i} = \frac{k_p [M][M \cdot]}{k_i [M][R \cdot]} \tag{1.20}$$

Furthermore, the number average molecular weight, M_n , is found by multiplying of the monomer molar mass, M_m , with average degree of polymerization, \overline{DP} .

The average degree of polymerization can be identified as the number average monomer molecule in a polymer. And after a certain derivations, the following equation was obtained and by using this equation \overline{DP} is calculated easily.

$$\overline{DP} = 2v \left(\frac{k_{tc} + k_{td}}{k_{tc} + 2k_{td}} \right) \quad (1.21)$$

In equation (1.22), k_{tc} and k_{td} are the rate constants for the termination by combination and disproportionation, respectively. Besides, if combination takes place mainly in the termination step in spite of disproportionation, \overline{DP} becomes equal to $2v$, in the opposite case, it equals to v .

Literature Survey for iCVD:

There are different types of polymeric materials produced by using iCVD for thin film coatings as acrylates, methacrylates, polytetrafluoroethylene (PTFE), styrenes, crosslinked polymers which are hydrogels and also copolymers (Bose, Lau et al. 2011). Additionally, these polymers have distinct properties, for examples, while some of them have superhydrophobic (Lau and Gleason 2007), superhydrophilic or antimicrobial (Martin, Lau et al. 2007) properties, the other ones possess low dielectric constants (Trujillo, Wu et al. 2010) or display some responsive features (Alf, Hatton et al. 2011) in terms of temperature or pH (Alf, Hatton et al. 2011, Coclite 2013). iCVD technique has a wide range of the application areas such as drug delivery, dielectric coatings, biosensors, and barrier coatings for protection of optical and electro optical systems owing to coating varies type of the polymers specified above.

In 2007, Martin and co-workers studied the polymeric antimicrobial coating, which prevents the growth of the *Escherichia coli* and *Bacillus subtilis* bacteria, on nylon fabric by iCVD technique and in this study dimethylaminomethylstyrene (DMAMS) was used as monomer due to having antimicrobial property. As initiator di-tert-amylperoxide (TAP) was utilized. iCVD method was preferred for coating the nylon fabric dyed with camouflage pattern that possesses porous structure because during coating process the clogging of pores and damaging dyed fabric by organic solvents were undesirable cases in this study. As the operating conditions, 331°C filament temperature, room temperature for substrate, 200 mTorr total pressure and 2.0 and 0.6 sccm monomer and initiator flow rates were used by the Martin and co-workers. According to the results of the tests, it was concluded that the coating was highly protective (99.99%) against gram negative *E. coli* and gram positive *B. subtilis* also there were no blockage in the pores and also any changes in color or feel of the fabric (Martin, Kooi et al. 2007).

Another study related with the biological field like the Martin and co-workers study was performed by Chan et al. as polymeric coating produced with iCVD for the application of antibiofouling surface. The hydrophilicity is very crucial property for the polymers that are used in the biomedical applications and polyvinylpyrrolidone (PVP) has this special feature also it is significant biocompatible polymer. In this study, Chan and co-workers were discussed that the PVP homopolymer and copolymer created with ethylene glycol diacrylate (EDGA) and vinylpyrrolidone (VP) coatings on silicon substrate were performed properly or not by using iCVD technique and observations were made regarding the functionality of the polymer. Also, effect of the VP flow rate was examined on the deposition rate. Tert-butyl peroxide (TBPO) was used as initiator in the operations. Results of this study indicated that there was a direct proportion between the deposition rate and partial pressure of monomer, also the hydrophilicity feature of PVP was conserved after coating with iCVD, in addition, copolymer coating performed efficiently with vapor flow control and supplied the property of swelling in water to the polymer (Chan, Kostun et al. 2006).

iCVD method is used not only for the flat or three dimensional shaped surfaces also it can be applied to particle substrates by producing encapsulating layers of polymers. There are many studies about polymeric coatings on particles and one of them was performed by Lau and Gleason. In their study, encapsulation layer around active particles, fluorescein in this study, was produced with copolymer that generated with the methacrylic acid (MAA) and ethyl acrylate (EA) and TBPO initiator by using iCVD method. Then, it was observed that copolymer coating that has property of swelling depending on pH ensured releasing of active materials in a controlled manner at certain pH values. While uncoated particles were released at pH of 1.2 and 6.8 in a short time, copolymer encapsulation did not allow releasing of fluorescein at pH 1.2 but facilitated fluorescein diffusion at pH 6.8 because of swelling (Lau and Gleason 2008).

Encapsulation of the particles by iCVD was performed also again Lau and Gleason in a different study. In this study encapsulation process was implemented for three different goals to create superhydrophobic surface, reactive surface and providing controlling drug release like the previous study. To generate the superhydrophobic surface that is important with regard to ensuring the self-cleaning feature, the carbon nanotubes arranged vertically were coated via polytetrafluoroethylene (PTFE) by using iCVD and as an initiator perfluorobutane-1-sulfonyl fluoride (PFBSF) was used. Water contact angle should be greater than 150° to for a superhydrophobic surface and water

contact angle was observed as approximately 170° by Lau and Gleason. Thus, it was concluded that carbon nanotubes coated with PTFE had the superhydrophobic property. Glycidyl methacrylate (GMA) was used as monomer for producing reactive coatings on glass microspheres and carbon nanotubes because PGMA showed the reactive feature owing to having epoxide ring. The reason for encapsulation of the particles was that providing the attachment of functional molecules to PGMA thus some properties altered. For instance, some aromatic molecules attached to the PGMA coating and thickness increased thus this caused to increase the refractive index of coating. And the last section of this study was the encapsulation process for the drug release. Ibuprofen was used as active particle and similar results with previous study were obtained as avoiding drug release at low pH value whereas allowing at higher pH value, that is, neutral pH (Lau and Gleason 2007).

Polymer coatings on the several material surfaces ensure possessing distinct properties to coated materials and this capability has led to evolve the smart coating idea for the materials. From the environment different stimuli reach to the materials and smart coatings responds as required. The most common ones are the pH and temperature responsive polymeric surfaces and these polymeric coatings produced by iCVD technique uniformly. For these coatings the unique polymers are used that have responsive property such as methacrylic acid (MAA) copolymers and polyhydroxyethyl methacrylate (PHEMA) hydrogels for pH responsive and polyN-isopropylacrylamide (pNIPAAm) for thermal responsive property (Coclite 2013). About the smart surfaces, Alf et al. investigated the creating thermal responsive surface of p(NIPAAm-co-DEGDVE) copolymer that generating the addition of diethylene glycol divinyl ether (DEGDVE) cross linker with (pNIPAAm) to the iCVD system. p(NIPAAm) has thermal responsive feature but copolymer was used in this study for providing durability against chain dissociation. 200°C and 50°C filament and substrate temperature were used respectively and TBPO was used as an initiator. Temperature responsivity was measured according to the low critical solution temperature (LCST). If the temperature is lower than the LCST that is 32°C for p(NIPAAm), polymer swells because of hydrophilicity and random coil shape occurs. However, when the temperature is higher than the LCST, globular shape forms. The shape changes depending on temperature stimuli were measured by using quartz crystal microbalance with dissipation (QCM-D) by Alf et al. According to the results, they concluded that the highly thermal responsive p(NIPAAm-co-DEGDVE)

copolymer coating created as uniformly with iCVD method and produced film could be used suitably in necessary applications (Alf, Hatton et al. 2011).

iCVD is an important CVD method preferred in the semiconductor industry except from the other application areas specified previously. Especially, in semiconductor industry, the integrated circuits undergo the changes continuously in terms of scaling of interconnect structures thus the interlayer dielectric (ILD) materials improved to meet the requirements. Besides, the low dielectric constant, k , ILD materials are developed because the materials having high k values cause occurring some undesired cases as high power consumption, forming cross talk, high delay time of signal distribution and increasing heat spread. There are many applications to overcome these problems with creating new low k materials and one of them was studied by the Trujillo and co-workers. In this study, polymer that have low k value was coated by using iCVD method. Among the aims of this study, using environmentally friendly process was one of the most important goal. PECVD was used in previous studies but the high energy consumption take place during the process therefore Trujillo et al. preferred to study with iCVD method which uses low energy and also with iCVD the film composition is adjusted appropriately. 1, 3, 5, 7-tetravinyltetramethylcyclotetrasiloxane (V4D4) was used as monomer because of similar structure presents in the V4D4 monomer with common low k monomer used in PECVD method. The results indicated that the mechanical properties of the film produced with p(V4D4) polymer by using iCVD developed with regard to modulus and hardness while the dielectric constant decreased and also it was observed that polymer functionality was not undergone any changes after coating. They were asserted that iCVD method permitted the removal of undesirable organic components and used low energy thus it was considered as environmentally friendly process (Trujillo, Wu et al. 2010).

In addition to all these application areas identified above, iCVD method can be utilized in producing protective polymer coatings for the optical components. The significant point is that the optic properties of the substrate material should not be affected from the polymeric coatings and also these components used in the adverse operating conditions in the electro optical systems therefore durability, self-cleaning property and reprocessing are the other crucial desired cases. In literature, there is not any study about the protective polymeric coatings on the optical components produced by iCVD technique therefore this study is quite unique compared to the other iCVD studies.

CHAPTER 2

EXPERIMENTAL WORK

In this chapter, information about iCVD system and its components like mass flow controllers, pump, heater, variacs, proportional–integral–derivative (PID) controllers etc., and materials used in this study are given. Furthermore, cleaning procedures of the substrates, coating process and the characterization methods applied after the coating process such as Reflectometry, Fourier transform infrared spectroscopy (FTIR), Optical Microscopy, Scanning Electron Microscopy (SEM), Atomic-force Microscopy (AFM) and mechanical tests are given in detail.

2.1. iCVD System

iCVD is a novel thermal process type of CVD and has many advantages as coating complex geometry substrates, having low energy consumption, higher deposition rate, nanoscale thickness control and being solvent-free process. During a deposition, thermal decomposition of initiator, adsorption of monomer and free radicals on substrate surface and free radical polymerization occur respectively to produce thin polymeric film coating and details were given in the Chapter 1. iCVD system includes different components as homemade vacuum chamber, filament array, mass flow controllers (MFC), pump, cooler, variacs and proportional–Integral–Derivative (PID) controllers. All these component types, models and working conditions were explained briefly as follows.

The vacuum chamber used in this iCVD system displayed in Fig. 2.1 below. This chamber has 31.6cm length and width and also 4.0 cm height. Besides, the chamber has backside cooled stage which possess 12 cm radius and in this stage temperature can be kept constant between -20 to 50°C by using a circulator (WiseCircu - refrigerated bath circulator). The reaction chamber was covered with a quartz plate (25 cm diameter, 2.5 cm thickness).

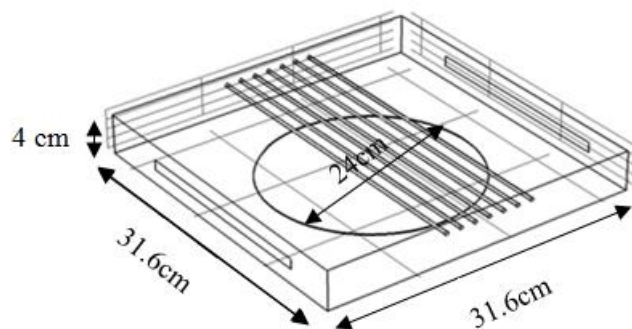


Figure 2.1. Vacuum chamber of iCVD system.

A filament array placed into the reaction chamber was used to supply thermal energy for decomposition of the initiator and there is space between cooled stage and Nichrome filaments (80% Ni/20% Cr) approximately 2 or 3 cm. Different filament temperatures between 230 and 330°C were used in this study and the temperature was measured by a thermocouple (Type K, Omega Engineering) attached to one of the filaments. The reactor pressure was kept between 0.1 to 1 Torr using the pump (2XZ-Rotary Vacuum Pump). To control the pressure in the reaction chamber, exhaust throttling butterfly valve (Model 253B, MKS type) was used. The monomers which needs to be heated were installed to the second channel of the system that was heated with heating tapes (Model FGR rope heater, Omegalux) and they transferred into the reaction chamber with mass flow controller 2, MFC2, (Model 1150C, MKS type). Other monomers and initiator were kept at room temperature and they were transferred into the reaction chamber by using first, third or fourth channel according to the flow amount, and MFC1, MFC3 (Model 1479A, MKS type) or Manual MFC were used in these channels, respectively. Furthermore, AC current was provided to some parts of the system like filaments and heating tapes by using different variacs (Servo-Matik) and PID controllers (TK4 series, Autonics) were used in order to set and monitor temperatures in certain parts of the system.

2.2. Materials

In this study polymeric thin films on different substrate materials were fabricated with iCVD method by using selected monomers (refractive indices between 1.3 and 1.7) and initiator. Vinyl monomers like acrylate and methacrylate and fluorine-containing

monomers were chosen and also tert-Butyl peroxide (TBPO, Sigma-Aldrich, 98%) was selected as initiator.

Glycidyl methacrylate (GMA, Sigma-Aldrich, 97%) was as epoxy monomer. As fluorine-containing monomers 1H, 1H, 2H, 2H-Perfluorodecyl acrylate (PFDA, Sigma-Aldrich, 97%), was used for this study. In addition to this, crystalline silicon (c-Si) and glass (microscope slide) were used as substrate materials because they are relatively inexpensive when compare the other substrate materials such as sapphire (Al_2O_3), calcite (CaCO_3), quartz etc. and they can be characterized easily. Two different cleaning procedures were applied to these substrate materials before using in the coating process. For the cleaning process of c-Si, deionized water (DIW), ammonium hydroxide (NH_4OH , Merck, 28-30%) and hydrogen peroxide (H_2O_2 , Merck, 35%) were used whereas for the glass substrate only liquid soap and deionized water were used. In addition to these, to detect solubility and cleanability of coated samples trichloroethylene, acetone and ethanol were used. In the following table some important properties of the materials used in this study were given.

Table 2.1. Properties of iCVD materials and substrate cleaning chemicals.

Materials	Chemical formula	Molecular weight (g/mol)	Density (g/ml) @ 25°C	Boiling Point (°C)
Glycidyl Methacrylate, 97%	$\text{C}_7\text{H}_{10}\text{O}_3$	142.15	1.042	189
1H, 1H, 2H, 2H-Perfluorodecyl acrylate, 97%	$\text{C}_{13}\text{H}_7\text{F}_{17}\text{O}_2$	518.17	1.637	90
tert-Butyl peroxide, 98%	$\text{C}_8\text{H}_{18}\text{O}_2$	146.23	0.796	109-110
Ammonium Hydroxide, 28-30%	NH_4OH	35.05	0.90 @ 20°C	32
Hydrogen Peroxide, 35%	H_2O_2	34.01	1.13 @ 20°C	110
Trichloroethylene	C_2HCl_3	131.39	4.53 (vapor density)	87
Ethyl alcohol	$\text{C}_2\text{H}_6\text{O}$	-	1.59 (vapor density)	78.5
Acetone	$\text{C}_3\text{H}_6\text{O}$	58.08	2 (vapor density)	56.2
Sodium Chloride	NaCl	58.44	-	1413

(Cont. on next page)

Table 2.1. (Cont.)

Materials	Flash Point (°C)	Refractive index, n	Supplier
Glycidyl Methacrylate, 97%	76	1.449	Sigma-Aldrich
1H, 1H, 2H, 2H-Perfluorodecyl acrylate, 97%	113	1.337	Sigma-Aldrich
tert-Butyl peroxide, 98%	1	1.389	Sigma-Aldrich
Ammonium Hydroxide, 28-30%	Not flammable	-	Merck
Hydrogen Peroxide, 35%	-	-	Merck
Trichloroethylene	-	-	Merck
Ethyl alcohol	18.5	-	Merck
Acetone	-20	-	Sigma-Aldrich
Sodium Chloride	-	-	Merck

2.3. Cleaning Procedures of the Substrates

In order to remove the organic or other types of contaminants like dust from the c-Si and glass substrates, two different procedures were used for each of them. For the c-Si, famous industry standard RCA procedure involving ammonium hydroxide (NH_4OH), about 27 %, hydrogen peroxide (H_2O_2), approximately 30%, and deionized water were used.

In this procedure, initially, 325 ml DI water was put into a beaker and then 65 ml NH_4OH added, after that, beaker containing DI and NH_4OH was placed on the hot plate (WiseStir, MSH-20D) and heated to 70-75°C. The beaker was then taken from the plate and 65 ml H_2O_2 was added to the beaker. After a few minutes (1-2 min.), it was observed that bubbles quickly formed into the solution and this indicated that solution was ready for use in cleaning of the c-Si substrates. Then, substrates were soaked in the solution for 15 minutes. Finally, substrates were removed from the solution and rinsed with deionized water one by one. They were dried in the vacuum oven (WiseVen, WOV-30) at 60°C for 2 hours to remove excess water residues. The following scheme shows the RCA cleaning procedure steps of c-Si substrates.

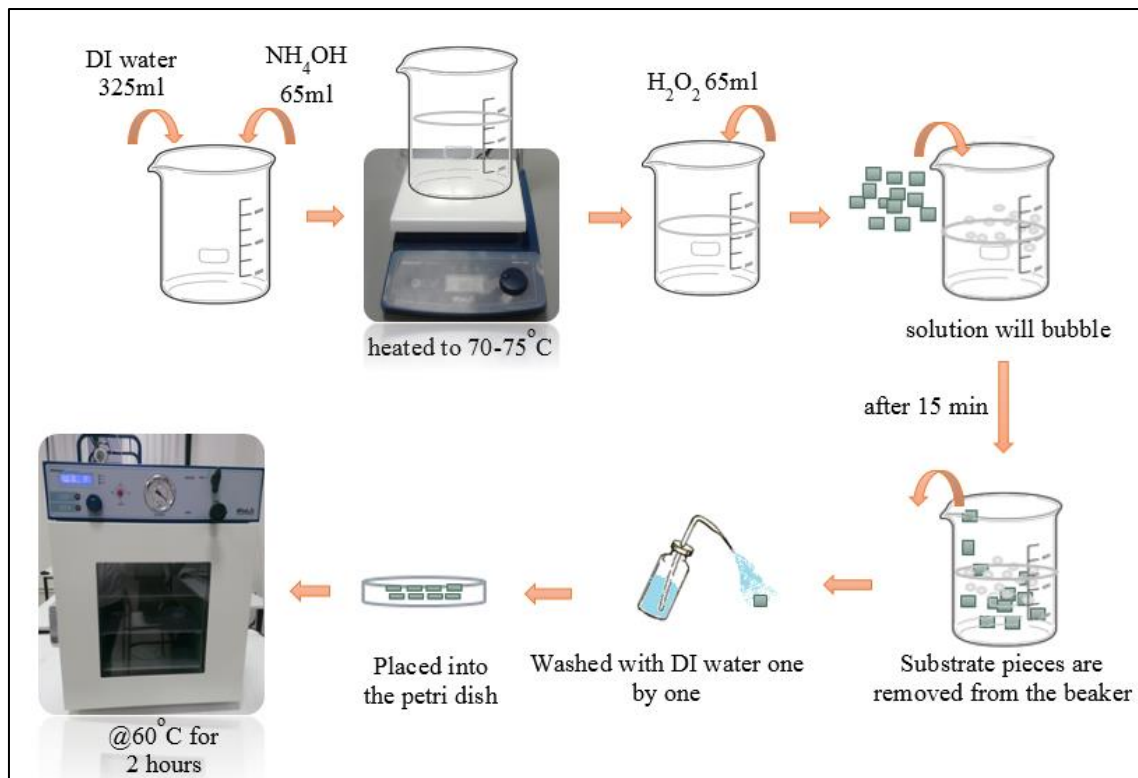


Figure 2.2. RCA cleaning procedure for c-Si substrates.

For the glass substrate, simpler cleaning procedure was performed. In this procedure soapy water was prepared and poured into a beaker. Glass substrates were placed into the beaker in ultrasonic bath (WUC-D06H, Wisd) at 50°C for 30 minutes for the first part of the cleaning procedure. Samples were then removed from the beaker and transferred to another beaker containing only DI water and the process was repeated. Glass substrates were then taken from the beaker and washed with the DI water one by one and put into the vacuum oven (WiseVen, WOV-30) at 60°C for 2 hours in order to carry out drying process. This cleaning procedure steps were clearly indicated in Figure 2.3.

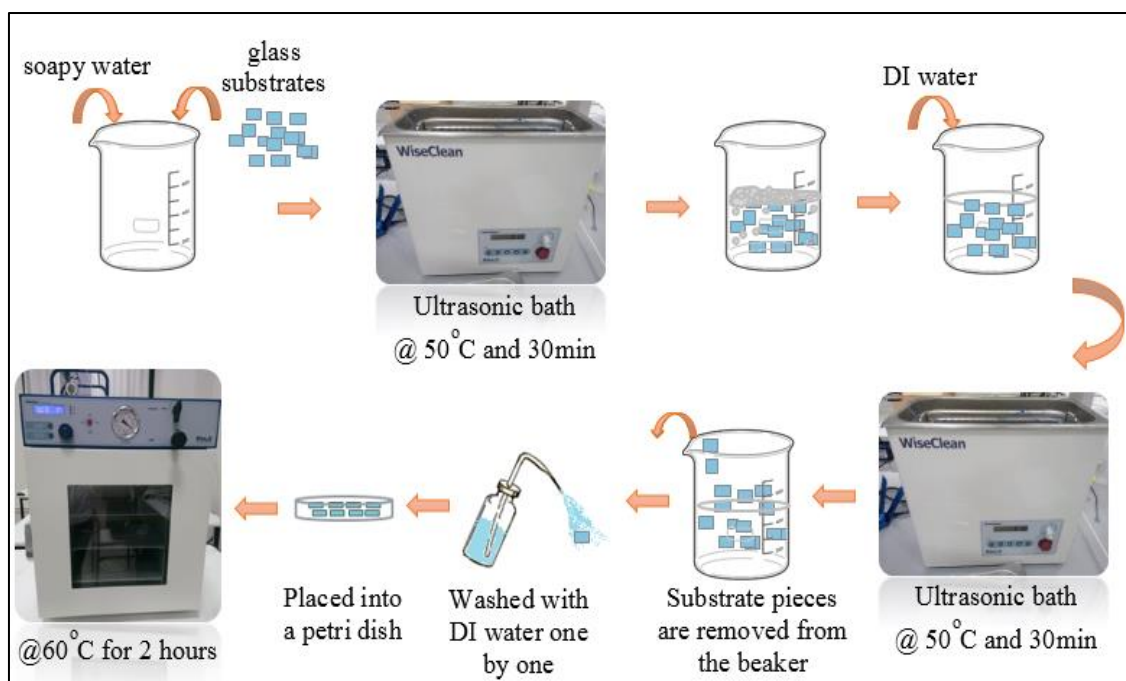


Figure 2.3. Cleaning procedure for glass substrates.

2.4. Polymeric Thin Film Coating Procedure in iCVD System

Thin film coating procedure in iCVD system consists of 3 main parts as startup, operating mode in iCVD and lastly shutdown. In the following sections, detailed information about each part was given clearly and briefly.

2.4.1. Startup of Thin Film Coating in iCVD System

Before the thin film coating process was taken place in iCVD system, initially necessary parts of the system as pump, control panel, mass flow controllers (MFCs), variacs etc. must be run therefore operations were alternately proceeded. Firstly, pump was turned on and manual valve was opened to provide vacuum to the system as 0.1-1 Torr. Then the control panel and MFCs were turned on and the flow positions were adjusted as external mode. Temperature values of the PID controllers selected in order to use in the experimental section were set to necessary values. Thereafter, monomer and initiator jars were installed to the system and flow positions of the MFCs were changed to the flow modes. Variacs were turned on to supply energy to the heating tapes for heating the system channels. After that, substrate materials desired to coat with thin film was

inserted into the reaction chamber and it was performed by closing manual valve, pressure sensor and reactor inlet valve and removing of the quartz plate on the reactor. After placing of the substrate materials on the cooled section of the chamber, filament array was placed on the substrate, thermocouple was attached one of the filaments, quartz plate put back and again system became under the vacuum with opening the manual, reactor inlet valve and pressure sensor. Finally, cooler was turned on and it was provided that desired temperature of the cooled section of the reaction chamber (substrate temperature) was adjusted as $<50^{\circ}\text{C}$.

2.4.2. Operating Mode in iCVD System

In this part of the thin film coating process, initially, setting of intended flow rate value of the monomer and initiator and reaction pressure were performed. Then, flow of monomer and initiator was provided from the channels to the reaction chamber. When all flow rates and reactor pressure reached their set values, variac 5 (V5), which has been used for supplying energy to the filaments, was turned on and filament temperature was set to the desired value. Time was started when the filament temperature reached approximately to 180°C . After the desired thickness was obtained, deposition was stopped by turning of the V5 and then shutdown operation was followed. For all different type of the iCVD chemicals that are monomer and initiator the same thin film coating procedure was applied but only the operating conditions as flow rate of monomer and initiator, deposition pressure, filament and substrate temperatures etc. were changed.

2.4.3. Shutdown Procedure in iCVD System

After the thin film coating was carried out, flow of monomer and initiator was stopped by closing the channel valves and MFCs. Then, manual valve was opened and system again returned to vacuum condition and flush of the system using nitrogen gas was performed 3 or 4 times to remove excess monomer or initiator residues from the system. Variacs and cooler was turned off. Thereafter, isolation of the chamber was performed like in the startup part and coated substrate material was removed from the reactor and then again chamber was closed with quartz plate and vacuum was supplied to the system.

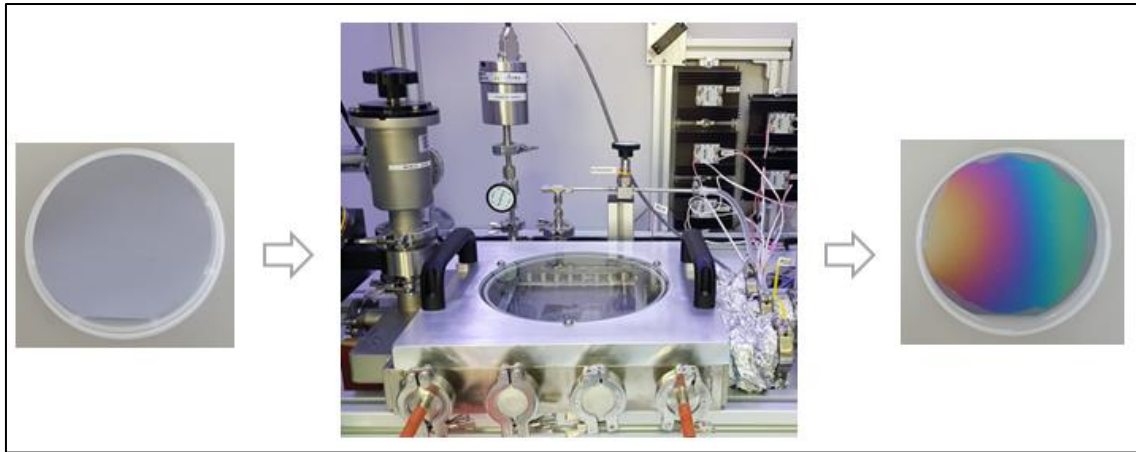


Figure 2.4. General substrate coating scheme in iCVD system.

2.5. Characterization

After coating process was performed in iCVD system, a reflectometry device, Mprobe-Vis20 system, was used for the thickness measurement, reflection measurement, single or multilayer film-stack modeling and performing simulations for the coated thin films. The necessary data was obtained from reflected light from the surface of the substrate. After that, necessary procedures could be performed by using the software of the system (TF Companion). Spectral range of this system is 400-1100 nm and also thickness range is 15 nm-50 nm. The following figure demonstrates the Mprobe-Vis system and its units.

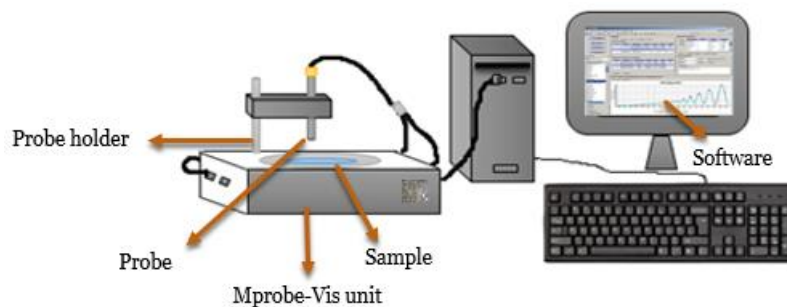


Figure 2.5. Mprobe-Vis system.

In addition to this characterization, Fourier transform infrared spectroscopy (FTIR) analysis were performed by using PerkinElmer Inc.-Spectrum BX FTIR Spectrometer in order to investigate whether polymerization was performed efficiently,

in other words, whether or not monomer units have fully participated in the free radical polymerization reaction. FTIR spectra of the coated silicon wafer substrates were collected between 450-4000 cm^{-1} scan range and at 4 cm^{-1} resolution. In addition to polymer film, also FTIR analysis of the monomer samples used in the deposition were performed to provide comparison with polymers.

Surface roughness of thin films fabricated with iCVD was examined by using Atomic-force Microscopy (AFM) and for this analysis Nanosurf-Flex Axiom system with 10 μm image size, 0° rotation, 0V tip voltage and 200-2 mV free vibration amplitude was used.

In order to detect the holes and scratches on film surface coated with iCVD, optical microscopy, BEL MPL-2 polarization microscope, was used and surface images were taken as 5x, 10x, 40x and 80x magnifications.

Moreover, surface uniformity and structure of the coated film in nano and micro scale were investigated by using Scanning Electron Microscopy (SEM), at 5kV with FEI QUANTA 250 FEG and surface images were taken at different magnifications.

Contact angle measurement was performed to investigate the water repellent property (hydrophobicity) of the coated film surface synthesized by using iCVD system and for this measurement Theta Optical Tensiometer was used. Also, water was selected as test liquid and static contact angle measurements were performed by dropping 5 μl water on the coating surfaces.

Physical quality control of the coating surface was carried out particularly with Military Standards (MIL-STD) that are used in defense and aerospace applications. In this study MIL-F-48616 military standard was followed for the performance tests. MIL-F-48616 standard includes general performance and durability tests of thin film coatings. It covers test methods as surface quality (scratches and holes) and surface resistance (adhesion, moisture, solubility in different chemicals, salt resistance and water solubility).

CHAPTER 3

MODELING OF OPTICAL COATINGS

In this study, modeling of single or multilayer, polymeric or hybrid thin film optical coatings was also done. The significant point is that these coatings should not affect the optical performance of the coating surfaces.

For the modeling of polymeric coatings, TF Companion software that is provided with Mprobe-Vis system was used. Therefore thickness and reflection measurements, film-stack modeling and simulations were performed easily as described in the experimental section. In this part of the study, initially, transmission behavior of substrate material and effects of coating features such as layer thickness, number of layers and refractive indices of the coating materials were examined, respectively.

The results of modeling studies are given as transmittance vs wavelength plots between the wavelengths of interests. Furthermore, for the modeling and simulations, fluoro and vinyl polymers like acrylates and methacrylates whose refractive indices between 1.3 and 1.7 were chosen.

In this part, firstly, the transmission behavior of the substrate materials that were BK7, sapphire (Al_2O_3), BaF_2 , CaF_2 , MgF_2 , Fused silica UV grade, Fused Silica IR grade, Si, ZnSe and Ge were investigated in literature and their transmission curves were formed by using the literature data (Web-9 , Web-10) as the following figure.

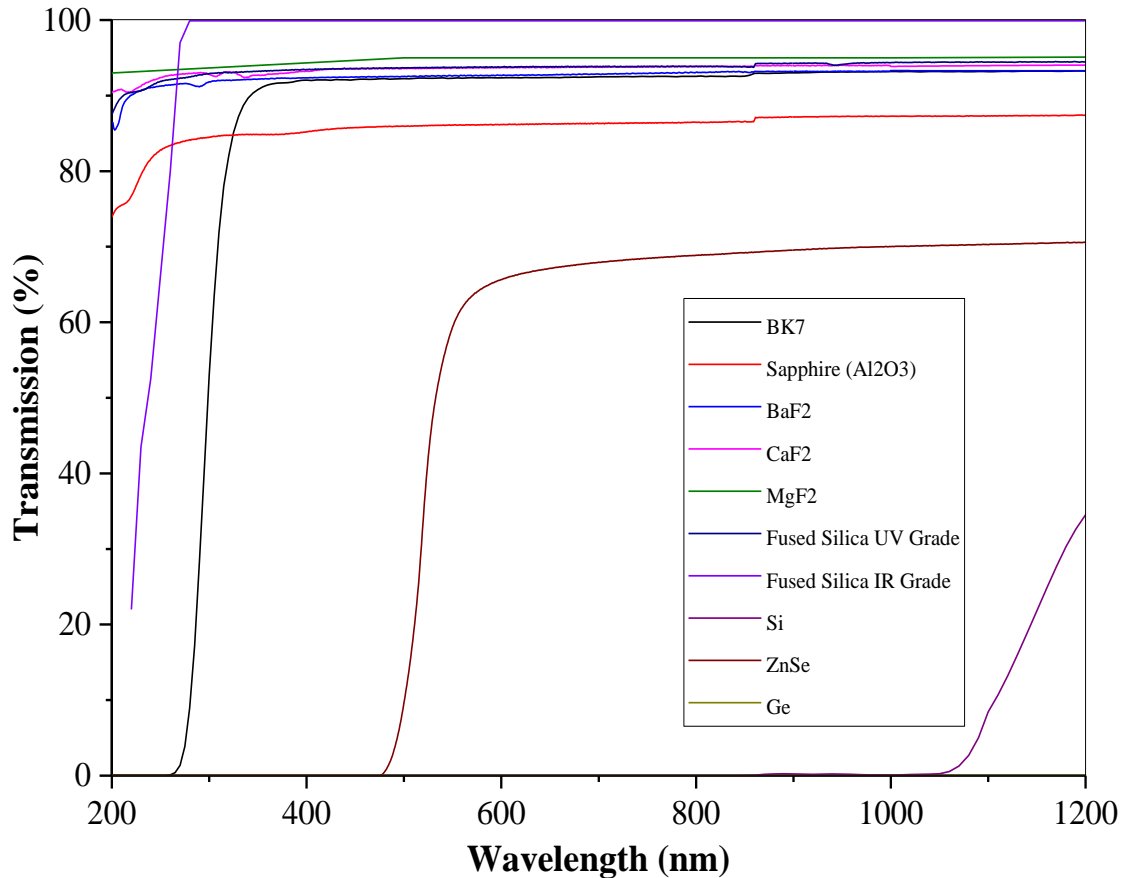


Figure 3.1. Transmission curves of substrate materials.

In this graph, wavelength region was selected as 200-1200 nm, which includes the region of near infrared, visible and far UV, the reason for this, transmission behavior of the substrate materials was needed to be examined in wide range. According to Figure 3.1, it was observed clearly that all substrate material transmissivity exceeded the point of 80% except for ZnSe and Silicon in this wavelength region.

Additionally, the effects of thickness and layer number of film stack and refractive indices of the coating materials were examined in this part. For this reason, substrate material and polymeric materials had different refractive indices were chosen then thickness and layer number of the coating were changed separately to monitor their effects on the transmission and reflection behavior of the substrate. In this system, simulations were performed easily when the necessary parameters were entered to the related part of the system software (TF Companion) as transmission range, angle of incident light, number of point, thickness, layer number of the coating elements etc. and also some necessary reflection and transmission calculations were performed at the background, however, the calculation steps were not monitored because only results were given by the

software as graphical or tabulated form. In accordance with this purpose, “Bragg mirror” type reflection expressed in the Chapter 1 as consisting of film stack formed consecutively with high and low index material was investigated and it was observed that height of the high reflection zone increases with increasing of the layer number and refractive indices of the materials and also when the difference of high and low refractive indices increases, the width of the high reflection zone increases also. In order to demonstrate these effects clearly by using the reflectometer device, a simple modeling was performed by using sapphire (Al_2O_3) as substrate material for simulation owing to obtaining more clear and prominent thickness and layer number change effects when compare the other substrates. Besides, poly (methyl methacrylate) (PMMA) and poly (tetrafluoroethylene) (PTFE) were used in this simulation part as high index (n: 1.49) and low index material (n: 1.32), respectively. The number of layer in the film stack was identified as $2p+1$ where p is pair and examinations were done according to this information.

Bragg mirror modelling was started with the 100 nm PTFE/100 nm PMMA on sapphire substrate and number of layer was found as 3 from $2p+1$ because there was one pair. Then, the thickness of the PTFE and PMMA layers were increased from 100 to 150 nm and thickness effects were examined from the following simulation graphs.



Figure 3.2. Film stack model of 1 pair PTFE/PMMA

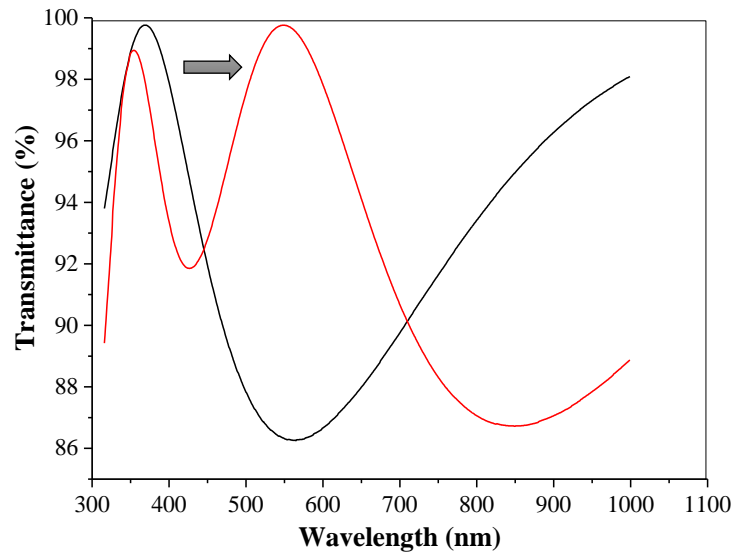


Figure 3.3. Transmission graphs of 1 layer-100 nm PTFE/100 nm PMMA (black) and 10 layer-150 nm PTFE/150 nm PMMA (red) on sapphire substrates.

According to the Figure 3.3, it was demonstrated clearly that the thickness of the layer increased from 100 to 150 nm caused to number of sine wave increased and also high reflection zone shifted to the right side.

After that, the same type film stack was formed but number of pair was increased from 1 to 10 therefore the number of layer also increased from 3 to 21 by using the $2p+1$ relation. Film stack model formed in the Mprobe-Vis system again illustrated in below.

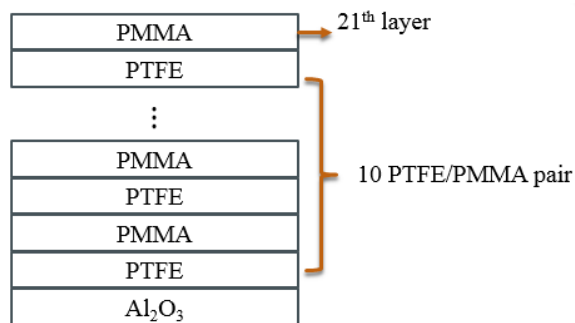


Figure 3.4. Film stack model of 10 pair PTFE/PMMA

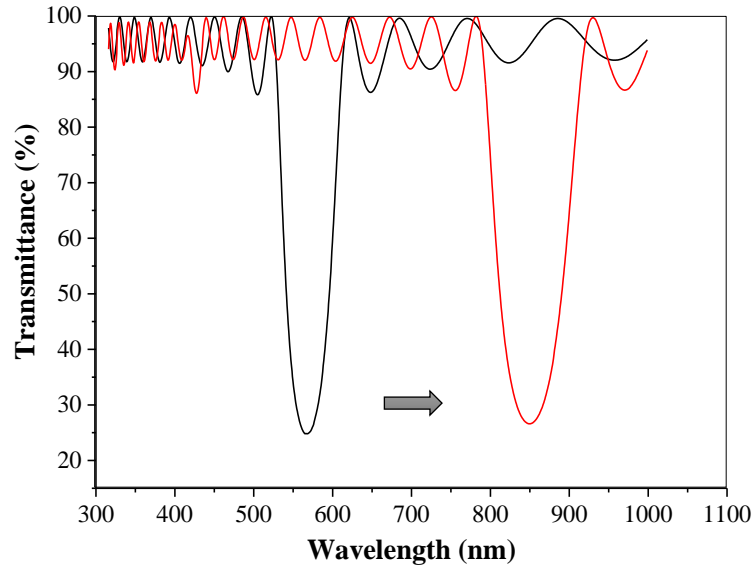


Figure 3.5. Transmission graphs of 10 layer-100 nm PTFE/100 nm PMMA (black) and 10 layer-150 nm PTFE/150 nm PMMA (red) on sapphire substrates.

In the figure above, thickness of layer increased from 100 to 150 nm as 1 pair film stack and it was observed that number of sine wave again increased when the thickness of layer improved. In addition to this, when Figure 3.5 was compared with Figure 3.3, it was represented that the number of pair in the film stack increased from 1 to 10 then the height of the high reflection zone increased also and this manner could be observed clearly in Figures 3.3 and 3.5 above.

Finally, the number of pair in the film stack was increased to 100 and according to the $2p+1$ relation the number of layer in film stack was obtained as 201. The film stack model formed in the software was shown below.

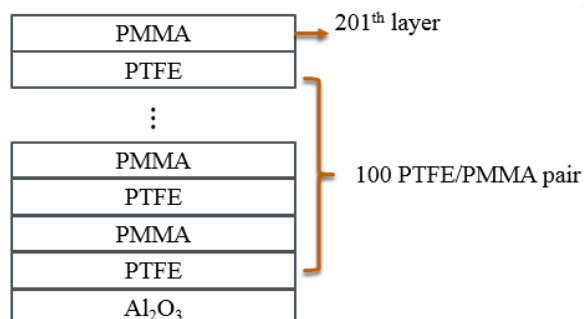


Figure 3.6. Film stack model of 100 pair PTFE/PMMA

Thereafter, the necessary parameters were set in the software in order to form the simulation graphs and two different thickness values were chosen again like the previous ones to examine and demonstrate the thickness effect and also number of layer changed in each set to observe the layer number effect. In this section, results obtained from the software of the Mprobe-Vis system were given in the following figure.

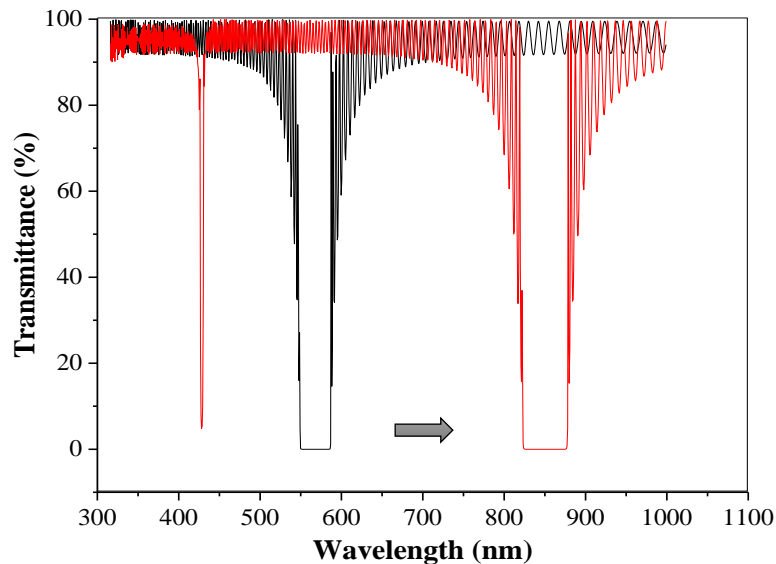


Figure 3.7. Transmission graphs of 100 layer-100 nm PTFE/100 nm PMMA (black) and 100 layer-150 nm PTFE/150 nm PMMA (red) on sapphire substrates.

When the Figure 3.7 was observed, it was seen that the number of sign wave increased extremely thus the high reflection zones could be observed more specifically and the small peaks were eliminated almost wholly with this way. Also, the high reflection zone shifted to the right side same as the previous ones and as a result of this new reflection zones came into sight. Moreover, in this section, number of pair was increased to 100 and total number of layer in the film stack was obtained as 201 by using $2p+1$ relation. When this section was compared with the sections of 10 and 1 number of pair, it was clearly observed that height of the high reflection regions became quite prominent.

Effects of thickness and layer number of film stack were explained and examined by using all these results given above. Moreover, one of the important aims clarified at the beginning chapter of the study is that the polymeric thin film coating should not affect the optical performance of the coated surface, in other words, it was desired that the polymeric film should not cause a measurable decline of the optical performance of the coated surface. Therefore, considering this critical point, in this study before the coating

process was taken place, modeling was performed to find out what are the optimum film thickness value does not affect the transmission behaviors of the selected substrates.

In this modeling section, BK7 glass and microscope slides were selected as substrate materials. However, in the modeling part, c-Si was not selected as a substrate because it is not a transparent material in the visible spectrum and it only transmits light in the infrared region as shown in Figure 3.1 previously. Therefore, it was used in the deposition experiments, and not used in the simulations. As a result, all thickness measurements and some characterization methods like FTIR were applied by using c-Si substrate instead of BK7 or microscope slide. Unlike glass substrates, thickness measurements with reflectometer device after depositions and FTIR characterization were performed easily, successfully and accurately by using the c-Si substrate.

Glass substrates have surface roughness, thus, some undesired internal reflections and reflection from stainless steel platform of the reflectometry result in difficulty during thickness measurements since the reflectometer used in this study is not suitable for transmission measurements. Various algorithms for reflectivity calculations for transparent substrates were tried to improve reliability of thickness measurements. Therefore, very accurate results would not be obtained in the measurements by using BK7 and microscope slide. Microscope slides are more affordable than BK7 due to higher defect density such as air bubbles and impurities, however, these defects are not clearly detectable in small volumes. Also, transmission behaviors resemble each other. Therefore, for the depositions microscope slide and c-Si substrate were used together. They were placed into reaction chamber and after the deposition, necessary measurements performed using reference (c-Si) substrate only. Since film thickness does not change with substrate type, these measurements were very helpful to determine the thickness of polymer films on glass substrates during and after deposition.

Moreover, poly (glycidyl methacrylate) (PGMA) ($n:1.54$) and an acrylate fluoropolymer (FP) was used in modeling. Refractive indices of fluoropolymers that would be used in this study like Poly(1H,1H,2H,2H-Perfluorodecyl acrylate) (PPFDA) are generally between 1.34 and 1.37. In addition to PGMA and fluoropolymer, copolymer consisting of PGMA and FP was used in the modeling. The reason for using a copolymer is that hydrophobic and self-cleaning properties of FPs and good mechanical properties of PGMA can be realized with a copolymer film coating.

In addition to these, actual substrate, glass type (BK7), has 1.5 refractive index and refractive indices of FPs and PGMA are 1.34 and 1.54, respectively. Therefore, transmission behavior of the substrate before and after the deposition does not alter remarkably, which is a desired result for this study. However, if the coating material refractive index has high values like 2 or 2.5, refractive index difference between the coating and substrate material increases and transmission behavior changes considerably. Therefore, PGMA and FPs were selected as the coating materials. The importance of this case was also demonstrated in the modeling results with graphical explanations.

During modeling, it was desired that after coating of the substrate surface, a total transmission change should not exceed 5%. In order to carry out simulations, TF Companion software was used and simulation graphs (transmittance vs wavelength) were obtained for each substrate and polymeric materials with varying thicknesses. Necessary parameters were adjusted in this modeling as 1 layer of the polymer or copolymer on substrate, 300-1100 nm spectral range, 0° incident light angle and 1000 simulated data points.

Modeling was started with BK7 substrate and PGMA, FP and copolymer, respectively, as coating materials. First, BK7 transmission curve was obtained with simulation as was given in Figure 3.8.

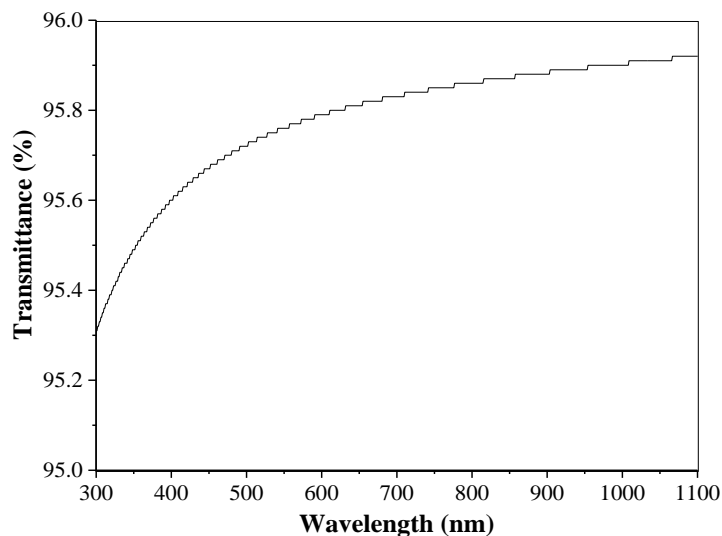


Figure 3.8. BK7 transmission behavior (transmission scale between 95-96%).

In BK7 transmission graph, it was observed that its transmittance changed from 95.3% to 95.9% and this transmission behavior was compared with simulation of coated

BK7 with three different polymeric materials; PGMA, FP and copolymer. In these simulations, film thicknesses were changed from 50 to 1 μm for each polymer. PGMA was used as the first polymer and the simulation results were given in Figure 3.9 as separately, and in Figure 3.10 as general graph containing all simulations.

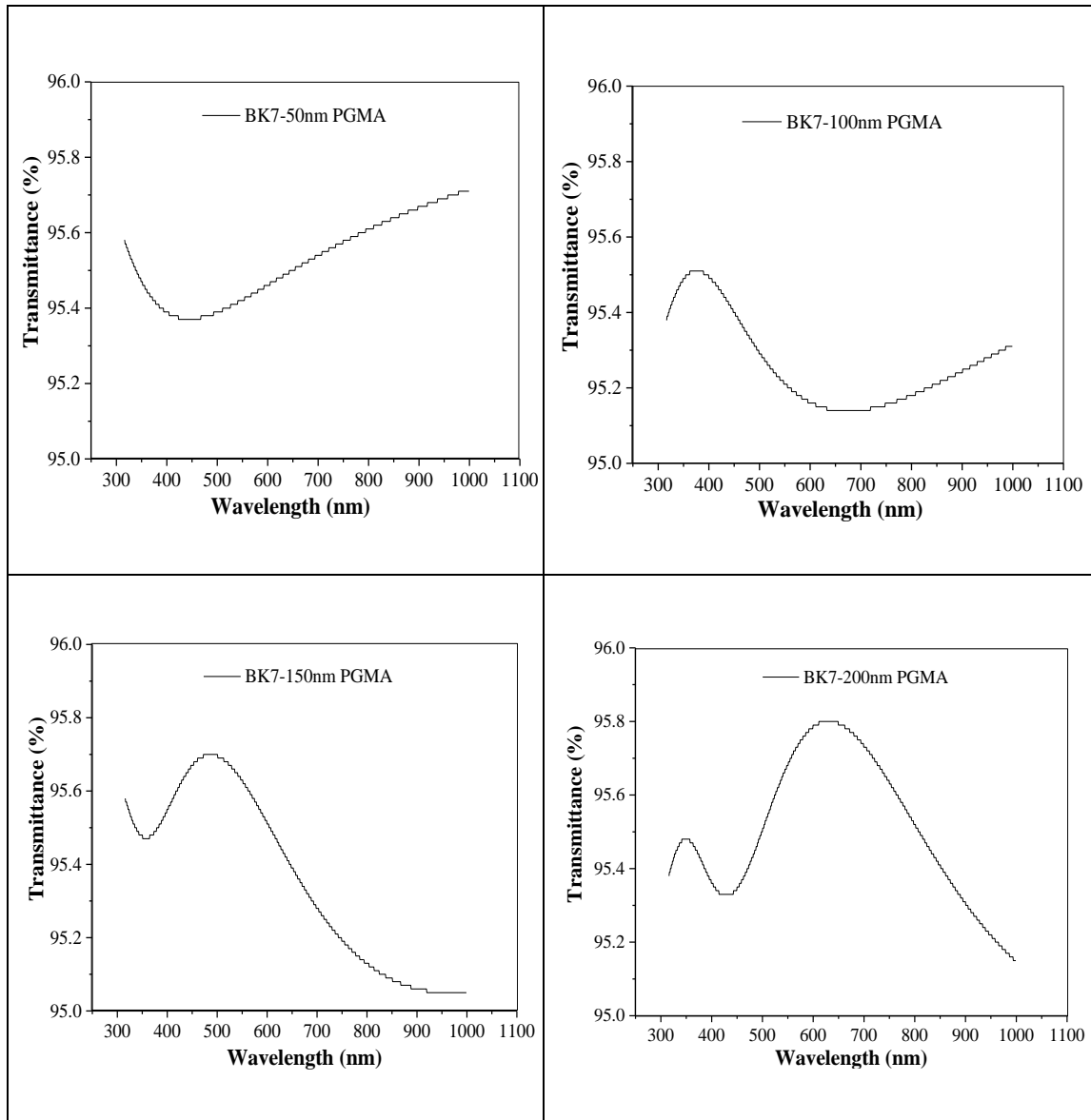


Figure 3.9. Simulation graphs of modeling BK7 coated with different thickness of PGMA.

(Cont. on next page)

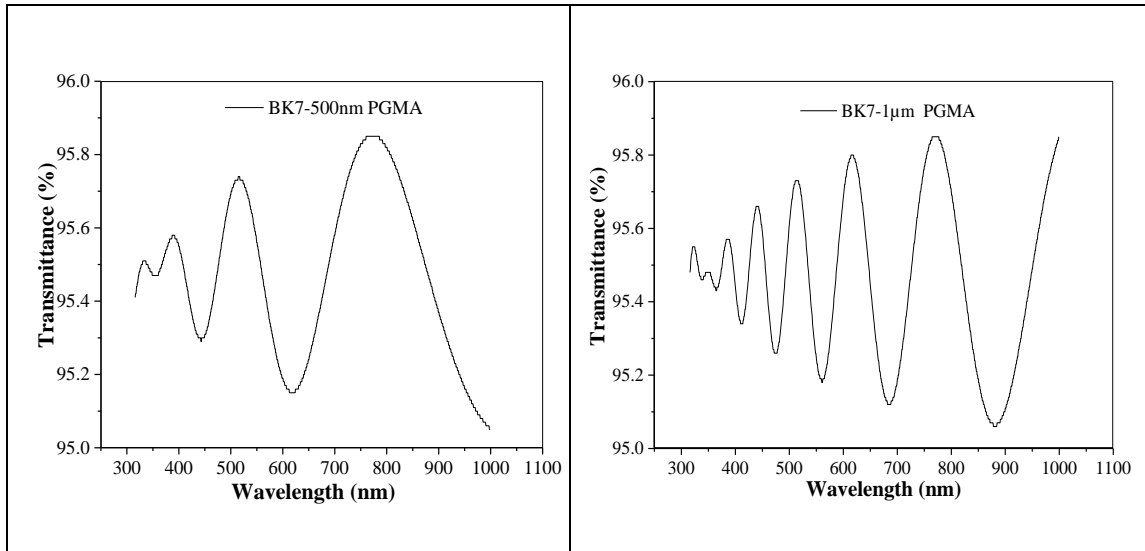


Figure 3.9. (Cont.)

Figure 3.9 illustrated the transmission graphs of BK7 coated with 1 layer of 50, 100, 150, 200, 500 nm and 1 μm PGMA, respectively. In these graphs, it was observed clearly that when the thickness was increased, the number of oscillations (sine waves) increased and high reflection zones shifted to the right. In order to illustrate the effect of thickness change from 50 nm to 1 μm on the transmission behavior a graph that contains all thickness variation curves was created in the following figure.

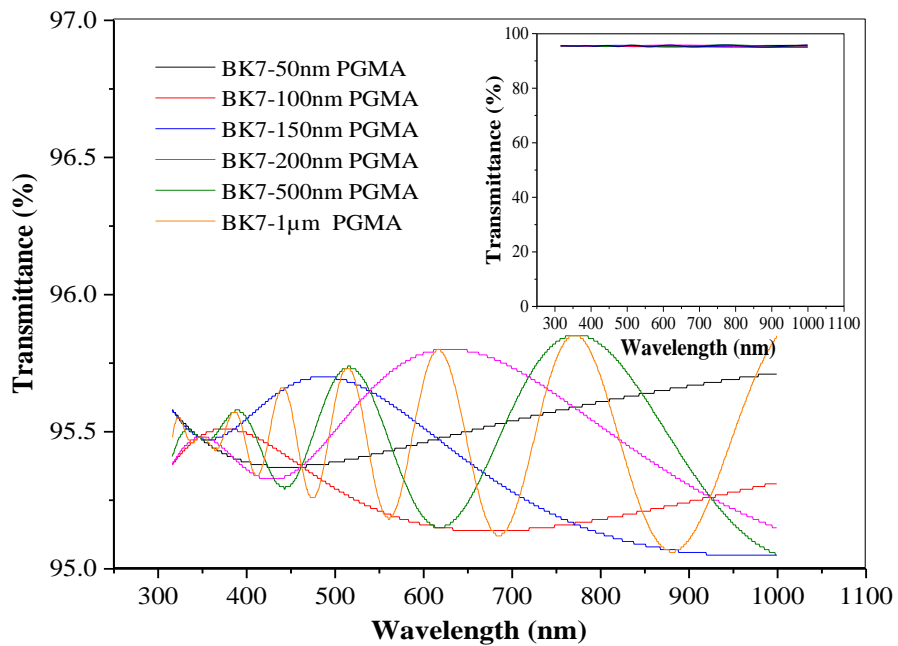


Figure 3.10. Transmission graph of BK7 coated with PGMA from 50 nm to 1 μm .

Figure 3.10 demonstrated that the transmission approximately changes from 95.1% to 95.8% and it was observed clearly when the transmission scale of graph was 95 to 97%. Besides, when the scale was adjusted as 0 to 100%, it was clearly seen that transmission not change dramatically with thickness changing from 50 nm to 1 μm . This result shows that PGMA coating from 50 nm to 1 μm on the BK7 did not affect significantly transmission behavior of BK7 because total change was 0.7%.

Similar transmission curves were obtained with simulation using FP and copolymer, and the same thickness change effect (increasing sine waves and shifting of the high reflection peaks to the right side with increasing thickness of the film) was also observed. Transmission graphs of BK7/FP, BK7/copolymer, Microscope slide/PGMA, Microscope slide/FP and Microscope slide/copolymer (thickness change from 50 nm to 1 μm) were given in the following figures.

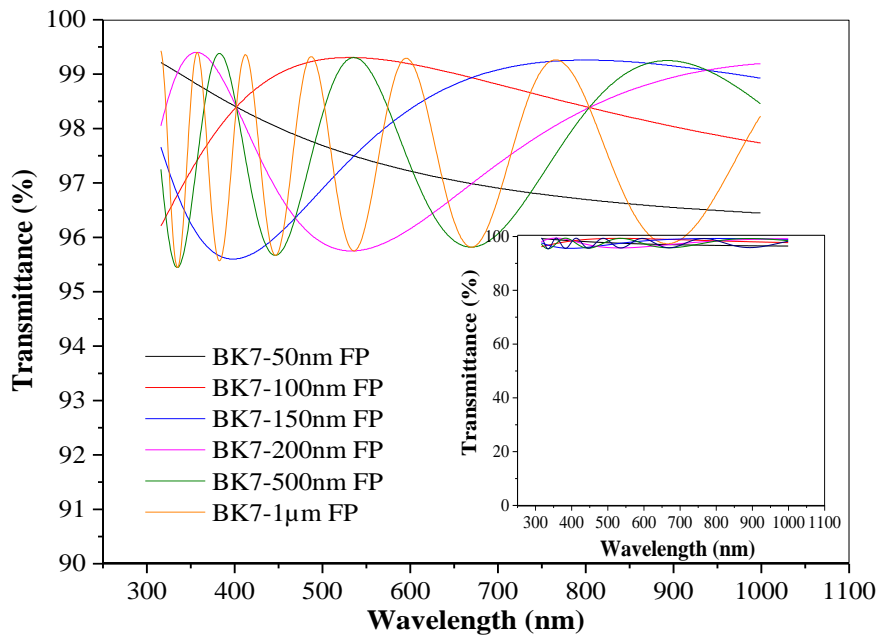


Figure 3.11. Transmission graph of BK7 coated with FP from 50 nm to 1 μm .

According to Figure 3.11, like general graph of PGMA it was seen clearly that transmission varies from 95.5% to 99.5% in the narrow scale of transmission. Furthermore, when the wide scale was examined, it illustrated that transmission not change significantly after coating of the substrate with FP. Total change was 4% and no transmission decrease observed. Therefore, it can be said that FP coating from 50 nm to 1 μm on BK7 was acceptable and this coating not altering the optical performance of the surface.

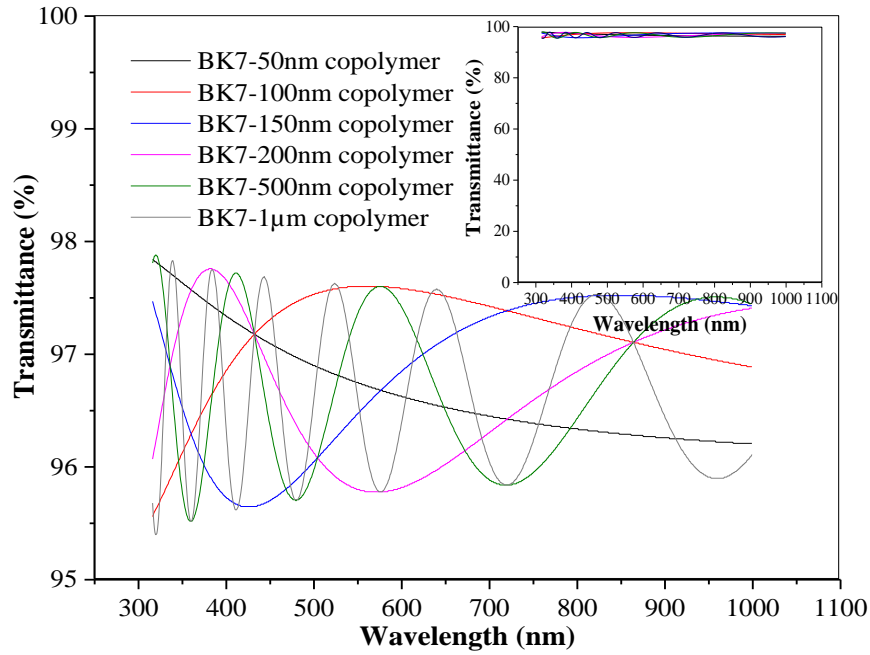


Figure 3.12. Transmission graph of BK7 coated with copolymer (PGMA-FP) from 50 nm to 1 μm .

In the large scale of Figure 3.12, changes of transmission with the coating thickness of the copolymer composed of PGMA and FP observed between 95.5% and 98%. According to this result, total transmission change was 2.5% and there is no decrease in transmission compared with the BK7 behavior. Also, when the wide scale was examined, no crucial change observed. Therefore, it can be said that copolymer coating on the BK7 does not affect the optical performance of the substrate.

Modeling work continued with using microscope slide as substrate and again PGMA, FP and copolymer as the coating materials. Similar to previous modeling with BK7 glass substrate, the transmission curve of microscope slide was acquired with simulation.

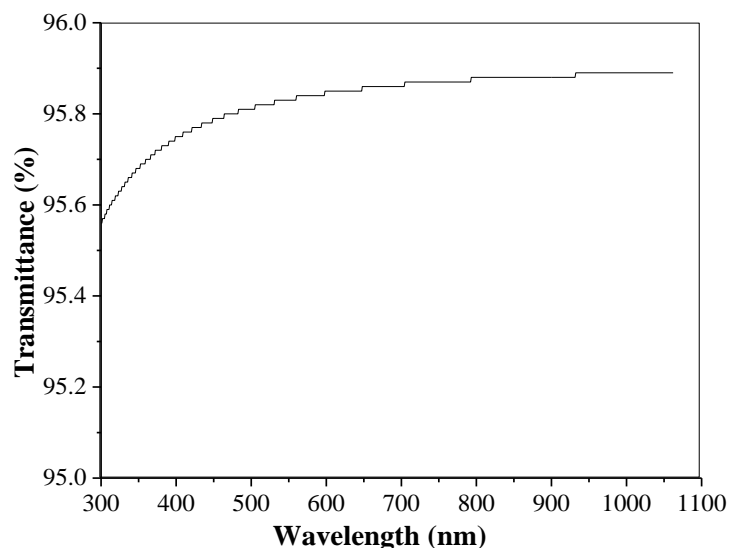


Figure 3.13. Microscope slide transmission curve.

Microscope slide (MS) transmission graph showed that transmittance changed from approximately 95.6% to 95.9%. The simulations of coated microscope slide with different thicknesses of PGMA, FP and copolymer which was changed from 50 nm to 1 μm , was investigated to evaluate the effect of film thickness on the optical performance of the substrate material.

In Figure 3.14, 3.15 and 3.16 general transmission graphs of PGMA, FP and copolymer that includes thickness alterations from 50 nm to 1 μm were given, respectively.

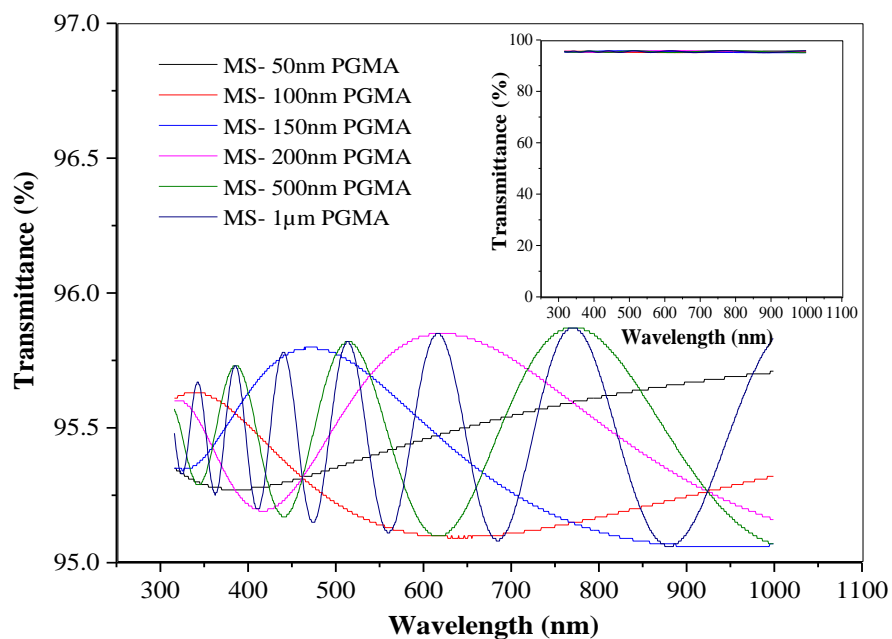


Figure 3.14. Transmission graph of MS coated with PGMA from 50 nm to 1 μ m.

Figure 3.14 illustrated that the transmission changes nearly from 95.1% to 95.8% in the narrow transmission scale. It was seen that total transmission change was 0.7% and about 0.2% transmission decrease was observed when compared with microscope slide transmission. Moreover, in the wide transmission scale (from 0 to 100%) no significant change was observed with thickness changing from 50 nm to 1 μ m. These results demonstrate that PGMA coating from 50 nm to 1 μ m does not affect the optical performance of the microscope slide.

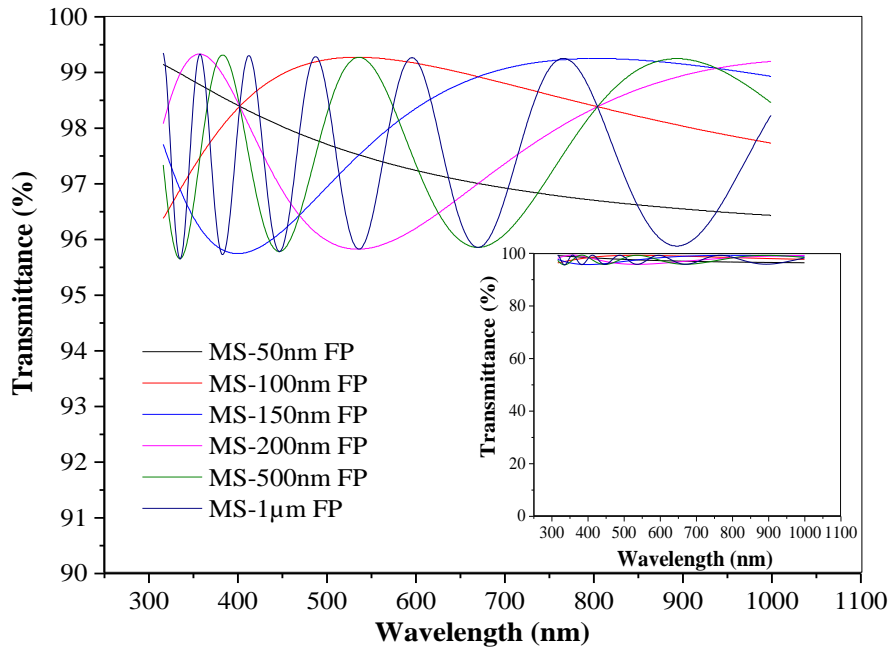


Figure 3.15. Transmission graph of MS coated with FP from 50 nm to 1 μm .

In Figure 3.15, when the narrow scale was examined, it was observed that transmission changes approximately from 95.5% to 99.5%, thus total transmission variation was found as 4% and there was no transmission decrease. Therefore, it can be said that the optical performance of the microscope slide was not affected from FP coating whose thickness varied from 50 nm to 1 μm .

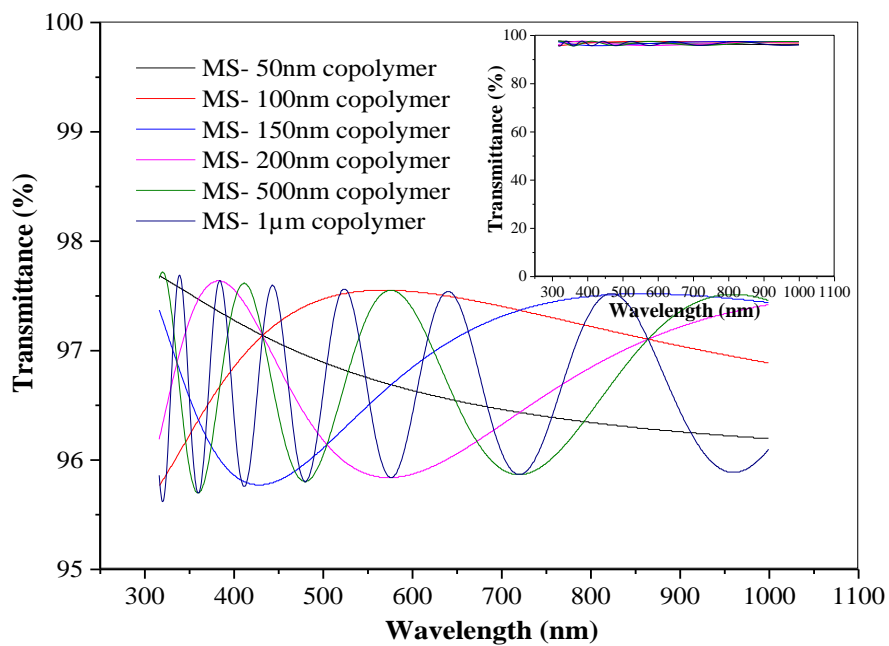


Figure 3.16. Transmission graph of Microscope slide coated with copolymer (PGMA-FP) from 50 nm to 1 μm .

According to the Figure 3.16, total transmission change was obtained nearly as 2.3% because fluctuation occurred between 95.5 and 97.8% and like the FP coating, in the copolymer there was no transmission decrease. When the wide scale graph examined it was concluded that copolymer coating on microscope slide from 50 nm to 1 μm thickness did not change optical performance of the substrate significantly.

After these examinations, all results containing PGMA, FP and copolymer coating whose thicknesses changed from 50 nm to 1 μm on BK7 and microscope slide demonstrated transmission behaviors of both substrate not affected significantly. The reason is that, refractive indices of PGMA, FP and copolymer (PGMA-FP) are 1.54, 1.34 and 1.44, respectively, and these values are close to that of BK7 and microscope slide which are 1.5. If these substrates coated with the materials that have higher refractive index values, optical performance of the substrates would be influenced significantly because transmission alters considerably. In order to observe this effect, simulation was performed by using silicon nitride (Si_3N_4) whose refractive index is 2.016, as the coating material on BK7 and microscope slide with changing film thickness from again 50 nm to 1 μm . The simulation graphs were given in the following figures.

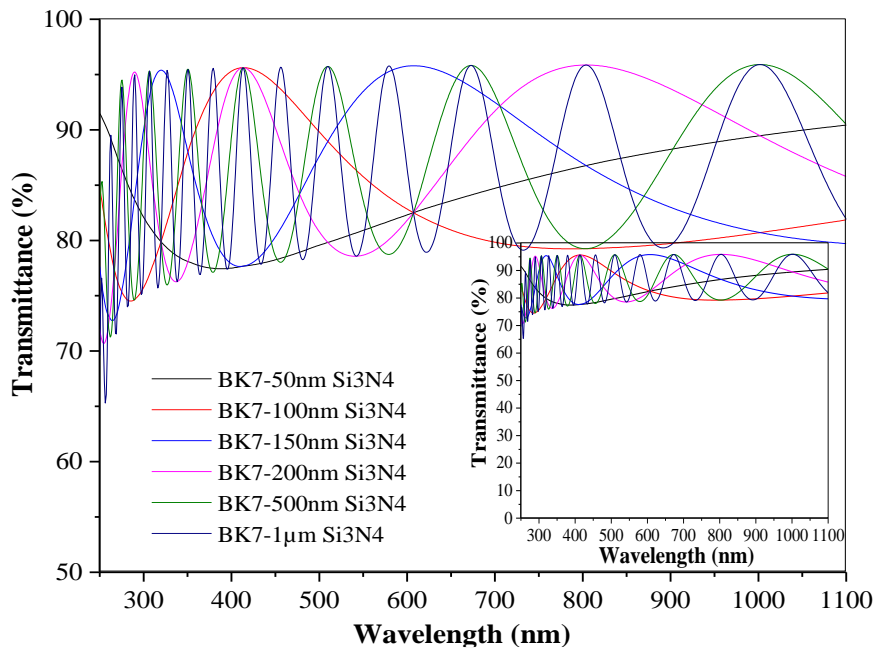


Figure 3.17. Transmission graph of BK7 coated with Si_3N_4 from 50 nm to 1 μm .

According to Figure 3.17, it was observed clearly in narrow scale that the transmission was changed from approximately from 65 to 95% and this large variation was also seen distinctly in wide scale graph. When compared with the previous results of

PGMA, FP and copolymer coating on BK and Microscope slide, there is an unacceptable amount of transmission change.

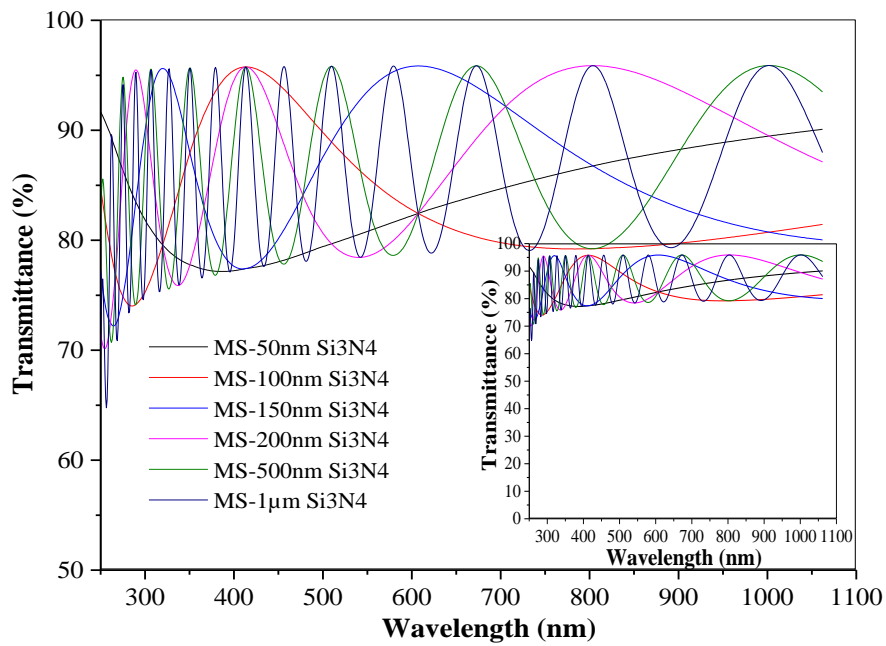


Figure 3.18. Transmission graph of MS coated with Si_3N_4 from 50 nm to 1 μm .

The same result for transmission change was obtained in the coating of Si_3N_4 on MS like that of Si_3N_4 on BK7 as about 30%. Besides, in the wide scale graph, change of the transmission can be seen and this shows that the optical performance of the MS was influenced considerably from the coating of Si_3N_4 regardless of the film thickness. Therefore, in order to maintain the transmission difference at minimum level, refractive index values of coating materials and substrates should be closer to each other.

CHAPTER 4

RESULTS AND DISCUSSION

In this chapter, results of deposition experiments which include PGMA, PPFDA and a copolymer P(GMA-PFDA) film coatings obtained using iCVD method and details about characterization of these coatings are given.

4.1. PGMA Deposition in iCVD System

Protective nano-coating fabrication with iCVD system is one of the purposes of this study and in order to achieve this aim. GMA was chosen as precursor owing to its significant features, for instance, it has quite good mechanical properties due to epoxy ring in its structure (Martin, Lau et al. 2007) as shown in Figure 4.1. Optical performance of the substrates can be protected by deposition of PGMA because of its well enough transparency (Bakker, Verlaan et al. 2007).

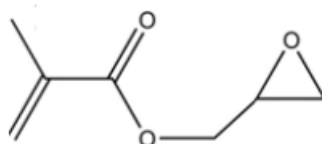


Figure 4.1. Glycidyl methacrylate (GMA) structure.

Polymeric thin film coating procedure steps in iCVD system were given explicitly in experimental part and this procedure is pretty much the same for all coating material. The main difference is that the deposition conditions of the materials are distinct from each other. Thus, in this study for all PGMA, PPFDA and copolymer film depositions, procedure explained in the experimental part was followed by using different operating conditions such as substrate and filament temperatures, flow rate values, reactor pressure, deposition time etc. Besides, before the starting of the depositions, operating conditions for the PGMA, PPFDA and copolymer were determined according to the desired film thickness based on modeling results.

Initially, for PGMA thin film deposition, for instance, Chan and Gleason studied with PGMA deposition in iCVD system and they determined the general operating conditions for this coating material and explained the effects of changing surface temperature and monomer (GMA) partial pressure on the deposition rate and molecular weight of polymer coated on the substrate surface (Chan and Gleason 2006). Mao and Gleason investigated the effects of altering the filament temperature and ratio of initiator to monomer (GMA) flow on the molecular weight of the polymer produced at the end of the deposition (Mao and Gleason 2004). Considering these studies, operating conditions for PGMA deposition in this study were selected in order to achieve intended thickness of the film, and some parameters were changed with regard to the results obtained at the end of each PGMA deposition experiments.

Before the depositions, flow calibrations were done for each coating material in different MFCs to determine the flow rate values of monomer and initiator provided by mass flow controllers (MFCs) to iCVD system. To decide how much flow can be provided, GMA flow calibration was performed in MFC2 (calibrated before with GMA) and Manual MFC (MMFC) and TBPO in both MFC1 and MFC3 (calibrated before with nitrogen) by following the steps below:

- Coating material which will be calibrated, monomer or initiator, installed to the process channel where the related MFC is present in a stainless steels or custom-made Pyrex-steel container.
- Desired MFC count value is set on the control panel, then flow is started.
- When the flow value reached the set-value, manual valve closed, chamber is isolated and timer is started.
- Pressure vs. time difference data are recorded.
- From the collected pressure data, using the volume of the reactor (5572 cm^3), and reactor temperature value (298K), flow rate value (ccm) is calculated.
- The same steps are repeated until at least 4 points are obtained.

The calibration results of the GMA in MFC2 and MMFC and TBPO in MFC1 and MFC3 were given in the following figure.

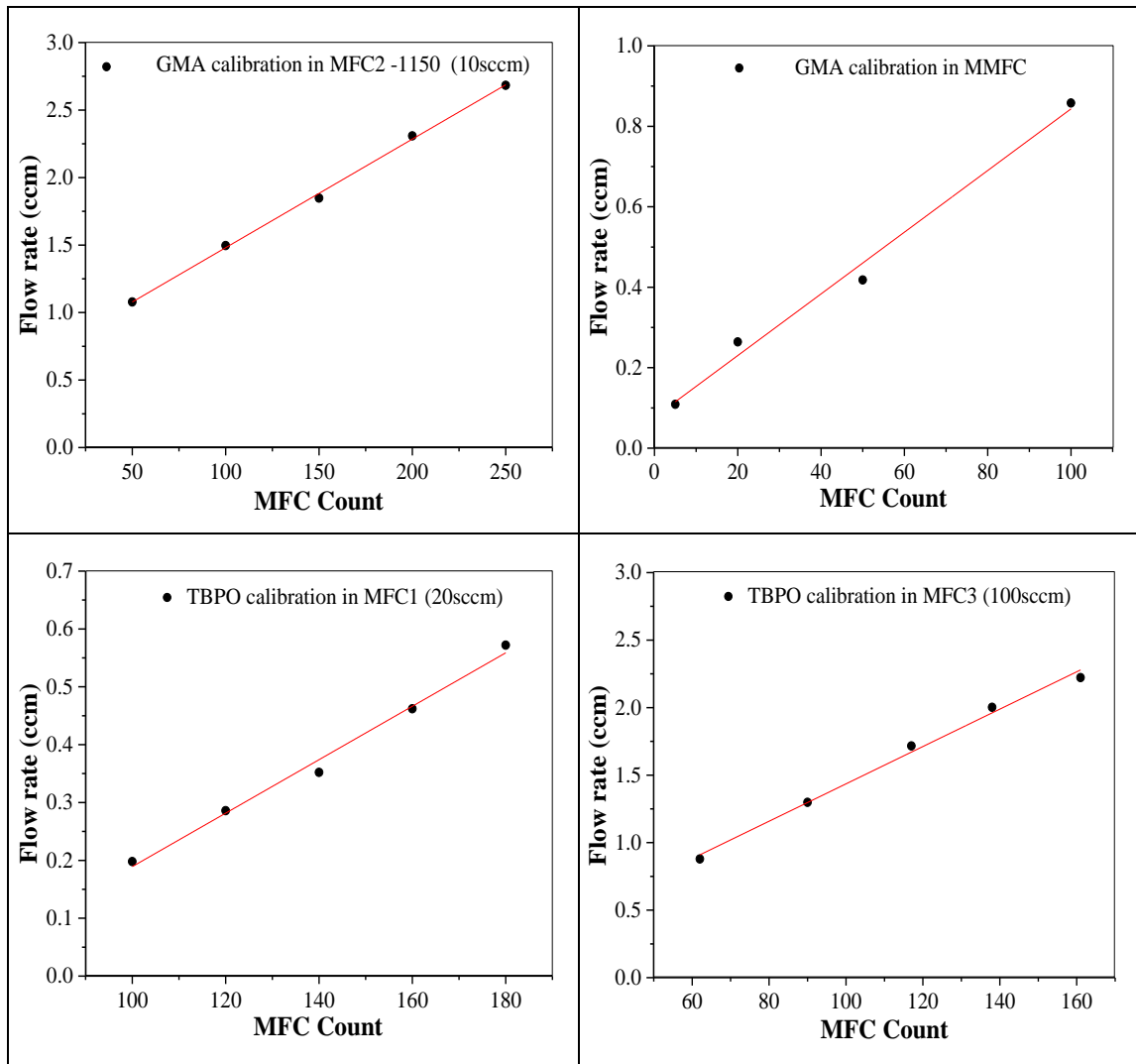


Figure 4.2. Calibration graphs of GMA in MFC2 and MMFC and TBPO in MFC1 and MFC3.

Flow rate values of GMA and TBPO were adjusted according to these calibration graphs and also other operating conditions were selected based on the literature studies.

The following table shows the deposition experiments that include operating conditions and thickness results of PGMA coating by using the iCVD system in this study.

Table 4.1. PGMA deposition experiment conditions and thickness results.

Monomer	Initiator	F_{monomer} (ccm)	$F_{\text{initiator}}$ (ccm)	P_{total} (mTorr)	$T_{\text{substrate}}$ ($^{\circ}\text{C}$)	T_{filament} ($^{\circ}\text{C}$)	Time (min)	Thickness (mm)	Deposition rate (mm/min)	P_M/P_{sat}	iCVD run
GMA	TBPO	1.5	1	250	35	330	6.5	78.2	12.03	0.02	61
GMA	TBPO	1.5	1	250	35	330	30	467	15.57	0.02	40
GMA	TBPO	1.5	1	300	35	330	30	580	19.33	0.03	62
GMA	TBPO	1.5	1	350	35	330	30	633	21.1	0.03	45
GMA	TBPO	1.5	1	400	35	330	30	702	23.40	0.03	42
GMA	TBPO	1.5	1	450	35	330	30	751	25.03	0.04	46
GMA	TBPO	1.5	1	500	35	330	30	813	27.1	0.04	44
GMA	TBPO	1.5	1	500	35	330	40	1080	27	0.04	53

In iCVD system, deposition influenced by flow ratio of initiator to monomer, $T_{\text{substrate}}$, T_{filament} and ratio of partial pressure to saturation pressure of monomer (P_M/P_{sat}). Therefore, suitable values to obtain good quality film coatings were selected on literature studies and previous experiments. For instance, the substrate temperature affects the adsorption of monomer to the substrate surface and as a result deposition rate is also affected. In order to improve the adsorption of monomer to the substrate surface $T_{\text{substrate}}$ kept lower than 50°C. However, when the temperature is decreased too much like 15 or 10°C, condensation will be observed because surface temperature also related with the saturation pressure of the monomer. When the P_M/P_{sat} approach to unity, the excess amount of monomer is adsorbed to the surface thus condensation occurs. At high temperatures like 45°C, monomer adsorption is not efficient and deposition rate becomes too low (Chan and Gleason 2006, Lau and Gleason 2006, Mittal 2013). In order to prevent these undesired cases, $T_{\text{substrate}}$ was chosen as 35°C which is not too low or too high, but this temperature value is not sufficient to obtain high quality coating, hence the flow ratio of initiator to monomer, T_{filament} and P_M/P_{sat} were also need to be considered. If the value of $F_{\text{initiator}}/F_{\text{monomer}}$ is very low, amount of monomer on the surface becomes high. On the other hand, if this ratio is very high, deposition rate excessively decreases owing to the inadequate monomer units and high amount of free radical that leads polymer chain termination instantly (Mao and Gleason 2004, Lau and Gleason 2006). Therefore, $F_{\text{initiator}}$ was selected as 1 ccm and F_{monomer} as 1.5 ccm to keep the deposition rate in average value preventing condensation and ensuring the uniform coating. Moreover, for polymerization reaction, free radicals in the reaction medium thus decomposition of the initiator with the hot filaments is significant. When the temperature of the filament is high, deposition rate increases. Additionally, T_{filament} and $T_{\text{substrate}}$ are related with each other in terms of transferring of free radicals to the surface of the substrate (Chan and Gleason 2006, Gupta and Gleason 2006, Lau and Gleason 2006). Thus, in this study, T_{filament} was selected as 330°C.

All these conditions were kept constant in this study but only total pressure was altered from 250 to 500 mTorr by considering P_M/P_{sat} value, to reach the desired film thicknesses. Because, the effect of P_M on deposition rate is very crucial (Lau and Gleason 2006, Mittal 2013) thus as in the Table 4.1, it was clearly observed that deposition rate rises when the pressure increases. However, pressure value is restricted between 250 and 500 mTorr. Very low P_{total} causes low partial pressure value of monomer and initiator that leads decreasing deposition rate. Also pressure upper limit was chosen as 500 mTorr

because at this pressure value approximately 800 nm film thickness was obtained at 30 min. In order to achieve 1 μm thickness, time was extended to 40 minutes.

After the depositions necessary thickness measurements and characterization methods were performed and results for PGMA coating were given in the following sections.

4.1.1. Thickness Measurement with Reflectometer for PGMA Coatings

After the coating of PGMA on the c-Si substrate with iCVD system, thickness measurements were carried out for all coatings of PGMA by using reflectometer device. In this measurement, estimated thickness value was added to the software then measured and calculated thickness results were analyzed and compared by the software. The actual thickness value was obtained when these results were in good agreement with each other. For PGMA coatings results were taken in tabulated form for each one, however, only three of them that are thin, medium thickness and thick coatings were demonstrated in the following graphs.

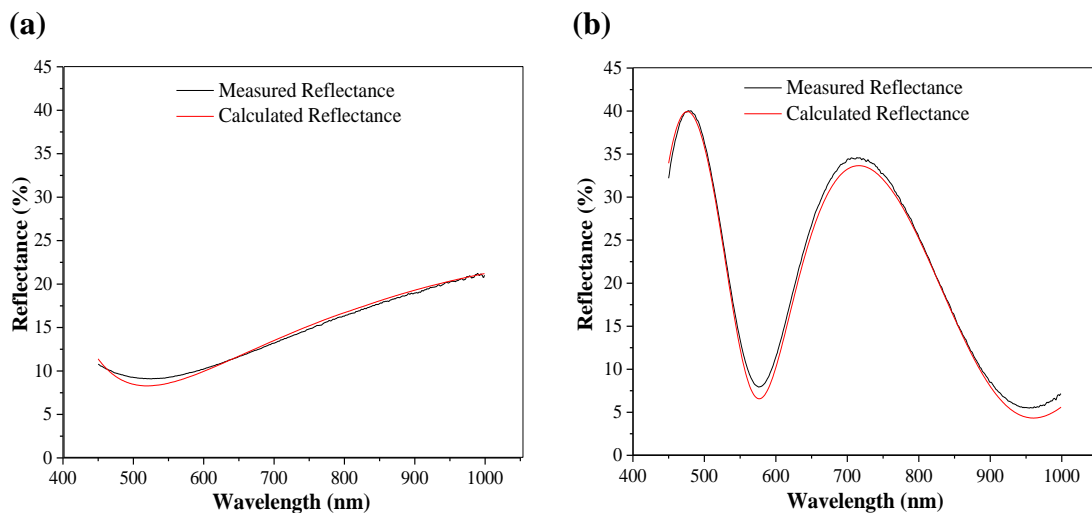


Figure 4.3. Reflectometer results of (a) iCVD61, (b) iCVD40 and (c) iCVD53 depositions for PGMA coatings on c-Si.

(Cont. on next page)

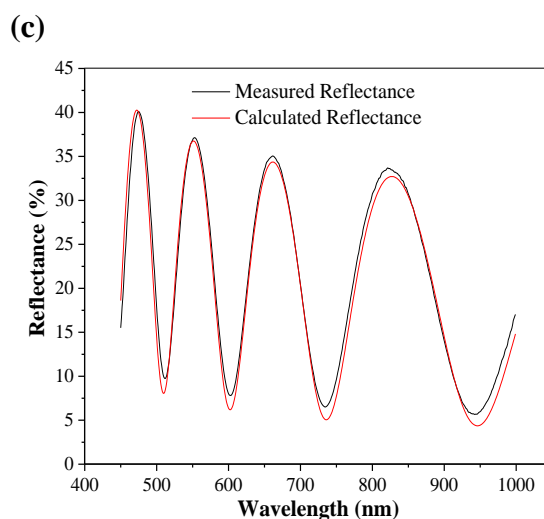


Figure 4.3. (Cont.)

Graphs in Figure 4.3 obtained by using the tabulated data taken from the reflectometer. Data belong to 78.2 nm, 467 nm and 1.08 μm thick PGMA films on c-Si substrates. According to these graphs, calculated and measured results agree well with each other although minor discrepancies observed at some points. It should be noted that during deposition, glass (microscope slide) and c-Si substrates were placed in iCVD chamber together, but measurement in the reflectometer could be performed only for samples on c-Si substrates. Since measured and calculated data did fit well, for iCVD61, iCVD40 and iCVD53 depositions, optical performance of the glass substrate coated with these coatings do not affect optical performance of glass as suggested as explained by simulation of PGMA films on glass substrates in Chapter 3.

4.1.2. FTIR Analysis of GMA Monomer and PGMA Film

In order to decide whether free radical polymerization properly takes place or not on the surface of the c-Si substrate and indicate the coating film purity FTIR analysis was performed for GMA monomer and PGMA film. FTIR spectra for both are given in Figure 4.4

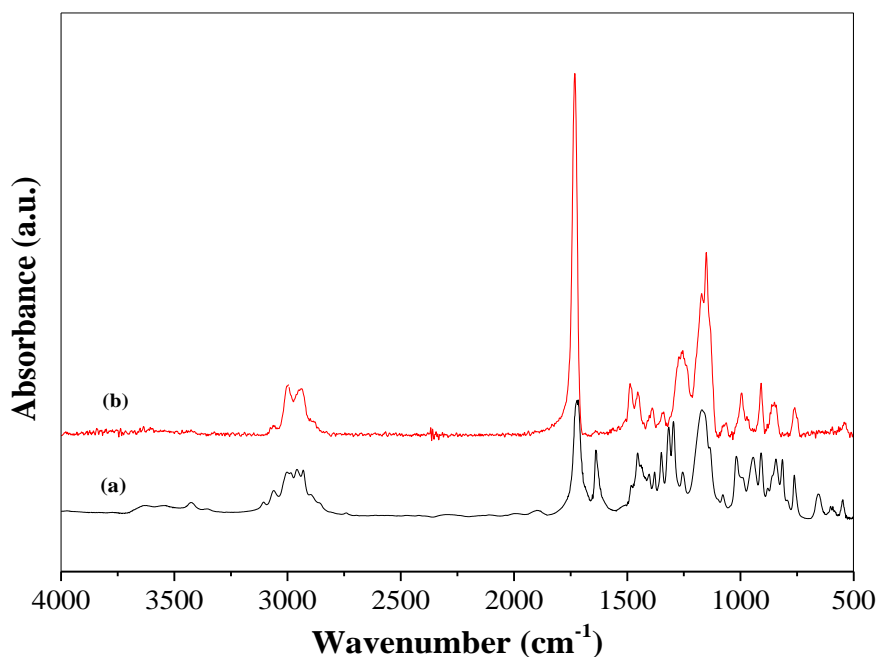


Figure 4.4. FTIR spectra of (a) GMA monomer and (b) PGMA film synthesized in iCVD system.

FTIR spectrum of PGMA belongs to the thickest film obtained by iCVD deposition, and Figure 4.4 illustrates that in both monomer (GMA) and polymer (PGMA) spectra, prominent characteristic peaks at about 3000 and 2932 cm^{-1} are clearly seen.

These peaks belong to C-H symmetry and asymmetry stretching caused by CH_3 and CH_2 groups are located in structures of the GMA and PGMA (Mohammed Safiullah, Abdul Wasi et al. 2014). Additionally, the peak at 1730 cm^{-1} that is the most distinct one is assigned to carbonyl group (C=O) stretching vibration (Bakker, Verlaan et al. 2007, Mohammed Safiullah, Abdul Wasi et al. 2014). The most significant peak is at 1640 cm^{-1} seen clearly in GMA spectrum while not observed in that of PGMA because it is the evidence that no monomer unit is present in the film after the deposition (Bakker, Verlaan et al. 2007). Lastly, the characteristic peaks of GMA which are at 906, 846 and 760 cm^{-1} and they belong to epoxy group stretching, clearly seen in both monomer and polymer spectra (Mao and Gleason 2004, Gupta and Gleason 2006, Mao and Gleason 2006, Bakker, Verlaan et al. 2007, Mohammed Safiullah, Abdul Wasi et al. 2014).

4.1.3. SEM Analysis of PGMA Film

In order to investigate film morphology and surface uniformity of coated PGMA film on c-Si substrate in iCVD system, SEM images (as shown in Figure 4.5) of uncoated c-Si substrate and coated with PGMA by using the iCVD53 were taken.

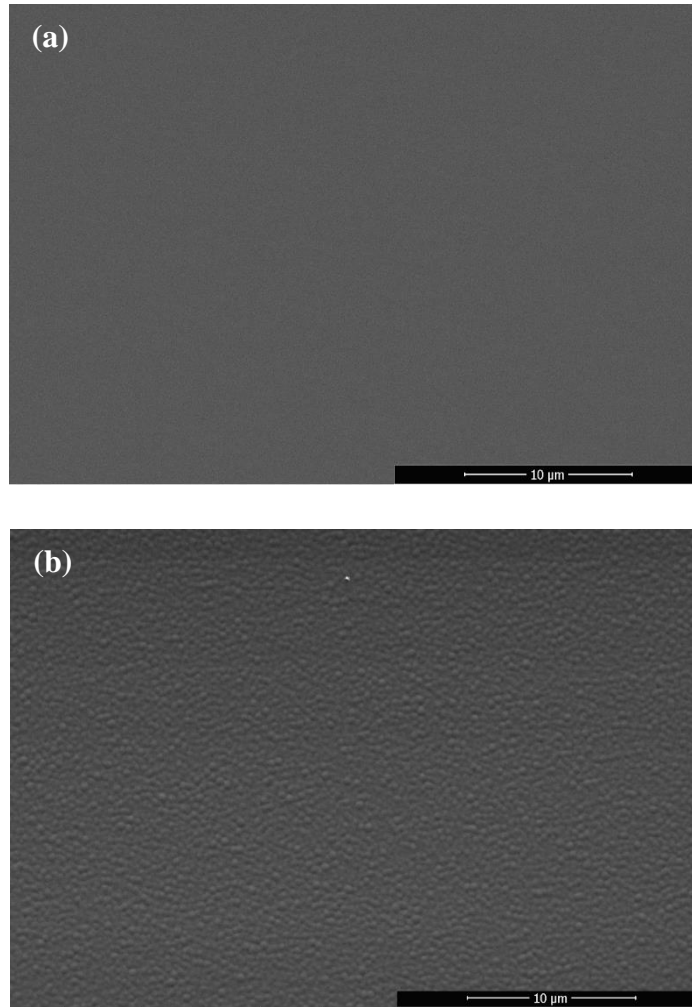


Figure 4.5. SEM images of (a) uncoated c-Si substrate (b) c-Si coated with $\sim 1 \mu\text{m}$ PGMA film.

In Figure 4.5, surface appearance of uncoated and coated substrate with PGMA can be seen. It was observed that PGMA film covered entire substrate surface uniformly without any visible defects such as pin holes and scratches etc. Besides, bead-like morphology was seen in PGMA film as previously reported in literature (Mao and Gleason 2004, Mohammed Safiullah, Abdul Wasi et al. 2014). It is claimed that $1 \mu\text{m}$ thickness film was obtained using 330°C filament temperature and this high temperature

causes high amount initiator activated, providing deposition with non-uniform manner. Therefore, spherical shapes are observed on the coating. However, if the filament temperature is lowered, disconnected curled rod shape morphology would be seen on the surface due to the inadequate free radical in the reaction medium.

4.1.4. AFM Results of PGMA Film

To investigate the surface roughness of the films which have different thicknesses after the deposition experiments, AFM analysis was performed. Results of bare c-Si and coated PGMA which have medium thickness and thick film were demonstrated in the Figure 4.6 and 4.7, respectively.

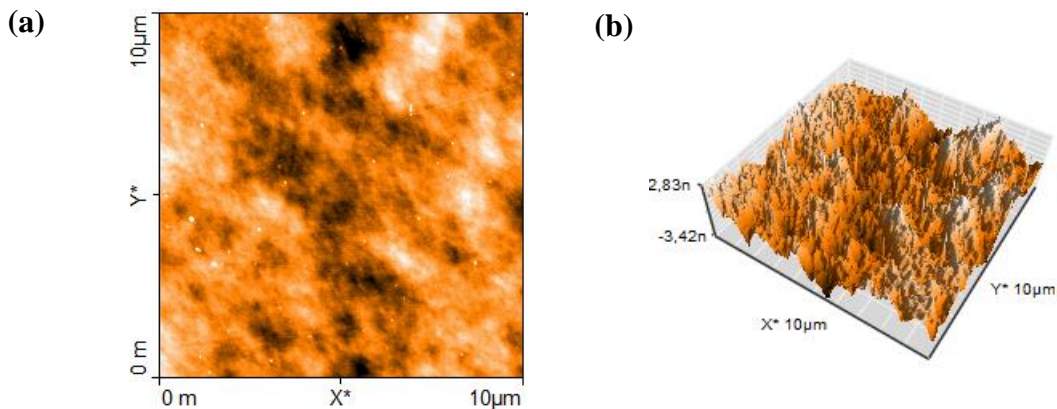


Figure 4.6. AFM results of bare c-Si substrate (a) color map (b) 3D view.

In Figure 4.6, AFM images of bare c-Si substrate were shown. Average surface roughness, R_a , and root mean square (RMS) roughness, R_q , of the substrate surface were found as 8.77 \AA and 10.9 \AA respectively. According to these results, the surface roughness of the c-Si is quite small and c-Si substrate surface is extremely smooth.

In order to demonstrate the effect of coating on the surface roughness, AFM analysis was performed for PGMA coatings deposited on c-Si substrate that have two different thickness values and results of them were given in Figure 4.7.

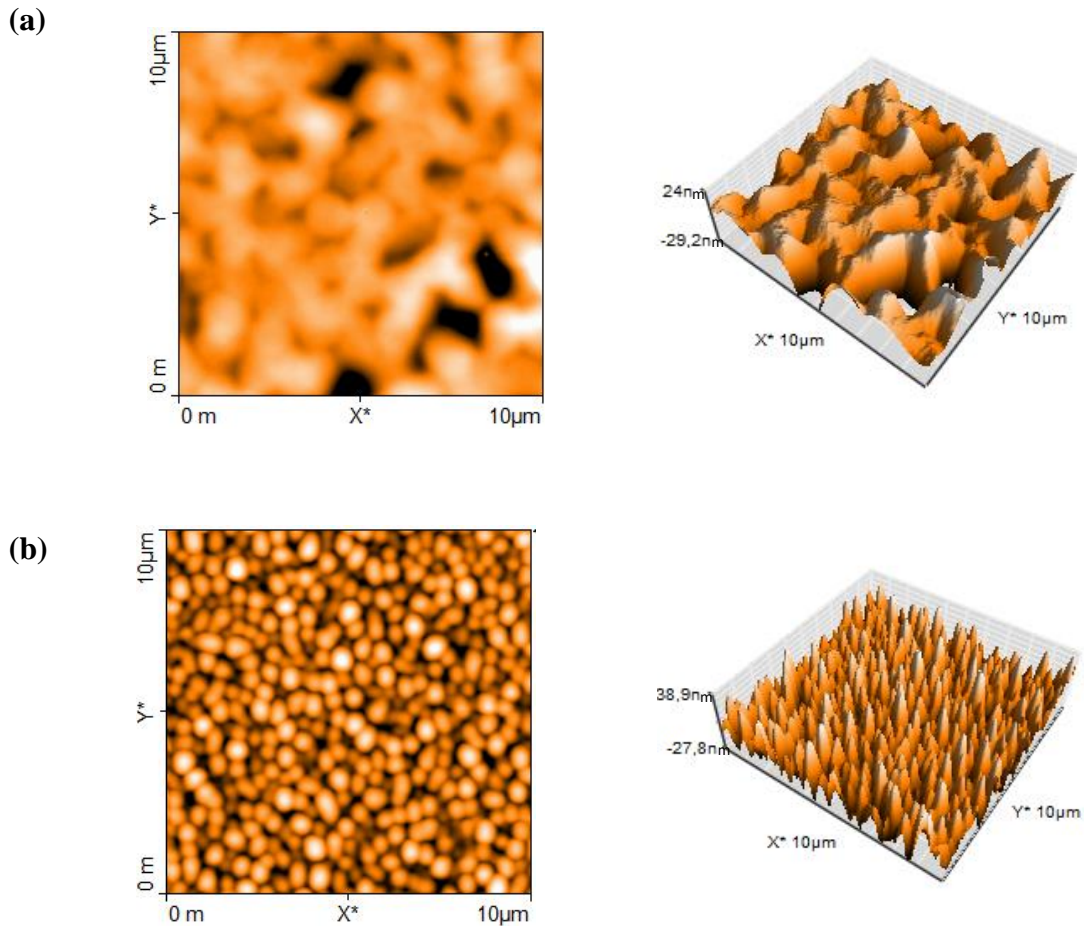


Figure 4.7. AFM color map and 3D images of PGMA coating with (a) ~500 nm and (b) 1 μm thickness.

In figure above, AFM images of PGMA coating with two different film thicknesses were shown and for both coatings R_a and RMS roughness, R_q , values were determined. For medium thickness PGMA coating R_a and R_q were found as 46.5 \AA and 54.9 \AA , respectively, and for thick coating R_a and R_q were determined to be 125.6 \AA and 149.4 \AA , respectively. When R_a and R_q values of PGMA coatings were compared with c-Si, it was observed that coating on c-Si increases surface roughness. Besides, when the difference of surface roughness between medium thickness and thick PGMA coatings were examined it was concluded that as the thickness of the coating increases, surface roughness also increases. This result is expected based on previous literature studies (Bakker, Verlaan et al. 2007, Park, Lee et al. 2015).

4.1.5. Contact Angle Measurement for PGMA Film

Although GMA films are not hydrophobic, contact angle measurement for PGMA film was performed to examine the surface roughness effect on the contact angle. In Figure 4.8 contact angle results of bare c-Si and 1 μm PGMA film were given.


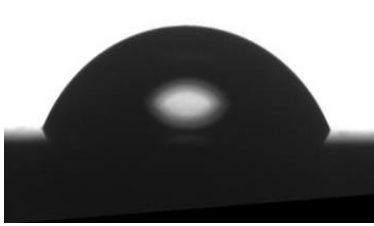
	Coated c-Si with PGMA
Uncoated c-Si	Thickness: ~500 nm
	
Contact Angle: 27°	Contact Angle: 64°

Figure 4.8. Contact angle results for bare c-Si substrate and c-Si coated with ~500 nm PGMA film.

It was observed that the contact angle for bare c-Si substrate is smaller than coated with PGMA film and this is the expected result because quite small surface roughness value of bare c-Si was obtained given in the AFM results in previous part while higher surface roughness value found for the PGMA film. Therefore, it can be concluded that surface roughness increasing leads to an observable increase of the contact angle value.

4.1.6. Surface Quality Test with Optical Microscopy for PGMA Film

In order to examine surface morphology and quality of the films optical microscopy analysis was performed. Any scratches and pin holes which may not be visible during visual inspection can be seen under optical microscope and defect density can be calculated. Surface images of 1 μm thick PGMA film was taken at 40x and 80x magnifications by using optical microscopy. These images were shown in Figure 4.9.

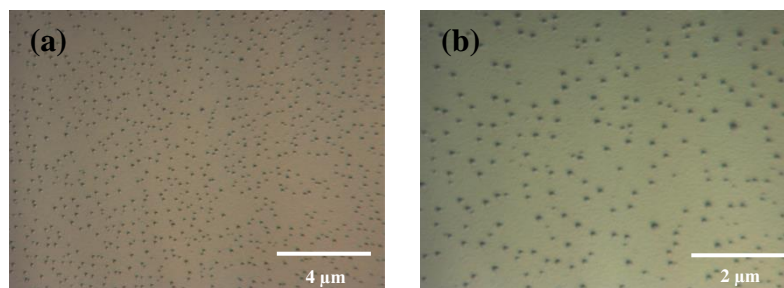


Figure 4.9. Surface images of 1 μ m PGMA film at (a) 40x and (b) 80x magnifications.

In Figure 4.9, small spherical structures were observed on the PGMA film surface. According to literature, this illustrates that polymerization reaction takes place properly thanks to the sufficient amount of free radicals activating monomer molecules on the substrate surface (Mao and Gleason 2004). No scratches or pin holes were found on the surface of PGMA film synthesized by iCVD. Since the mechanical properties of GMA is quite good handling of the samples after deposition did not result in any observable damage to PGMA films.

4.2. PPFDA Deposition in iCVD System

In this study, self-cleaning and super hydrophobic protective coating fabrication is one of the main objectives. For this reason, fluorinated acrylate monomer PFDA was chosen as precursor because it has low surface energy (5.6-7.8 mNm⁻¹) and high hydrophobicity due to CF₃ side groups in its structure (Martin, Lau et al. 2007, Gupta, Kapur et al. 2008, Gleason 2015).

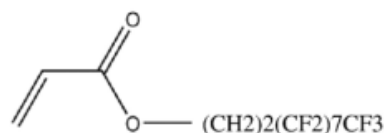


Figure 4.10. 1H, 1H, 2H, 2H, (Perfluorodecyl) acrylate (PFDA) structure.

As in PGMA deposition part, first flow calibration was performed to determine the flow rate values of PFDA in MFC2 (calibrated before with GMA) and the calibration result are given in Figure 4.11.

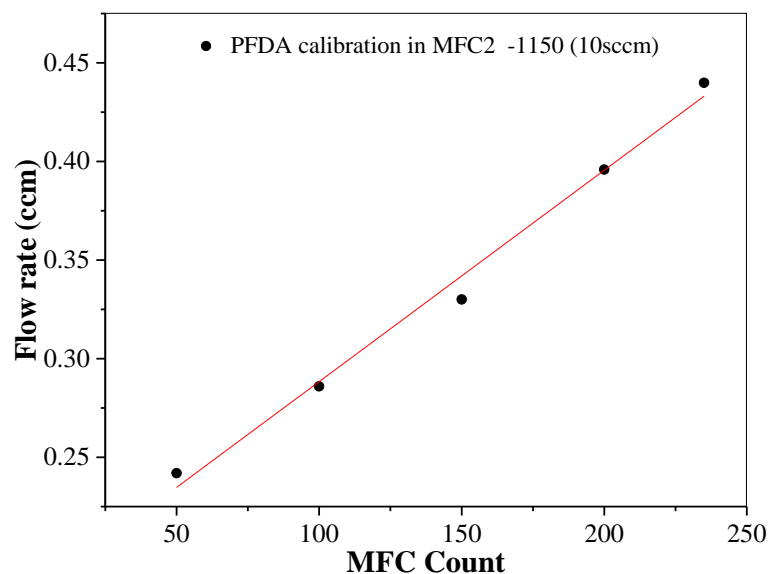


Figure 4.11. Calibration result of PFDA in MFC2.

Operating conditions of PPFDA deposition experiments were decided by examining the related literature studies of PFDA deposition by CVD. For instance, Gupta and Gleason used PFDA to produce low surface energy films and at the end of the depositions they concluded that with low substrate temperature and high monomer partial pressure deposition rate and molecular weight increased (Gupta and Gleason 2006). Conclite, Shi and Gleason used PFDA as monomer in their study to obtain super hydrophobic surfaces and also controlled crystallinity of the film by adjusting substrate and filament temperatures, and flow ratio of initiator to monomer (Coclite, Shi et al. 2013). Gupta and Gleason coated pores of membranes with PPFDA via iCVD to provide hydrophobic surfaces. They reported that deposition rate increases with low substrate temperature and high monomer partial pressure (Gupta and Gleason 2009). Based on these literature studies, the operating conditions for PPFDA depositions were decided by considering the desired thickness of the films.

PPFDA film depositions were performed using the PFDA monomer and TBPO as initiator.

Table 4.2. PPFDA deposition experiment conditions and thickness results.

Monomer	Initiator	F_{monomer} (ccm)	$F_{\text{initiator}}$ (ccm)	P_{total} (mTorr)	$T_{\text{substrate}}$ ($^{\circ}\text{C}$)	T_{filament} ($^{\circ}\text{C}$)	Time (min)	Thickness(mm)	Deposition rate (nm/min)	P_M/P_{sat}	iCVD run
PFDA	TBPO	0.35	0.5	50	35	260	5	154	30.80	0.035	73
PFDA	TBPO	0.35	0.5	50	35	260	30	1090	36.33	0.035	72
PFDA	TBPO	0.35	0.5	60	35	260	20	724	36.20	0.042	70
PFDA	TBPO	0.35	0.5	60	35	260	30	1170	39	0.042	68
PFDA	TBPO	0.35	0.5	60	35	260	10	352	35.2	0.042	69
PFDA	TBPO	0.35	0.5	60	35	260	5	222	44.40	0.042	71

In PGMA deposition part, effects of operating parameters such as $T_{\text{substrate}}$, T_{filament} , initiator to monomer flow ratio and P_M/P_{sat} were explained briefly. Considering the influence of these parameters, operating conditions were set carefully. For example, Gupta and Gleason changed the initiator to monomer flow ratio from 1.22 to 6.3 and results showed that when the ratio increased deposition rate decreased (Gupta and Gleason 2006). Also, Gupta, Kapur et al. used the initiator to monomer ratio became 2.3 for their study (Gupta, Kapur et al. 2008). Based on these studies, monomer and initiator flow rates were selected as 0.35 and 0.5 ccm for PPFDA to prevent monomer condensation and non-uniform coating. Substrate temperature, $T_{\text{substrate}}$ was set to 35°C as for PGMA depositions because this temperature is the suitable for the adsorption of the monomer and free radical on the substrate surface effectively. Total pressure of the system was set to between 50 and 60 mTorr. However, when the pressure increased further, monomer condensation was observed. At lower pressures deposition rate decreased to unacceptable levels. In order to achieve desired thickness values, T_{filament} was set to 260°C. At the end of the depositions, thickness measurements were performed by reflectometer before other characterization tools were applied.

4.2.1. Thickness Measurement with Reflectometer for PPFDA Coatings

For all PPFDA coatings, thickness measurement were performed using reflectometer, but only thin (~100 nm), medium (~500 nm) and thick (~1 μm) coating results were illustrated in Figure 4.12 below.

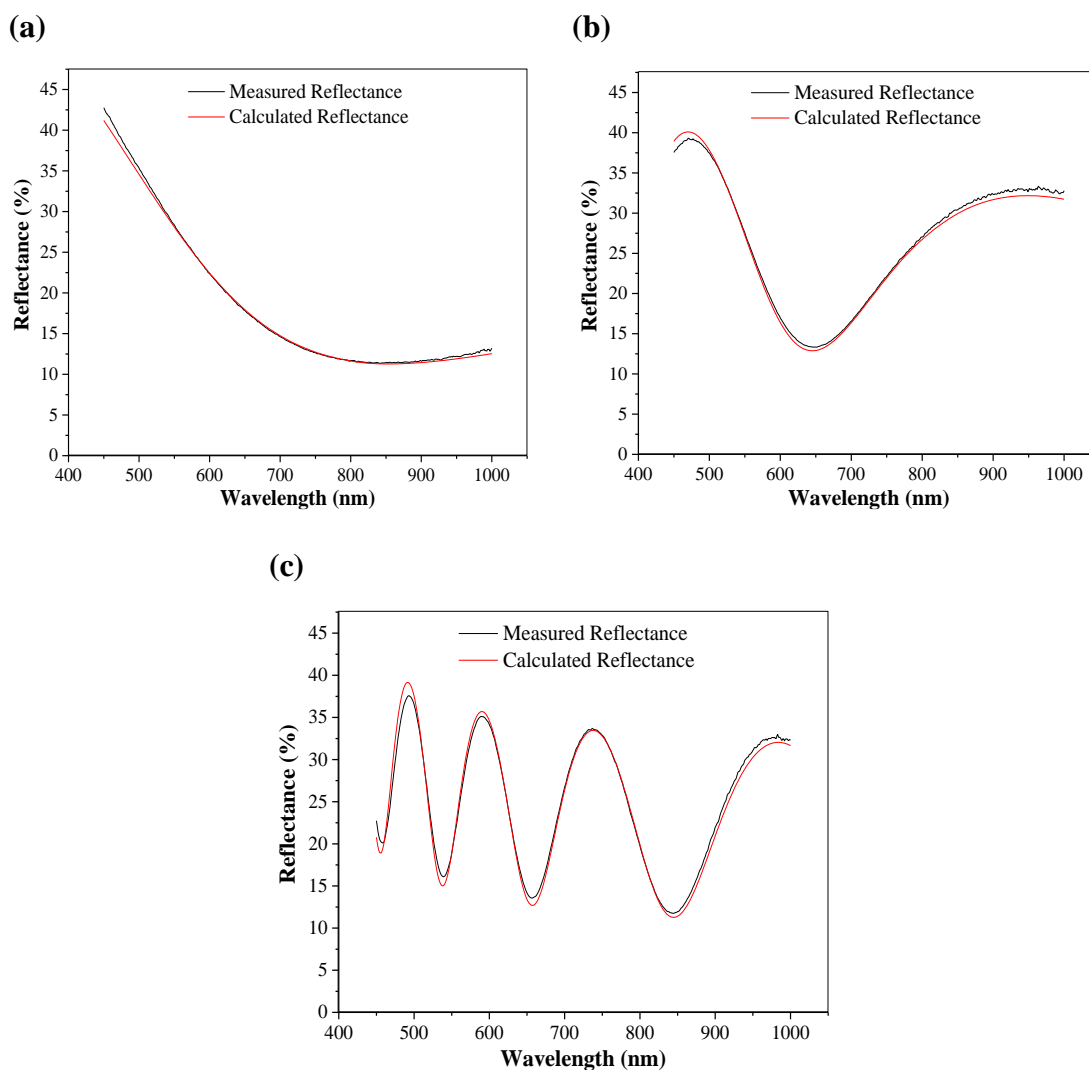


Figure 4.12. Reflectometer results of (a) iCVD73, (b) iCVD69 and (c) iCVD72 depositions for PPFDA coatings on c-Si.

According to Figure 4.12, 154 nm, 352 nm and 1.09 μm thicknesses were obtained for iCVD73, iCVD69 and iCVD72 samples, respectively. It was observed that calculated and measured results of these depositions mostly agreed with each other. Therefore, these thickness values are acceptable for the iCVD73, iCVD69 and iCVD72 deposition experiments. In PPFDA coatings, the same thickness effect observed on the reflectance curve behavior as observed in PGMA samples (increasing of sine wave with thickness and high reflection region shifting to right side). PPFDA film synthesis in iCVD system was also performed on glass substrates but thickness measurement could only be performed for coatings on c-Si substrates reliably. Therefore, c-Si used as reference substrate in this study. After depositions, thickness measurements and optical transmission curves of modeled and fabricated coatings were compared. In these

depositions, 154 nm, 352 nm and 1.09 μm thicknesses were achieved with quite good fitted data and it can be said that the optical performance of the glass surface is not affected in these samples as suggested by simulation results in Chapter 3.

4.2.2. FTIR Analysis of PFDA Monomer and PPFDA Film

FTIR analysis of PFDA monomer and PPFDA coating film were performed and their spectra compared with each other in the following figure to determine if the polymerization on c-Si substrate occur completely and if monomer molecules are still present on the substrate.

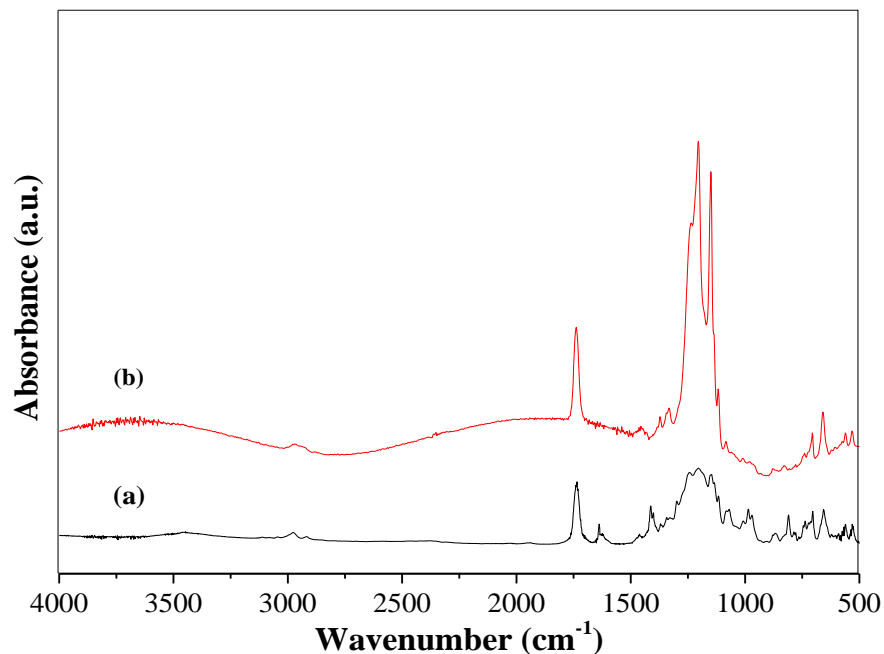


Figure 4.13. FTIR spectra of (a) PFDA monomer and (b) PPFDA film synthesized in iCVD system.

Figure 4.13 shows FTIR spectra of PFDA monomer and PPFDA polymer film. In monomer spectrum only, two specific peaks are present around 3020 cm^{-1} and 2980 cm^{-1} due to C=C double bond. These peaks are not seen in the polymer spectrum because in polymerization, unsaturated bonds in monomer transforms into saturated form (Gupta and Gleason 2006). Although in polymer spectrum the above peaks are not observed, the peaks observed at 2970, 2914 and 2864 cm^{-1} are assigned to C-H stretching and CH₂ vibrations due to saturated bond formed after the polymerization. Besides, the most specific peak seen in both spectra at 1740 cm^{-1} is associated with carbonyl group (C=O)

stretching (Gupta and Gleason 2006, Luis and Gleason 2013). Furthermore, in the monomer spectrum only the characteristic peaks observed at 1637, 1620, 1413, 1401, 995 and 968 cm^{-1} are assigned to C=C double bond and these peaks like 3010 and 2980 cm^{-1} are not seen in the polymer spectrum because after the polymerization saturated carbons consist of these unsaturated bonds (Gupta and Gleason 2006). Lastly, the most significant characteristic peaks at 1246, 1206 and 1150 cm^{-1} are clearly observed in both monomer and polymer spectra, and these peaks form due to asymmetric, symmetric stretching of -CF₂- group and -CF₂-CF₃ group, respectively (Gupta and Gleason 2006, Luis and Gleason 2013, Yoo, You et al. 2013).

4.2.3. SEM Analysis of PPFDA Film

SEM analysis was performed also for PPFDA films to examine film morphology. SEM image of a PPFDA film on c-Si substrate is given in Figure 4.14.

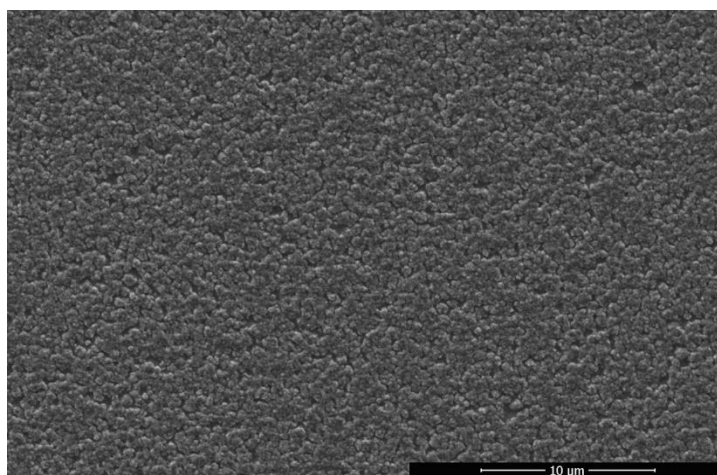


Figure 4.14. SEM image of c-Si coated with 352 nm PPFDA film.

It was seen that polymerization taken place successfully on the surface of the c-Si substrate because this image has uniform coating over the entire substrate surface and no apparent defects are visible. In addition, surface of the coating had sponge like structure.

PPFDA film deposition using iCVD was performed not only on the flat surface but also on porous and three dimensional surfaces. In order to show hydrophobicity of PPFDA coated surfaces, paper napkin was used as substrate material. SEM images of uncoated and coated napkins wetted with liquid dye are given in Figure 4.15.

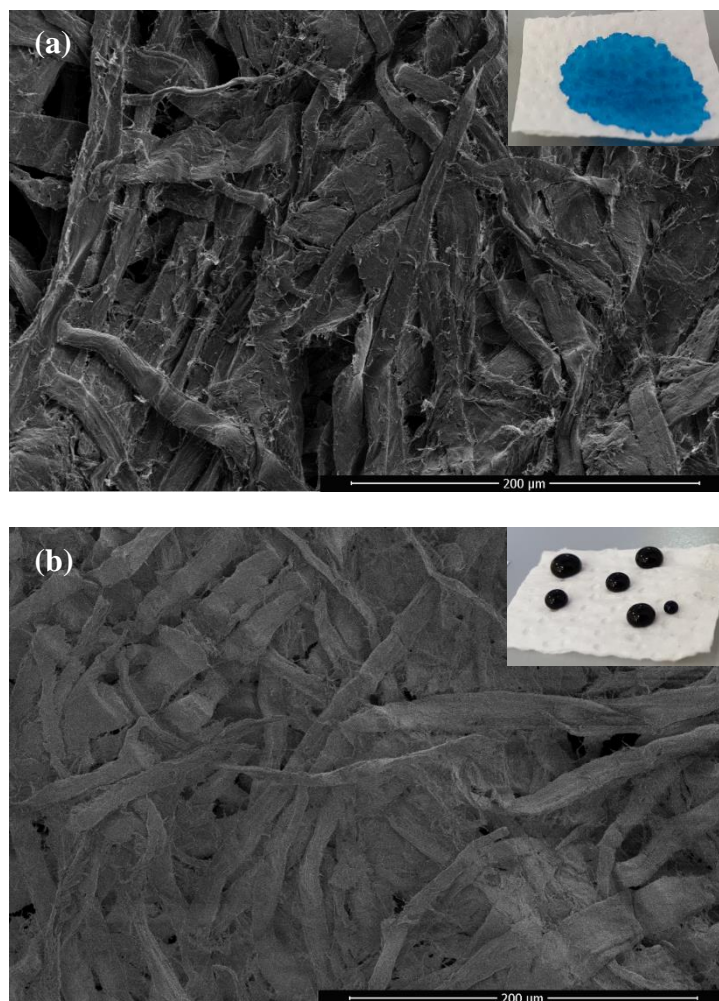


Figure 4.15. SEM images of (a) uncoated napkin (b) coated napkin with PPFDA film.

In Figure 4.15, it is clearly seen that the uncoated napkin has more porous structure and also the fiber appearance more distinct than the coated napkin because gaps were filled and smoother surface was obtained due to the deposition with PPFDA. Besides, when the dye dropped on the uncoated napkin, it was soaked immediately by napkin while dye droplets formed beads on the surface of the coated napkin due to very hydrophobic surface.

4.2.4. AFM Results of PPFDA Film

AFM analysis was performed for PPFDA coatings with different thicknesses to examine the effect of thickness on surface morphology as shown in Figure 4.16.

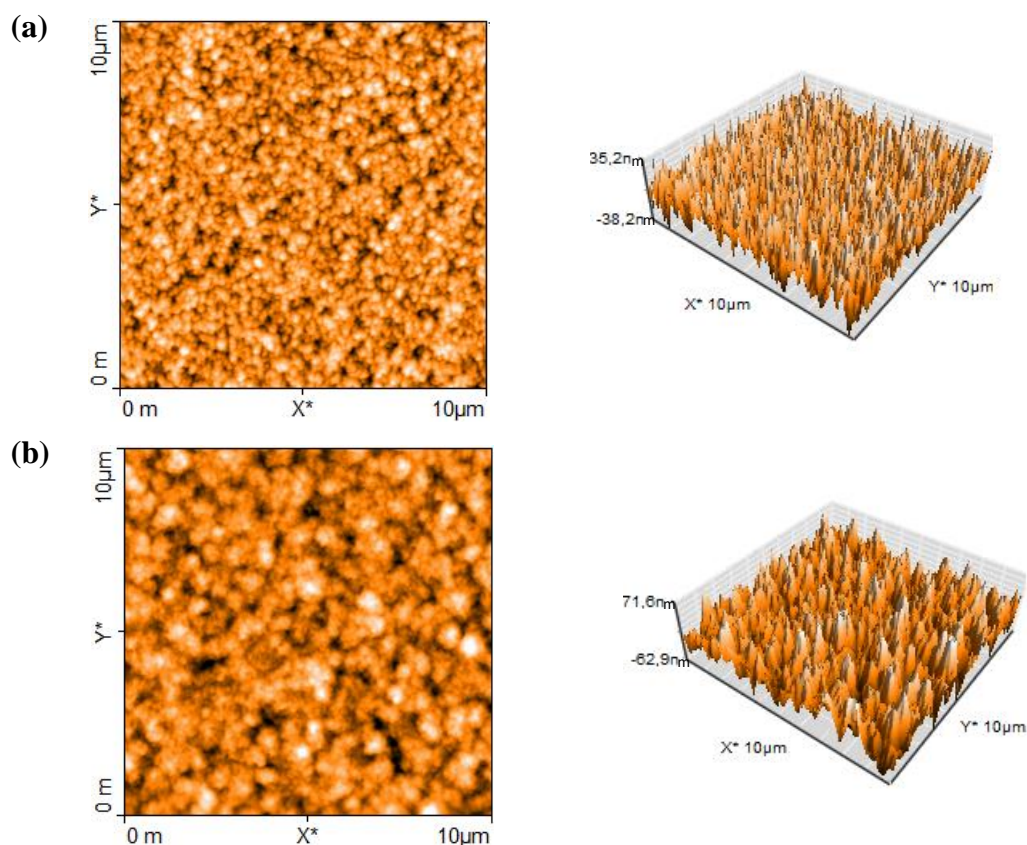


Figure 4.16. AFM color map and 3D images of PPFDA coating with (a) medium thickness 352 nm and (b) 1.09 μm thickness.

In Figure 4.16, AFM images of PPFDA coatings with two different thicknesses were given and according to these images, compact spherical clusters are present on the surface. Besides, Ra and RMS roughness, Rq, values were determined for both coatings. For 352 nm thick coating Ra and Rq values were 97.2 \AA and 120.9 \AA , respectively. Also for 1.09 μm thick coating Ra and Rq were found as 180 \AA and 224.8 \AA , respectively. When the surface roughness values of these two coatings were examined it was concluded that surface roughness increases with increasing of film thickness.

4.2.5. Contact Angle Measurement for PPFDA Film

In order to measure hydrophobicity of PPFDA films, contact angle measurement was performed for bare c-Si, and substrates coated with PPFDA. For this measurement 1.09 μm thick PPFDA was used and also the effect of surface roughness on the contact angle was examined.


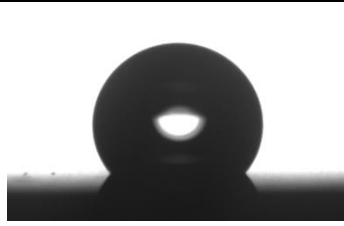
	Coated c-Si with PPFDA
Uncoated c-Si	Thickness: 1.09 μm
	
Contact Angle: 27°	Contact Angle: 132°

Figure 4.17. Contact angle results for bare c-Si substrate and c-Si coated with 1.09 μm PPFDA coating.

In figure 4.17 it was determined that the contact angle of 1.09 μm film is 132°, clearly showing a very hydrophobic surface. Besides, surface roughness increment causes increasing of contact angle value as can be seen when AFM and contact angle results of bare c-Si and PPFDA films are compared with each other. Ra and Rq values of bare c-Si were determined as 8.77 Å and 10.88 Å, respectively. On the other hand, Ra and Rq values of PPFDA film were found to be 180 Å and 224.8 Å. Therefore, contact angle of coated c-Si substrate with PPFDA film found as quite high (132°) when compare with bare c-Si contact angle (27°) and this provides super hydrophobic surface for the coating on flat surface which is very significant property and desired result for this study (Gupta and Gleason 2006, Gupta, Kapur et al. 2008, Gupta and Gleason 2009).

4.2.6. Surface Quality Test with Optical Microscopy for PPFDA Film

Surface quality tests which are based on MIL standards, were performed for 1.09 μm thick PPFDA coating by optical microscopy. Surface images were taken at 40x and 80x magnifications, respectively. These images are given in Figure 4.18.

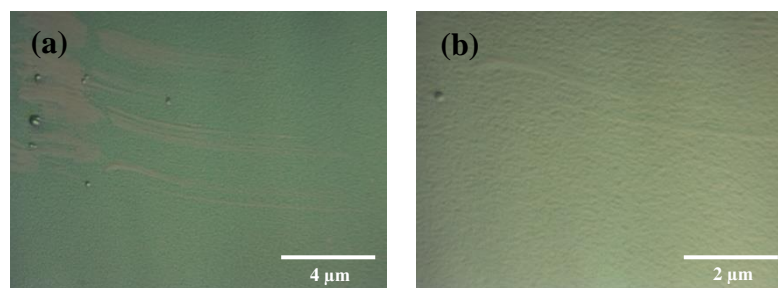


Figure 4.18. Surface images of 1.09 μm PPFDA film at (a) 40x and (b) 80x magnifications.

Relatively non-uniform surface morphology was observed for PPFDA films under optical microscope. Additionally, scratches on the coating surface were observed but these were not related to iCVD deposition but formed when the coated substrate was taken from the reactor using Teflon tweezers thanks to poor mechanical properties of PFDA. Although substrates and reaction chamber were cleaned before every deposition, some dust particles were observed film surface. It is reasonable to assume that during the transport the samples from reaction chamber to the sample box, and during characterization dust particles in the laboratory environments stick to freshly coated surface.

4.3. Copolymer P(GMA-PFDA) Deposition in iCVD System

In order to synthesize thin films which have good mechanical properties and self-cleaning and super hydrophobic surface, copolymer thin films was performed in iCVD system by using GMA and PFDA as monomers. To carry out the copolymerization, GMA monomer jar was installed to the Manual MFC channel and PDA monomer container was attached to the MFC2 channel. Because the maximum flow rate value of PFDA in MFC2 channel was ~ 0.4 ccm, GMA flow rate adjusted according to PFDA.

Copolymer deposition parameters were selected based on previous studies of homopolymer deposition. To avoid monomer condensation, slightly lower flow rates were used to lower P_m/P_s ratio, but still get a decent polymerization rate. Also, $T_{\text{substrate}}$ was adjusted as 35°C similar to PGMA and PPFDA deposition. T_{filament} was set to 300°C to increase the deposition rate. Total pressure value selected as 200 mTorr.

Table 4.3 list the process conditions used in copolymer deposition using GMA and PFDA monomers.

Table 4.3. Copolymer deposition experiment conditions and thickness results.

iCVD run	Monomer 1	Monomer 2	Initiator	F _{monomer,1} (ccm)	F _{monomer,2} (ccm)	F _{initiator} (ccm)	P _{total} (mTorr)	T _{substrate} (°C)
iCVD59	GMA	PFDA	TBPO	0.42	0.42	1.2	200	35
iCVD77	GMA	PFDA	TBPO	0.27	0.42	1.2	200	35

Table 4.3. (Cont.) Copolymer deposition experiment conditions and thickness results.

iCVD run	Monomer 1	Monomer 2	Initiator	T _{filament} (°C)	Time (min)	Thickness (nm)	Deposition rate (nm/min)
iCVD59	GMA	PFDA	TBPO	300	7.5	670	89.33
iCVD77	GMA	PFDA	TBPO	300	5	574	114.80

4.3.1. Thickness Measurement with Reflectometer for Copolymer Films

For two different copolymer coatings, thickness measurements were performed using the reflectometer device and results were shown in Figure 4.19.

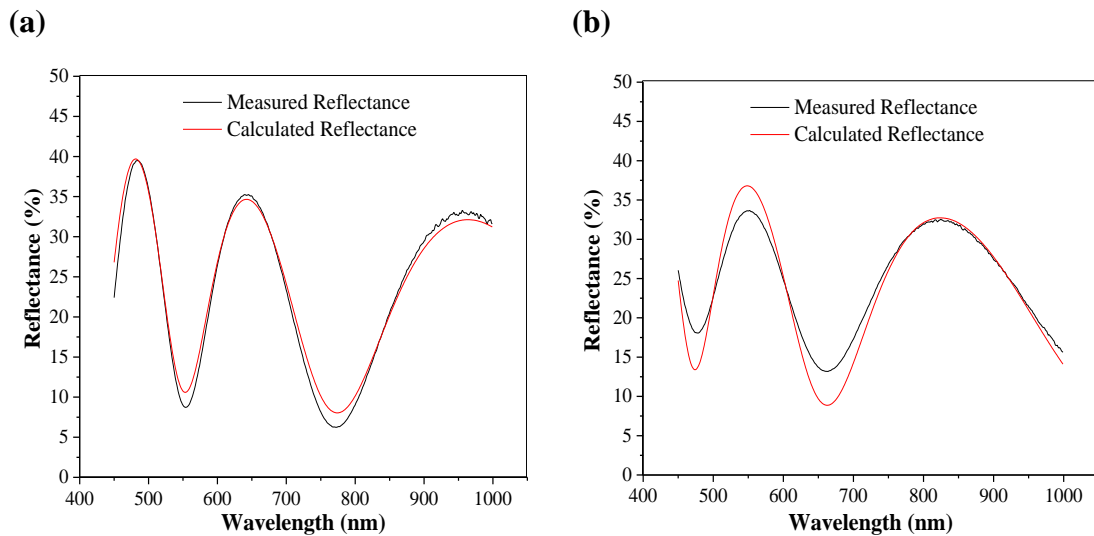


Figure 4.19. Reflectometer result of (a) iCVD59 and (b) iCVD77 depositions for Copolymer coatings on c-Si.

In Figure 4.19, thickness measurement results of iCVD59 and iCVD77 are given. Measured and calculated values of iCVD59 and iCVD77 coating films fits reasonably well with each. There is no significant difference between measured and calculated data of the thickness results of the films, therefore, these results are acceptable and thickness of the films were calculated as 670 and 574 nm, respectively. Therefore, according to this

experimental and simulated data, optical performance of the surface does not change with copolymer film coating.

4.3.2. FTIR Analysis of Copolymer Films

In order to investigate the composition of PGMA and PPFDA in the copolymer, FTIR analysis was performed. FTIR spectra of homopolymer PGMA and PPFDA and also copolymers having different composition of PGMA and PPFDA are given in Figure 4.20.

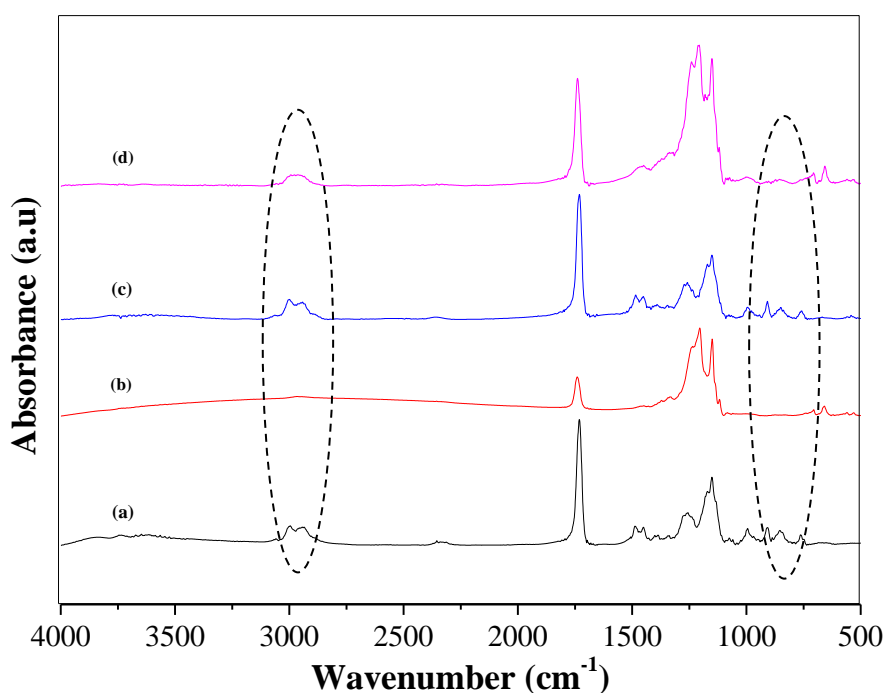


Figure 4.20. FTIR spectra of (a) homopolymer PGMA, (b) homopolymer PPFDA, (c) copolymer P(GMA-PFDA) deposited in iCVD59 and (d) copolymer P(GMA-PFDA) deposited in iCVD77.

In figure above FTIR spectra of homopolymer and copolymer films were compared with each other. It was observed that FTIR spectrum of copolymer film deposited in iCVD59 experiment contains epoxy peaks at 908, 847 and 760 cm^{-1} similar to homopolymer PGMA spectrum. Besides, the characteristic symmetry and asymmetry C-H stretching peaks at about 3000 cm^{-1} are clearly observed in copolymer iCVD59. On the other hand, in spectrum of copolymer deposited in iCVD77 experiment, very small epoxy peaks appear. Homopolymer PPFDA do not include any of these peaks like that of the peaks at around 3000 cm^{-1} . However, characteristic -CF₂- and -CF₂-CF₃ stretching

peaks of pure PPFDA at around 1250 and 1150 cm^{-1} clearly observed in also copolymer iCVD77 in addition to homopolymer PPFDA. As a result, it can be concluded that copolymer iCVD59 contains higher amount of PGMA in its composition while higher amount of PPFDA found in iCVD77 copolymer film according to the FTIR spectra results. However, FTIR analysis is not enough for composition determination and detailed Nuclear Magnetic Resonance (NMR) spectroscopy should be used in future studies.

4.3.3. SEM Analysis of Copolymer Films

SEM analysis for copolymer P(GMA-PFDA) films was performed to examine the film morphology. In Figure 4.21 and 4.22, SEM images of copolymer films of the iCVD59 and iCVD77 depositions are given, respectively.

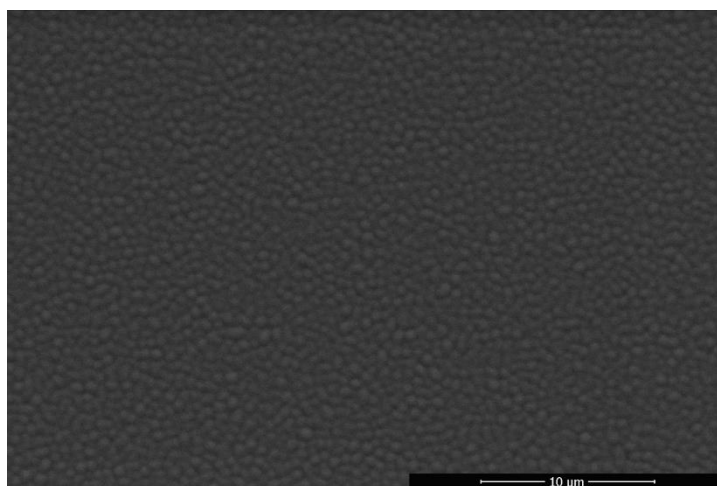


Figure 4.21. SEM image of c-Si coated with copolymer P(GMA-PFDA) film which contains higher amount of PGMA.

In Figure 4.21, SEM image of iCVD59 was shown and it was observed that surface of the coating looks more like the homopolymer PGMA coating because smoother surface and spherical shapes as previously observed. Since GMA monomer flow rate is also higher than PFDA monomer flow rate during deposition in iCVD59, composition of PGMA in the copolymer can be considered higher than PPFDA. This is also supported by FTIR analysis.

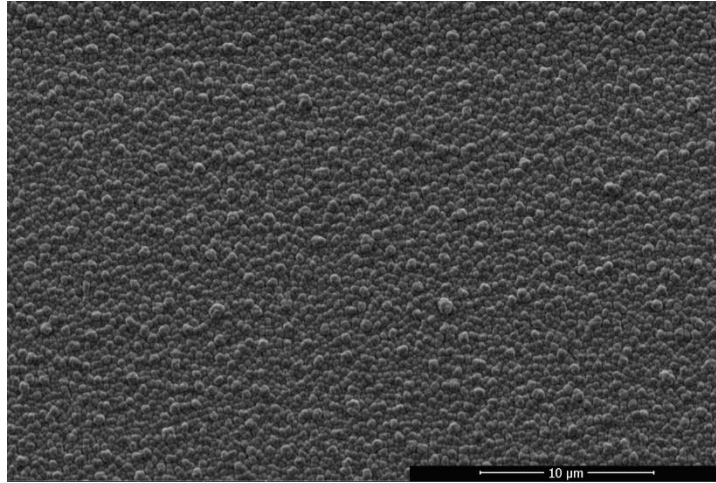


Figure 4.22. SEM image of c-Si coated with copolymer P(GMA-PFDA) film which contains higher amount of PFDA.

SEM image of iCVD77 shown in Figure 4.22. It is clearly seen that film morphology more resemble to homopolymer PFDA coating because its surface appears prominently rough and compact even though spherical shapes also observed due to the PGMA. As a result, it can be said that opposite of the iCVD59 in this copolymer coating, PFDA composition are higher than PGMA.

4.3.4. AFM Results of Copolymer P(GMA-PFDA) Film

In Figure 4.23, AFM analysis of copolymer films which have different amount of PGMA and PFDA compositions are given. Surface roughness values of these films were determined and evaluated based on their composition.

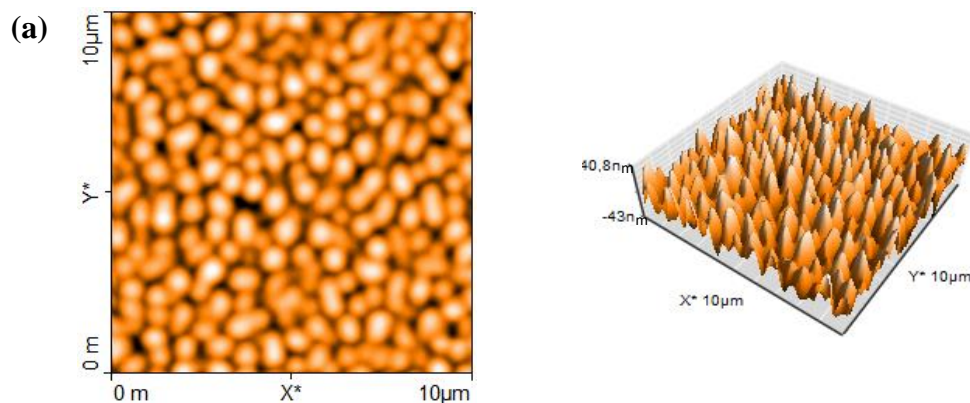


Figure 4.23. AFM color map and 3D images of copolymer coatings synthesized in (a) iCVD59 run and (b) iCVD77 run.

(Cont. on next page)

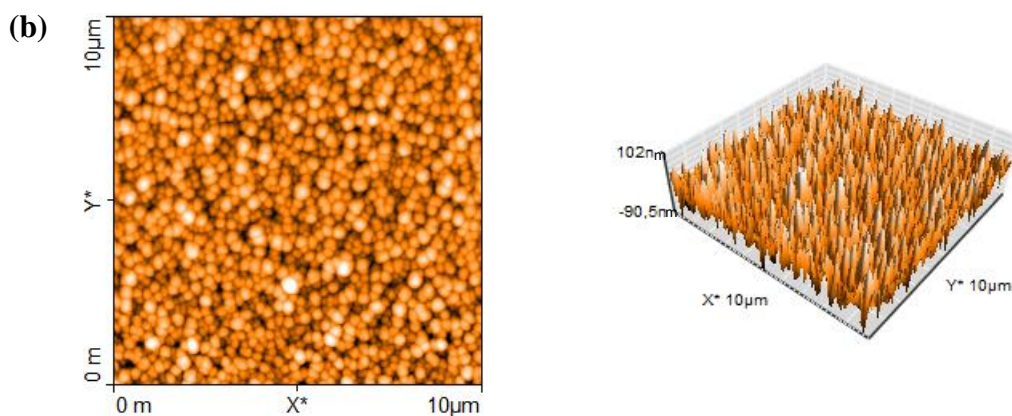


Figure 4.23. (Cont.)

In AFM color map and 3D images, it is clearly observed that Figure 4.23 (a) resemble to PGMA coating, and Figure 4.23 (b) is similar to PPFDA coating when these results compare with that of homopolymers of PGMA and PPFDA.

The average roughness and RMS roughness values of iCVD59 and iCVD77 samples were found as Ra: 131 Å, Rq: 158 Å, and Ra: 233.8 Å, Rq: 289.8 Å, respectively. These results show that surface roughness values of iCVD59 sample is lower than iCVD77. This was an expected result because both in FTIR and SEM analysis, it was concluded that PGMA in copolymer coating is higher in iCVD59 sample while PPFDA polymer is present slightly more than PGMA in iCVD77 copolymer coating.

4.3.5. Contact Angle Measurement for Copolymer Films

In order to determine hydrophobicity of the copolymer coating film, contact angle measurement was performed for two copolymer films and results are given Figure 4.24.

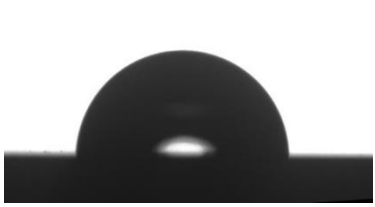
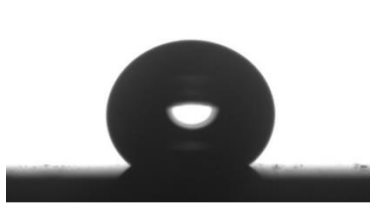
Coated c-Si with Copolymer films P(GMA-PFDA)	
iCVD59	iCVD77
	
Contact Angle: 85°	Contact Angle: 142°

Figure 4.24. Contact angle results for c-Si substrate coated with copolymer films.

For iCVD59 sample, contact angle was measured as 85° whereas contact angle of iCVD77 sample was determined to be 142°. These results indicate that the surface hydrophobicity of iCVD77 is higher than the other copolymer film. As confirmed by FTIR, SEM and AFM results, high composition of PPFDA in the iCVD77 copolymer coating is responsible for higher contact angle.

It is reasonable to assume that surface hydrophobicity and mechanical properties of copolymer films can be finely tuned by controlling the flow rate of each monomer during deposition thus controlling the ratios in the final copolymer film composition.

4.3.6. Surface Quality Test for Copolymer P(GMA-PFDA) Films

In addition to homopolymer PGMA and PPFDA coatings, surface quality test also performed for copolymer coatings and results of iCVD59 and iCVD77 films are shown in Figure 4.25.

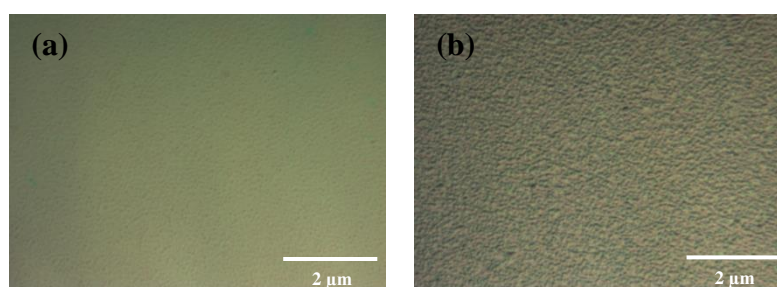


Figure 4.25. Surface images of (a) iCVD59 and (b) iCVD77 deposition samples at 80x magnification.

According to Figure 4.25, uniform coatings were obtained in both iCVD59 and iCVD77 depositions. While quite smooth surface was obtained in copolymer film synthesized in iCVD59, rougher surface appears in iCVD77 copolymer film and this verifies that this copolymer include higher amount of PPFDA than PGMA. Besides, in both copolymer film, there is no visible scratches, pin holes or other defects unlike what was observed in homopolymer films of PPFDA. This is clearly a results of improved mechanical properties of copolymer films compared to pure fluoropolymer due to incorporation of GMA.

4.4. Performance Tests for Homopolymer and Copolymer Films

In order to examine the physical quality of both homopolymer and copolymer coating surfaces, Military Standard (MIL-STD) which is MIL-F-48616 was followed. In each homopolymer and copolymer films, surface quality tests, scratches and holes detections were performed using optical microscopy. In addition, humidity, swelling in water, salt resistance, solubility in different chemicals, and adhesion test results are given in this section.

4.4.1. Humidity Test

Humidity tests was performed to investigate the coated film resistance to the moisture. Before applying this test, coated film thicknesses were measured in reflectometer and the same thickness measurement were performed after the test to examine whether any changes occurred. For humidity tests, coated substrates with both homopolymer and copolymers placed into a test chamber which contained an ultrasonic humidifier, temperature measurement device and moisture meter. In this test chamber, temperature was set to 35°C and relative humidity was kept at 80-95% while samples were exposed for 24 hours. After that samples were removed from the chamber and placed into the vacuum oven at 60°C for 30 minutes to dry the samples as instructed by MIL standard used in this study. Thereafter, again thickness and reflection measurements at the same time were performed. The results are given in Table 4.4.

Table 4.4. Thickness results of coated films on c-Si substrate.

Coatings on c-Si	Thickness Results	
	Before Humidity Test	After Humidity Test
Homopolymer PGMA	1.07 μm	1.07 μm
Homopolymer PPFDA	1.17 μm	1.15 μm
Copolymer P(GMA-PFDA) (contains higher amount of PGMA)	620 nm	618 nm
Copolymer (P(GMA-PFDA)) (contains higher amount of PPFDA)	572.4 nm	571.8 nm

When the results were examined it was observed that there is no significant difference in film thicknesses and the little change in the thickness values may be seen originating from the measurement errors. Below, only PGMA reflectance graph is given in Figure 4.26, in order to show perfect agreement before and after humidity tests.

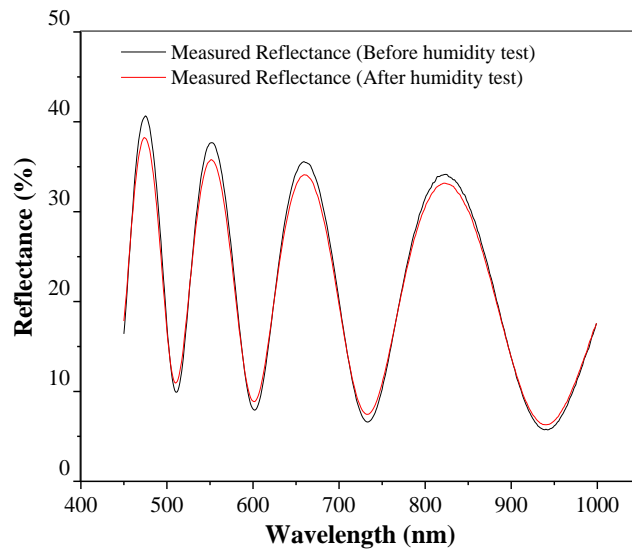


Figure 4.26. Thickness and reflection inspection of PGMA film produced in iCVD system before and after humidity test.

In figure 4.26, measured reflectance before and after humidity test at the same thickness values were shown. According to this figure, reflectance data obtained before and after humidity test fitted with each other properly. As a result, it can be concluded that the coated films by using iCVD show excellent resistance to humidity at given conditions.

4.4.2. Swelling-Solubility in Water Test

In order to examine the resistance of coatings fabricated in iCVD system to various solvents and swelling in water, a test was implemented based on MIL standard. Before the test, thickness measurement was performed by using reflectometer device. In this test, coated samples were placed separately into beakers which contain only deionized (DI) water at room temperature for 48 hours. At the end of this time period, samples removed from the beakers and dried one by one by holding to nitrogen flow. After the drying step, coated film thicknesses measured again to check whether there is any effect of test on the films. Results are given in Table 4.5 below.

Table 4.5. Swelling-Solubility in Water Test results of coating films on c-Si substrate.

Coatings on c-Si	Thickness Results	
	Before Swelling-Solubility Test	After Swelling-Solubility Test
Homopolymer PGMA	876 nm	875.7 nm
Homopolymer PPFDA	871.6 nm	872.8 nm
Copolymer P(GMA-PFDA) (contains higher amount of PGMA)	661 nm	661 nm
Copolymer (P(GMA-PFDA) (contains higher amount of PPFDA)	487.4 nm	491 nm

It was clearly seen that there is no remarkable change in the thickness of the films before and after the test and little alteration may occur due to the measurement error in reflectometer. The thickness measurement result data shown in Figure 4.27 for PGMA film as an example because nearly the same data were obtained before and after the test for the other films.

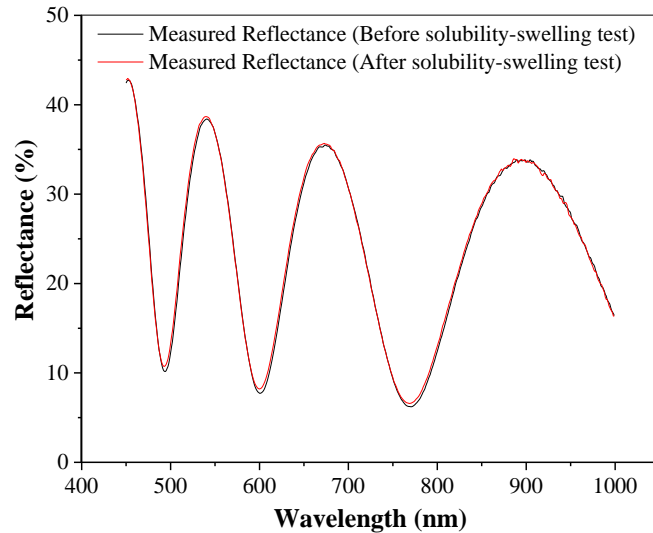


Figure 4.27. Thickness and reflection inspection of PGMA film produced in iCVD system before and after swelling-solubility in water test.

As seen in the figure, measured reflectance data before and after the tests fit very well with each other and this result show that produced film in iCVD system is quite resistant to swelling and solubility in water.

4.4.3. Salt Solubility Test

Salt solubility tests were applied to films on c-Si substrates. Before this test, thickness measurement was performed. In this test a solution of distilled water and sodium chloride, NaCl, (salt) was prepared by using 80 ml water and 3.58 g NaCl. Then, samples were immersed into the solution at room temperature for 24 hours. At the end of the test, samples were taken from the solution and washed with DI water one by one to remove salt residuals on the surface. Samples were dried in vacuum oven at 60°C and approximately 30 minutes, then again thickness measurements were performed to compare the results before and after the test. Results are given in Table 4.6.

Table 4.6. Salt Solubility Test results of coating films on c-Si substrate.

Coatings on c-Si	Thickness Results	
	Before Salt Solubility Test	After Salt Solubility Test
Homopolymer PGMA	748 nm	750 nm
Homopolymer PPFDA	1.2 μm	1.2 μm
Copolymer P(GMA-PFDA) (contains higher amount of PGMA)	665 nm	664 nm
Copolymer (P(GMA-PFDA) (contains higher amount of PPFDA)	499 nm	500 nm

The thickness results before and after the test were very close. Therefore, it can be said that all coatings produced with homopolymers and copolymers showed excellent resistance to salt water, and did not showed any swelling. The reflectance curve of a PGMA coating is given in Figure 4.28 as an example to show that optical performance of the coating does not change after the salt solubility test. It was observed that there is no significant variation in the reflectance of the coating even if salt solubility test applied, thus this illustrates that films coated on c-Si substrates in iCVD system highly resist to the salt solubility.

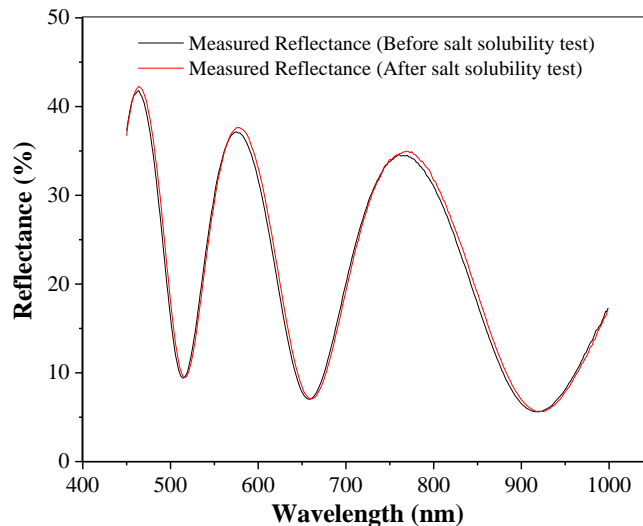


Figure 4.28. Thickness and reflection inspection of PGMA film produced in iCVD system before and after salt solubility test.

4.4.4. Solubility and Cleanability Test

For the solubility and cleanability test, polymer film coatings were immersed into three different solutions which are trichloroethylene, acetone and ethyl alcohol, respectively and samples were kept into each solution approximately for 20 minutes, as instructed by MIL-F-48616 standard.

After removal of the samples from the solution, to remove excess solvent present on the surface of the samples, they were exposed to air for 5 minutes without applying any drying process and then immersed in next solution. As expected polymer films were dissolved completely. MIL standards that were used in this study are originally designed for inorganic thin film coatings, not for polymeric materials. There are no standard procedures for testing polymer thin films for the same purpose. That said, from previous studies in the literature, it is expected that cross-linked homo and copolymer films would survive this solubility tests and for the future studies, cross-linking of polymeric films developed in this study should be considered.

4.4.5. Adhesion Test

In adhesion test, 1.27 cm wide cellophane tape is used and it is pressed on the copolymer film surfaces then removed from the surface at an angle that is normal to the coated surface as instructed by MIL-F-48616 standard. After that, visual inspections and thickness measurements were performed by using optical microscopy and reflectometer device, respectively. The results are given in Figure 4.29.

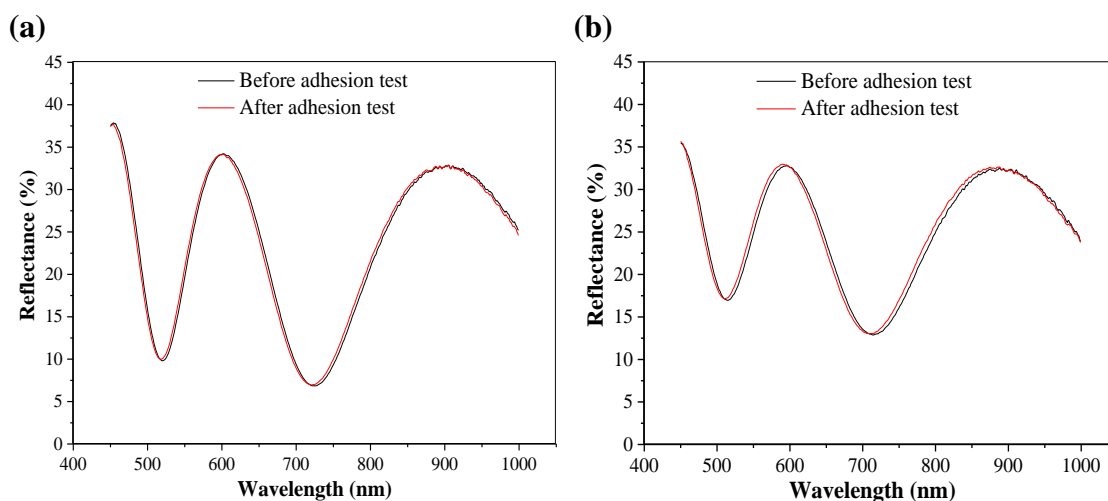


Figure 4.29. Thickness measurement results before and after adhesion test for (a) Copolymer (iCVD59) and (b) Copolymer (iCVD77) films produced in iCVD system.

Before and after the adhesion test, thickness values obtained from the reflectometer device were 628 and 625 nm for copolymer (iCVD59), and 618 and 614 nm for copolymer (iCVD77) film, respectively. According to these thickness results shown in figures above, it can be stated that there is no significant difference in terms of thickness of the coatings.

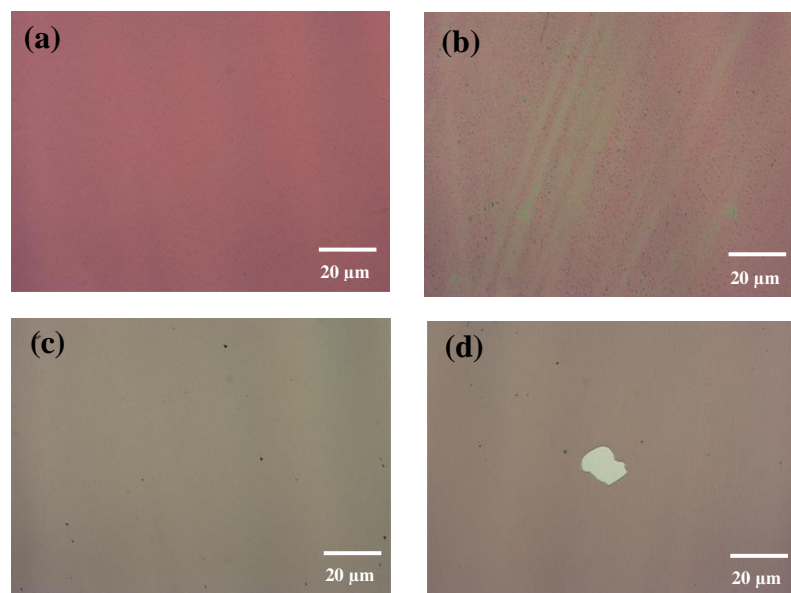


Figure 4.30. Before and after adhesion test visual inspection results of (a) and (b) Copolymer (iCVD59) and (c) and (d) Copolymer (iCVD77) film surface images at 5x magnifications.

When optical microscopy analysis was performed, it was observed that after the adhesion test, there is no significant change on the coating surface of the copolymer (iCVD59) film thus concluded that copolymer (iCVD59) survived adhesion test successfully. However, in copolymer (iCVD77) coating, a small piece of the film stuck to the cellophane tape and was removed from the surface. This was expected because the mechanical properties of this copolymer film was expected to be poorer than the iCVD59 film due to higher amount of PFDA in its composition. However, compared to total area of the film that the area of piece of film that was removed from the substrate is still within acceptable range. So by carefully controlling the copolymer film composition, mechanical strength and adhesion of the film to the substrate surface can be improved. As a result, even if iCVD77 copolymer film not show very high resistance to the adhesion test as seen in the copolymer iCVD59, it can still be said that this copolymer film also was durable to this test when both thickness and visual inspection results considered.

CHAPTER 5

CONCLUSIONS

In this study, fabrication of protective, self-cleaning and super hydrophobic polymeric film coatings for optical surfaces of the electro-optical systems were performed on both c-Si and glass substrates. In order to achieve desired mechanical, chemical and surface properties as well as to meet minimum optical performance criteria optimum operating conditions in iCVD system were determined for a variety of homo- and copolymer film coatings.

In order to obtain coatings with unique properties specified by the application GMA and PFDA were used as monomers; GMA for excellent mechanical and adhesion properties and PFDA for providing super hydrophobicity. Another reason for using these monomers in this study is that their refractive indices are close to glass substrate and this is very significant to preserve optical performance of especially glass type optic surfaces used in the electro-optical systems. Before depositions, modeling and simulation of the coatings to determine optimum film thickness was completed and simulation results showed that optical performance of the substrate surfaces preserved successfully even if the film thickness varied from 50 nm to 1 μm .

Homopolymers of PGMA and PPFDA thin films with varying thicknesses were deposited on c-Si and glass substrates via iCVD process. PGMA homopolymer films showed excellent mechanical and optical properties, however, hydrophobicity of the surface was not sufficient to be used as protective optical coatings in EO systems. On the other hand, PPFDA homopolymer films showed excellent surface hydrophobicity but also showed very poor mechanical properties, and were very prone to scratches and other surface damage by mechanical handling.

In order to take advantage of good mechanical properties of PGMA and hydrophobicity of PPFDA, P(GMA-PFDA) copolymers were fabricated via iCVD process. It was found that optical and mechanical properties of copolymers can be finely tuned by controlling the flow rates of monomers during iCVD deposition process.

To investigate the suitability of using these thin films as protective optical coating in EO systems, additional tests based on MIL-F-48616 standard were performed for homopolymer and copolymer films.

It was concluded that both homopolymer and copolymer films deposited in iCVD system show high resistance to humidity, salt solubility, swelling and solubility in water. Also, copolymer film which has higher amount of GMA is quite resistance to adhesion test. Therefore, it can be concluded that especially copolymer films produced in this study are quite suitable for coating on optical surfaces of the electro-optical surfaces.

REFERENCES

- Alf, M. E., T. A. Hatton and K. K. Gleason (2011). "Initiated chemical vapor deposition of responsive polymeric surfaces." Thin Solid Films **519**(14): 4412-4414.
- Allcock, H. R., F. W. Lampe and J. E. Mark (2003). Contemporary Polymer Chemistry, Prentice Hall.
- Andrews, D. L. (2009). Encyclopedia of Applied Spectroscopy, Wiley.
- Bakker, R., V. Verlaan, C. H. M. van der Werf, J. K. Rath, K. K. Gleason and R. E. I. Schropp (2007). "Initiated chemical vapour deposition (iCVD) of thermally stable poly-glycidyl methacrylate." Surface and Coatings Technology **201**(22–23): 9422-9425.
- Bass, M., C. DeCusatis, J. Enoch, V. Lakshminarayanan, G. Li, C. MacDonald, V. Mahajan and E. Van Stryland (2009). Handbook of Optics, Third Edition Volume IV: Optical Properties of Materials, Nonlinear Optics, Quantum Optics (set), McGraw-Hill Education.
- Bose, R. K., K. Lau, U. Drexel and E. College of (2011). Initiated chemical vapor deposition of polymer thin films and coatings for biological applications, Drexel University.
- Callister, W. D. (2007). Materials Science And Engineering: An Introduction, John Wiley & Sons.
- Campana, S. (1993). The Infrared & Electro-Optical Systems Handbook. Passive Ellectro-Optical Systems, Infrared information and analysis center ann arbor mi.
- Chan, K. and K. K. Gleason (2006). "A Mechanistic Study of Initiated Chemical Vapor Deposition of Polymers: Analyses of Deposition Rate and Molecular Weight." Macromolecules **39**(11): 3890-3894.
- Chan, K., L. E. Kostun, W. E. Tenhaeff and K. K. Gleason (2006). "Initiated chemical vapor deposition of polyvinylpyrrolidone-based thin films." Polymer **47**(20): 6941-6947.
- Coclite, A. M. (2013). "Smart surfaces by initiated chemical vapor deposition." Surface Innovations **1**(1): 6-14.
- Coclite, A. M., Y. Shi and K. K. Gleason (2013). "Super-Hydrophobic and Oloophobic Crystalline Coatings by Initiated Chemical Vapor Deposition." Physics Procedia **46**: 56-61.
- Dorval Dion, C. A. and J. R. Tavares (2013). "Photo-initiated chemical vapor deposition as a scalable particle functionalization technology (a practical review)." Powder Technology **239**: 484-491.

- Driggers, R. G., P. Cox and T. Edwards (1999). Introduction to Infrared and Electro-optical Systems, Artech House.
- Dudzik, M. (1993). The Infrared & Electro-Optical Systems Handbook. Electro-Optical Systems Design, Analysis, and Testing, Infrared information and analysis center ann arbor mi.
- Fox, C. (1996). The Infrared and Electro-optical Systems Handbook: Actives electro-optical systems, Environmental research institute of Michigan.
- Gleason, K. K. (2015). CVD Polymers: Fabrication of Organic Surfaces and Devices, Wiley.
- Gupta, M. and K. K. Gleason (2006). "Initiated Chemical Vapor Deposition of Poly(1H,1H,2H,2H-perfluorodecyl Acrylate) Thin Films." Langmuir **22**(24): 10047–10052.
- Gupta, M. and K. K. Gleason (2006). "Large-scale initiated chemical vapor deposition of poly(glycidyl methacrylate) thin films." Thin Solid Films **515**(4): 1579-1584.
- Gupta, M. and K. K. Gleason (2009). "Surface modification of high aspect ratio structures with fluoropolymer coatings using chemical vapor deposition." Thin Solid Films **517**(12): 3547-3550.
- Gupta, M., V. Kapur, N. M. Pinkerton and K. K. Gleason (2008). "Initiated Chemical Vapor Deposition (iCVD) of Conformal Polymeric Nanocoatings for the Surface Modification of High-Aspect-Ratio Pores." Chemistry of Materials **20** (4): 1646–1651.
- Johnson, R. W., A. Hultqvist and S. F. Bent (2014). "A brief review of atomic layer deposition: from fundamentals to applications." Materials Today **17**(5): 236-246.
- Jones, A. C. and M. L. Hitchman (2009). Chemical Vapour Deposition: Precursors, Processes and Applications, Royal Society of Chemistry.
- Lau, K. K. S. and K. K. Gleason (2006). "Initiated chemical vapor deposition (iCVD) of poly(alkyl acrylates): An experimental study." Macromolecules **39**(10): 3688-3694.
- Lau, K. K. S. and K. K. Gleason (2006). "Initiated chemical vapor deposition (iCVD) of poly(alkyl acrylates): A kinetic model." Macromolecules **39**(10): 3695-3703.
- Lau, K. K. S. and K. K. Gleason (2007). "Particle functionalization and encapsulation by initiated chemical vapor deposition (iCVD)." Surface and Coatings Technology **201**(22–23): 9189-9194.
- Lau, K. K. S. and K. K. Gleason (2008). "Applying HWCVD to particle coatings and modeling the deposition mechanism." Thin Solid Films **516**(5): 674-677.

- Lau, K. K. S. and K. K. Gleason (2008). "Initiated chemical vapor deposition (iCVD) of copolymer thin films." Thin Solid Films **516**(5): 678-680.
- Luis, Y. J. and K. K. Gleason (2013). "Enhanced Cross-Linked Density by Annealing on Fluorinated Polymers Synthesized via Initiated Chemical Vapor Deposition To Prevent Surface Reconstruction." Macromolecules **46**(16): 6548–6554.
- Lvovsky, A. I. (2013). Fresnel Equations. In Encyclopedia of Optical Engineering, Taylor and Francis: New York: 1-6.
- MacLeod, H. A. (2001). Thin-Film Optical Filters, Third Edition, Taylor & Francis.
- Mao, Y. and K. K. Gleason (2004). "Hot Filament Chemical Vapor Deposition of Poly(glycidyl methacrylate) Thin Films Using tert-Butyl Peroxide as an Initiator." Langmuir **20**(6): 2484-2488.
- Mao, Y. and K. K. Gleason (2006). "Vapor-Deposited Fluorinated Glycidyl Copolymer Thin Films with Low Surface Energy and Improved Mechanical Properties." Macromolecules **39**(11): 3895-3900.
- Martin, T. P., S. E. Kooi, S. H. Chang, K. L. Sedransk and K. K. Gleason (2007). "Initiated chemical vapor deposition of antimicrobial polymer coatings." Biomaterials **28**(6): 909-915.
- Martin, T. P., K. K. S. Lau, K. Chan, Y. Mao, M. Gupta, A. S. O'Shaughnessy and K. K. Gleason (2007). "Initiated chemical vapor deposition (iCVD) of polymeric nanocoatings." Surface & Coatings Technology **201**(22-23): 9400-9405.
- Mittal, V. (2013). Encapsulation Nanotechnologies, Wiley.
- Mohammed Safiullah, S., K. Abdul Wasi and K. Anver Basha (2014). "Preparation of poly(Glycidyl methacrylate)–copper nanocomposite by in-situ suspension polymerization – A novel synthetic method." Materials Letters **133**: 60-63.
- Nalwa, H. S. and S. Miyata (1996). Nonlinear Optics of Organic Molecules and Polymers, Taylor & Francis.
- Park, S. W., D. Lee, H. R. Lee, H.-J. Moon, B. R. Lee, W.-K. Ko, S.-J. Song, S. J. Lee, K. Shin, W. Jang, J.-K. Yi, S. G. Im and I. K. Kwon (2015). "Generation of functionalized polymer nanolayer on implant surface via initiated chemical vapor deposition (iCVD)." Journal of Colloid and Interface Science **439**: 34-41.
- Parker, T. C., D. Baechle and J. D. Demaree (2011). "Polymeric barrier coatings via initiated chemical vapor deposition." Surface and Coatings Technology **206**(7): 1680-1683.
- Piegari, A. and F. Flory (2013). Optical Thin Films and Coatings: From Materials to Applications, Elsevier Science.

- Pierson, H. O. (1999). Handbook of Chemical Vapor Deposition, 2nd Edition: Principles, Technology and Applications, Elsevier Science.
- Riche, C. T., C. Zhang, M. Gupta and N. Malmstadt (2014). "Fluoropolymer surface coatings to control droplets in microfluidic devices." The Royal Society of Chemistry **14**: 1834–1841.
- Schaub, M. P. (2009). The Design of Plastic Optical Systems, Society of Photo Optical.
- Stenzel, O. (2006). The Physics of Thin Film Optical Spectra: An Introduction, Springer Berlin Heidelberg.
- Stuart, B. H. (2004). Infrared Spectroscopy: Fundamentals and Applications, Wiley.
- Träger, F. (2012). Springer Handbook of Lasers and Optics, Springer.
- Trujillo, N. J., Q. G. Wu and K. K. Gleason (2010). "Ultralow Dielectric Constant Tetravinyltetramethylcyclotetrasiloxane Films Deposited by Initiated Chemical Vapor Deposition (iCVD)." Advanced Functional Materials **20**(4): 607-616.
- Turner, T. and R. Kirschner. "Thin-Film Coatings." Retrieved (2015 September, 11), from <http://www.photonics.com/EDU/Handbook.aspx?AID=42399>.
- Wakaki, M. (2012). Optical Materials and Applications, Taylor & Francis.
- Web-1. (2012). "Refraction of Light." Retrieved (2015 September, 8), from <http://sciencelearn.org.nz/Contexts/Light-and-Sight/Science-Ideas-and-Concepts/Refraction-of-light>.
- Web-2. "Light Properties: Absorption, Reflection and Transmission." Retrieved (2015 September, 11), from <http://www.easycoursesportal.com/basicphotographycourseiii/coursesec/Less-8.htm>.
- Web-3. "Crystal Systems." Retrieved (2015 September, 13), from <https://www.imperial.ac.uk/earthscienceandengineering/rocklibrary/viewglossre cord.php?Term=crystal%20system>.
- Web-4. "Tracking Solar Flares." Retrieved (2015 September, 18), from <http://solar-center.stanford.edu/SID/activities/ionosphere.html>.
- Web-5. "Anti-Reflection Coatings." Retrieved (2015 September, 18), from <http://hyperphysics.phy-astr.gsu.edu/hbase/phyopt/antiref.html>.
- Web-6. "Optical Coatings." Retrieved (2015 September, 19), from http://cvilaseroptics.com/Frontend/PDFs/optical_coatings.pdf.
- Web-7. "Hot&Cold Mirrors." Retrieved (2015 September, 28), from http://www.uqgoptics.com/product_custom_filters_mirrors.aspx.

Web-8. "Optical Filters: Hot and Cold Mirrors." Retrieved (2015 September, 28), from <http://www.optical-filters.com/Filters.aspx>.

Web-9. "Transmission spectra of substrate materials." Retrieved (2016 January, 2), from http://www.thorlabs.de/NewGroupPage9.cfm?ObjectGroup_ID=3982.

Web-10. "Material Transmission Data." Retrieved (2016 January, 2), from <http://rmico.com/support/tech-notes/material-data#mgf2>.

Weber, M. J. (2002). Handbook of Optical Materials, Taylor & Francis.

Wypych, G. (2011). Handbook of Polymers, ChemTec Pub.

Yoo, Y., J. B. You, W. Choi and S. G. Im (2013). "A stacked polymer film for robust superhydrophobic fabrics." Polymer Chemistry **4**(5): 1664-1671.